International Materials Reviews
Material challenges in hydrogen-fuelled gas turbines
--Manuscript Draft--

| Abstract: | With the increased pressure to decarbonize the power generation sector several gas turbine manufacturers are working towards increasing the hydrogen-firing capabilities of their engines towards 100%. In this review, we discuss the potential materials challenges of gas turbines fuelled with hydrogen, provide an updated overview of the most promising alloys and coatings for this application, and highlight topics requiring further research and development. Particular focus is given to the high-temperature oxidation of gas turbine materials exposed to hydrogen and steam at elevated temperatures and to the corrosion challenges of parts fabricated by additive manufacturing. Other degradation mechanisms such as hot corrosion, the dual atmosphere effect and hydrogen diffusion in the base alloys are also discussed. |

Materials challenges in hydrogen-fuelled gas turbines

Elena Stefan*[1], Belma Talic*[1], Yngve Larring[1], Andrea Gruber[2], Thijs A. Peters[1]

[1] SINTEF Industry, P.O. Box 124 Blindern, N-0314, Oslo, Norway

[2] SINTEF Energy Research, Thermal Energy Department, Trondheim, Norway

*These authors contributed equally to this work.

Contents

Abstract

With the increased pressure to decarbonize the power generation sector several gas turbine manufacturers are working towards increasing the hydrogen-firing capabilities of their engines towards 100%. In this review, we discuss the potential materials challenges of gas turbines fuelled with hydrogen, provide an updated overview of the most promising alloys and coatings for this application, and highlight topics requiring further research and development. Particular focus is given to the high-temperature oxidation of gas turbine materials exposed to hydrogen and steam at elevated temperatures and to the corrosion challenges of parts fabricated by additive manufacturing. Other degradation mechanisms such as hot corrosion, the dual atmosphere effect and hydrogen diffusion in the base alloys are also discussed.

1 Introduction

Gas turbines are among the most widely used power-generation technologies today. Their theoretical basic principle, the Brayton thermodynamic cycle, relies on thermal energy conversion of a chemically reactive fuel and leverages on an abundantly available gas (air) as working fluid to generate electric power or to mechanically drive rotating equipment (*e.g.* in compressor stations). State-of-the-art combined cycle gas turbines offer the advantages of a high total efficiency (>60 % [1]), low NO_x and SO_x emissions, and high fuel flexibility. However, despite being considered the cleanest of the conventional fossil-fuel power generation technologies, gas turbines fuelled with hydrocarbon-based fuels inevitably lead to considerable CO_2 emissions (ca. 440 gCO_2/kWh for natural gas [2]). These CO_2 emissions could be greatly reduced or even eliminated if the gas turbine instead is fuelled with hydrogen produced using either renewable energy [3] or natural gas reforming combined with carbon capture and storage (CCS) schemes [4]. Gas turbines are complementary to other hydrogen-conversion technologies such as fuel cells as they currently are more cost-efficient at large scale and can utilize lower-purity hydrogen, for example produced during the synthesis of aromatics and olefins or hydrogen from chlor-alkali plants. The hydrogen available from these sources amounts to > 10 000 metric tons per year in the US alone [5].

A jet engine powered by hydrogen was demonstrated already in 1937, which shows that the hydrogen-fuelling of gas turbines is not novel [6]. However, practical considerations and the historically lower price of natural gas compared to hydrogen favoured the development of gas turbines highly tuned for operation with natural gas. With the increased pressure to decarbonize the power generation sector in order to limit global warming, the industry is re-considering hydrogen as a viable fuel. In a few countries such as the Netherlands, small amounts (<20 vol.%) of hydrogen are being mixed into the natural gas grid and used to fuel conventional gas turbines [7]. While this is an important step in the right direction, adding hydrogen to natural gas has only a minor effect on the CO_2 emissions because of the low volumetric energy density of hydrogen relative to methane. For example, adding 10 vol.% hydrogen to methane will only reduce CO_2 emissions by 2.7 % [8]. For a completely CO_2-emission free operation, gas turbines capable of operating on 100 % hydrogen are hence required.

As illustrated in Figure 1, several commercially-available gas turbines based on diffusion-flame combustion systems can already be operated with 100 % hydrogen [9]. However, these systems require the addition of large quantities of treated water (or nitrogen) in order to adequately decrease the flame temperature and NO_x emissions in wet low emission (WLE) combustors, which results in a more complex, bulkier, and expensive system with a lower overall efficiency. Therefore, recent research and development efforts have focused on hydrogen-firing of state-of-the-art dry low-emission (DLE) combustion systems that have greater potential to simultaneously ensure high efficiencies and emissions-compliant operation. In DLE combustors the flame temperature is typically

moderated by ensuring that fuel-lean conditions are achieved before combustion occurs, thereby avoiding any significant production of NO_x. This is achieved through an highly-optimized injection and mixing of the fuel with the oxidant (air) before the resulting burnable mixture enters the combustion chamber.

None of the commercially available DLE combustion systems today, however, can be operated with more than 30-60 vol.% of hydrogen [10]. While the Japanese company Kawasaki reported in July 2020 the world's first demonstration of a 100% hydrogen-fuelled gas turbine using a DLE combustion system [11], this achievement was obtained in the context of a small combined heat and power (CHP) application featuring relatively low electrical efficiency (~28%) and, therefore, requiring a relatively low firing temperature. Significant outstanding issues remain if 100 % hydrogen DLE operation has to be implemented in gas turbines capable of state-of-the-art electrical efficiencies that reach ~43% in open cycles configurations (~63% in combined cycles) and require high firing temperatures [12]. The gas turbine industry in Europe is targeting to achieve this by 2030 [10].

The main challenges encountered in the operation of DLE systems with 100 % hydrogen are related to the combustion characteristics of hydrogen [9,13] that become increasingly difficult to handle, from the combustion system's design point of view, for higher flame temperatures. This is a significant issue since the flame temperature is the single most important quantity controlling the turbine inlet temperature, the power output and the efficiency of the gas turbine, *i.e.* its ability to produce work (electricity or mechanical drive). Among the most important characteristics that differentiate hydrogen from conventional hydrocarbon fuels (*e.g.* natural gas) is the combustion burning rate, *i.e.* the rate at which the flame is able to consume the combustible mixture, increasing the working fluid's temperature to accelerate it towards the turbine stage. The burning rate (flame speed) in laminar hydrogen flames is nominally three to seven times higher compared to methane (the main component of natural gas) at equal flame temperature because of hydrogen's fast reaction and diffusion rates [8,13]. Even larger differences are observed in the highly turbulent flames found in the combustion system of modern gas turbines [14]. The augmented burning rate can lead to flame instability issues, increasing the risk of unwanted flame displacement into the upstream mixing section of the burner (flashback) and resulting in early combustion of a sub-optimal (still fuel-rich) mixture of fuel and oxidant. In turn, this causes very high local flame temperatures that promote pollutants formation (NO_x) and exposure above the melting point of the stainless-steel alloy construction materials.
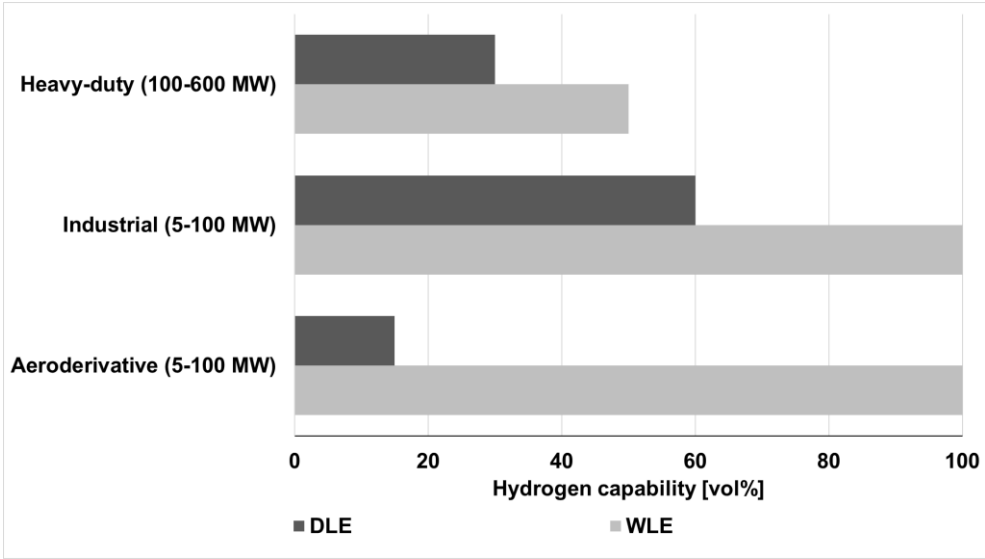
An additional important challenge introduced by hydrogen combustion that is of specific relevance to the material-science aspect of the technology development is related to the flame characteristic quenching distance (δ_q). This quantity defines the minimal distance between a hot flame and a (relatively) cold solid surface at which quenching nominally occurs. Both fundamental modelling and experimental investigations have indicated that δ_q is significantly smaller (by a factor of 1/2) for hydrogen flames compared to hydrocarbon flames [15], implying the possibility of a greatly enhanced heat-flux to the solid surfaces that are in vicinity of the hydrogen flame stabilization location. The quenching heat-flux from the flame to the combustor walls is further amplified in the presence of characteristic near-wall turbulence structures [16], establishing an unsteady spatial pattern with peaks exceeding 1 MW/m^2 that, when opportunely modulated by the controlling time and length scale of the turbulent flow, can result in severe thermal stress of the solid material.

While many of the above-mentioned challenges related to the combustion of hydrogen can be handled through modifications to the design of the burner, factors such as an increased temperature and steam content may also require the development of new materials. One potential challenge from the materials' perspective is that hydrogen combustion results in a higher steam concentration in the exhaust gas relative to natural gas combustion. The exhaust from natural gas fired land-based turbines typically contains 10 vol.% steam and 5 vol.% CO_2. State-of-the-art DLE operation with pure hydrogen
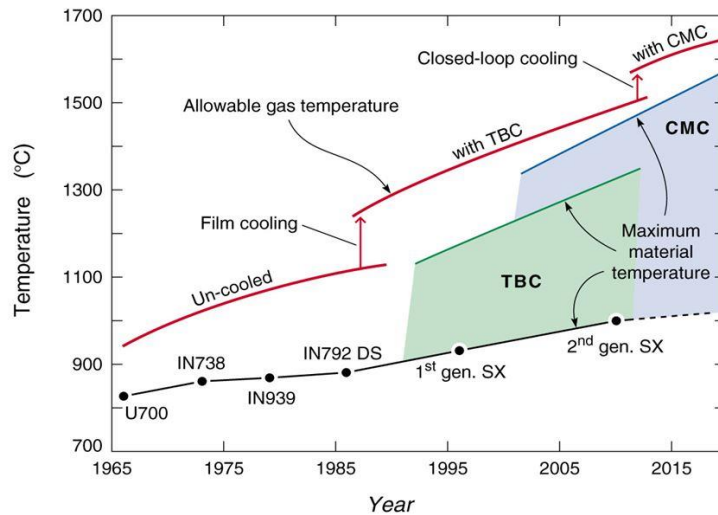
3

(yet to be achieved) would theoretically increase the steam fraction in the combustion products to 16 vol.%, while legacy technologies utilizing steam dilution or water injection result in exhaust steam content up to 85 vol.% [17,18]. One of the impacts of increased water content in the combustion products is that the heat transfer coefficient between the hot gas and all solid surfaces exposed to it is increased, resulting in higher temperatures of the metal blades in the first, critical turbine stages that are subjected to the largest heat load [13]. This effect can be compensated by decreasing the flame and the turbine inlet temperatures, but at the expense of a lower efficiency [19].

There are several reviews available that provide an overview of the latest developments in materials for gas turbines [20–27]. Most of these discuss the possible challenges with using natural gas as the fuel, while less literature is available regarding the possible materials challenges with using hydrogen. To our own knowledge, only the 2007 review by Wright and Gibbons [20] considered the suitability of applying state-of-the-art materials developed for "conventional" gas turbines in gas turbines burning coal-derived syngas or hydrogen. They concluded that the combustion environment with coal derived hydrogen or syngas was possibly more corrosive than natural gas, because of the greater level of impurities such as sulphur, water vapour and particulates that affect the durability of some components. The development of materials for gas turbines has significantly progressed since Wright and Gibbons [20] published their review. The most important trend is the development of new materials enabling a higher operating temperature, and thus higher turbine efficiency, as shown in Figure 2. Another trend is the increased application of additive manufacturing or 3D printing to fabricate complex gas turbine combustor designs, such as those currently being developed for hydrogen-fuelled gas turbines. The time is therefore mature to review the current state-of-the art materials and their suitability for application in hydrogen-fuelled gas turbines.

In this review, we aim to present an overview of the materials challenges in gas turbines fuelled with 100 % hydrogen, provide an updated overview of the most promising alloys and coatings for this application, and highlight topics requiring further research and development. Particular focus is given to the high-temperature oxidation of gas turbine materials exposed to hydrogen and steam at elevated temperatures and the potential corrosion issues for gas turbine components made by additive manufacturing.
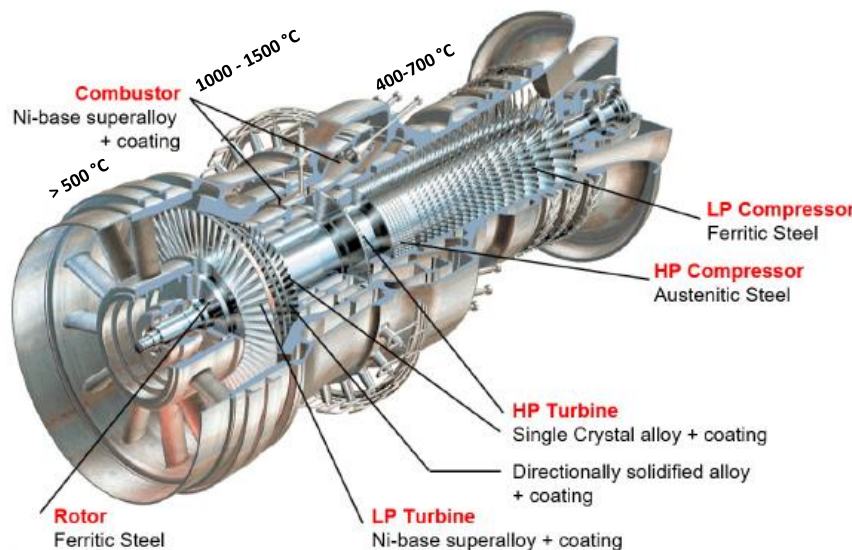

Figure 1 Types of gas turbine burners fuelled with hydrogen-fuel mixtures, adapted freely after [8,9,28]. DLE = dry low emission, WLE = wet low emission.

Figure 2 Material improvements with firing temperature capability of industrial gas turbines (TBC – thermal barrier coatings, CMC – ceramic matrix composites), after [19].

2 Materials used in gas turbines

The materials used in the different parts of a gas turbine must meet a demanding set of requirements in terms of mechanical and thermal properties, manufacturability into complex geometries, and stability under the working conditions. Figure 3 illustrates the range of exposure conditions for different parts of the gas turbine and highlights commonly employed materials. Since a single material in most cases cannot provide the necessary combination of mechanical robustness/strength and sufficient oxidization resistance, some of the gas turbine components are coated and/or internally cooled.

Figure 3 Main parts of an Alstom gas turbine, exposure conditions and materials used in different sections, after [29,30].

The following sections contain a description of the exposure conditions in the different parts of the gas turbine and how these may be influenced when the gas turbine is fuelled with hydrogen instead of natural gas. An overview of the most commonly used turbine materials and the most promising new

developments is presented. In the previous two decades, several companies and research programs focused on developing syngas (*i.e.* CO + H$_2$) fuelled gas turbines, which has given some experience with use of hydrogen containing fuels [13]. Much of the more general materials development has otherwise been driven by the development of aeroturbines, as these operate at harsher conditions and have stricter requirements for high efficiency and low weight. Industrial-scale land-based turbines have tougher requirements of low cost that, alongside challenges with upscaling certain manufacturing methods, imposes restrictions on which materials that can be adopted. For example, single crystal alloys are attractive because of their high temperature tolerance, but difficult to manufacture without defects in the large size required for industrial scale gas turbines [12,19,21].

2.1 Materials for the compressor section

The temperature in the air compressor part of the turbine is typically limited to 400-500 °C, making it possible to use relatively inexpensive alloys such as martensitic stainless steels, *e.g.* AISI 403 or AISI 403 Nb [23]. In small and intermediate scale gas turbines operated with relatively clean air, these alloys do not suffer from any significant materials challenges [21]. The materials requirements are harsher for gas turbines installed in industrial settings where the air is contaminated by acids and/or salts. In these situations, alloys such as the precipitation hardened martensitic stainless steel GTD-450 is a good alternative [23]. This alloy has a higher Cr and Mo content compared to AISI 403, which provides corrosion resistance to moisture containing acids and salts [23,24].

Hydrogen fuelling does not have any intrinsic requirements for higher or lower compressor output compared to natural gas fuelling of gas turbines. Thus, no changes are expected for this part of the gas turbine when switching to hydrogen.

2.2 Materials for combustor parts

State-of-art DLE combustion systems for stationary gas turbines are based on a lean premixed combustion approach and typically consists of a mixing section where fuel is injected and mixed into the oxidant stream and a combustion chamber. In stationary applications, longitudinal or radial (co-axial) fuel staging designs are often adopted in order to optimize the combustion process and limit pollutants formation. However, footprint and weight constraints severely limit the adoption of staged combustion systems in aero-applications which, because of flame stability and high-altitude relight requirements, traditionally employ a non-premixed combustion approach with important consequences on emissions from the diffusion-type flame. The combustion chamber is the hottest part of the gas turbine where temperatures can reach 1600 °C or even higher [20]. The materials used for some specific parts of the combustion system must therefore meet a series of strong requirements including high temperature creep rupture strength, good oxidation resistance, and endurance against thermal and cycle fatigue. The materials should also have good formability and weldability to enable fabrication of complex shapes [20,21].

Commonly applied materials able to meet the mechanical requirements are wrought Ni base superalloys such as Hastelloy X, IN617, Nimonic 263, Haynes 188 or Haynes 230 and SS309 [21,23,24,31]. In order to keep the surface of these alloys sufficiently below their melting point, internal air cooling and thermal barrier coatings (see Section 2.4) or ceramic tiles are applied as the combustor lining.

Land-based gas turbines are striving to reduce costs by exchanging the low-Re (Rhenium) second generation superalloys to Re-free first-generation alloys such as 1483, or to directionally solidified superalloys such as 247. Other research, motivated by cost reductions, is to replace the relatively expensive Ni-based superalloys in parts of the gas turbine with cheaper Cr-based alloys. Cr-based alloys have other advantages besides a low cost, such as a 400-500 °C higher melting temperature and 2-4

times higher thermal conductivity. However, challenges such as decreased high temperature strength and ductility, and lower oxidation and corrosion resistance compared to Ni-based superalloys need to be overcome before the Cr-based alloys can be applied in gas turbines. Dorcheh and Galetz [32] have reviewed the challenges with using Cr-based alloys with focus on their oxidation resistance and reported volatilization and nitridation to be the major obstacles for the use of these alloys in air above 900 °C. Gu et al. [33] also pointed out embrittlement resulting from nitridation during high temperature air exposure as a major problem for Cr-based alloys and reviewed various strategies for improving the high temperature strength and other mechanical properties. It is worth noting that the addition of water vapour to a N_2-1%O_2 atmosphere has been found to decrease and even completely supress the nitridation of high purity chromia [34]. Thus, in this respect, fuelling with hydrogen (and the resulting increase in water vapour) may actually prove to be beneficial.

The desire to operate gas turbines at higher efficiencies and with hydrogen as the fuel puts even stronger requirements on the combustor materials due to the increase in temperature and steam content. Alternative alloys such as oxide-dispersion-strengthened (ODS) superalloys, ferritic alloys (*e.g.* PM2000 and Incoloy MA956) and ceramic matrix composites such as SiC/SiC based composites are therefore being considered [20,21,35]. ODS superalloys are advanced high temperature materials able to retain strength up a high fraction of their melting point and are therefore attractive to use for the hot gas path components [36]. However, high costs and a brittle nature limiting how large the ODS components can be made, restricts the use of ODS superalloys mostly to aircraft turbine vanes.

SiC/SiC ceramic matrix composites (CMC) have been used as an alternative to Ni-based superalloys in the hot section of commercial aircraft turbine engines for the last few years. Compared to Ni-based superalloys, the CMCs offer a lower weight and better resistance to higher operating temperatures. This reduces some of the need for internal cooling, which improves the turbine efficiency. During service, the SiC will form a slow growing, dense layer of SiO_2 on the surface, which greatly slows down further oxidation. Because of the high volatility of SiO_2 in humid conditions (see Section 3.1.4) the CMCs have to be coated with environmental barrier coatings such as rare earth (Yb, Y, Mo - Yb_2SiO_5 and $MoSiO_2$) disilicates. As will be further discussed in Section 3.1.4, hydrogen-fuelling of the gas turbine will likely strengthen the need for coatings with a low Si-volatility due to the higher steam content in the combustion gas.

2.3   Turbine components

In the turbine expansion stage, the hot exhaust gasses from the combustor are passed through a series of discs and vanes connected to a drive shaft that transmits the generated power. The temperature of the turbine inlet can be up to 1300-1600 °C and decreases towards the outlet. The turbine discs have to tolerate the axial loadings from the blades attached to it and the thermal, vibrational and centrifugal stresses during operation. This requires the turbine discs materials to have superior tensile strength, creep and high fatigue strength, as well as resistance to oxidation and corrosion attack. For turbine discs operating at the highest temperatures, Ni-based superalloys are preferred [21]. Cast and wrought processing is commonly applied for Ni-based alloys like IN718, IN706, Waspaloy and U720Li [21]. To mitigate some of the challenges with obtaining large forgings of segregation-free Ni-based superalloys by forging, machining and welding, the alloy Udimet 720Li has been developed specifically for land based gas turbines [23,37].

Turbine blades and vanes are exposed to elevated temperatures, rotational and gas bending stress and thermo-mechanical loading cycles during start-up and shut down. The gas temperature at the turbine entry can exceed 1350 °C. The elevated temperatures and stress may lead to creep, requiring alloys with excellent creep strength, tensile strength and toughness. In the colder end of the turbine (<

800 °C), bare Ni-based superalloys can be used, while air cooling and thermal barrier coatings are used in the hotter end to avoid severe corrosion and erosion (see Section 2.4).
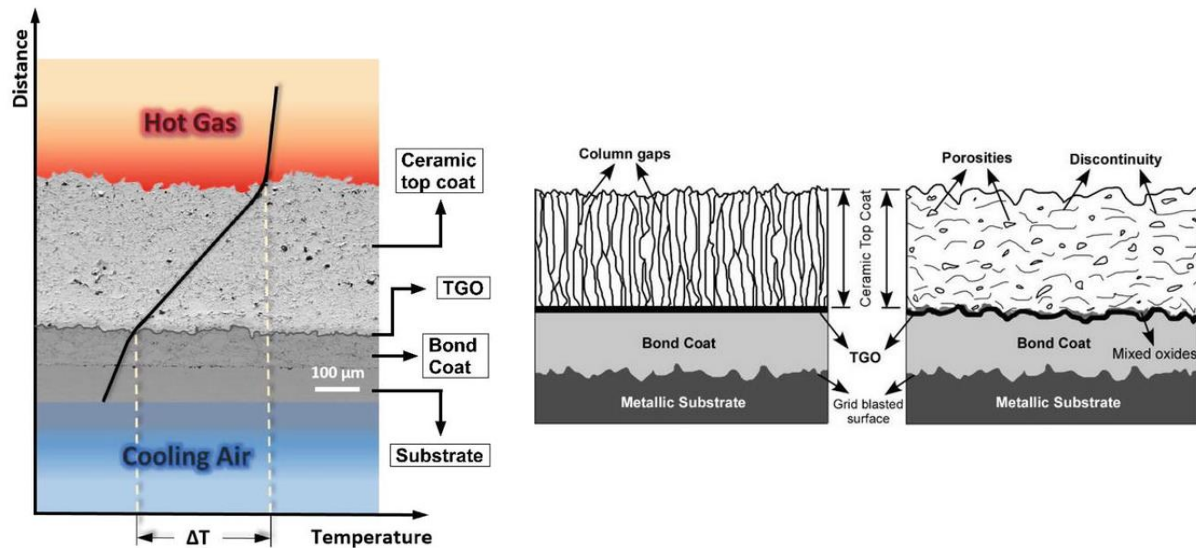
The alloys and processing methods for this application have evolved from conventionally cast Ni-base superalloys, to directionally solidified alloys, followed by the single crystal technology development. The single crystal alloys are categorised into generations based on the Re and Ru content. Re-free (CMSX-7) and low Re (CMSX-8) content alloys have been developed as 6th generation of single crystal alloys, but 2nd generation alloys, such as CMSX-4, René N5 and PWA 1484 with 3% Re are still commonly used [25]. The alloy development has enabled an increased temperature tolerance, from around 800 °C for the first generation of polycrystalline superalloys up to ca. 1100 °C for the newest single-crystal superalloys. In parallel, the creep strength has been improved by higher levels of alloying (Al, Ti, Ta, Re, W, Ru) to increase the content of the γ' strengthening phase [38]. Higher levels of alloying by addition of refractory elements such as Mo, W, Re and Ru also increase the thermal stability [39]. However, while this approach provides an excellent creep resistance, it reduces the corrosion resistance, thereby putting stronger requirements on the thermal barrier coatings [20,21,23,24]. Like the combustion parts, the components in the turbine expansion stage will be exposed to higher temperature and a greater steam content with the switch from natural gas to hydrogen fuelling. The impact this may have on the durability of these components is discussed in Section 3.

Material development for turbine blades and vanes is lately directed towards additive manufacturing (AM), which is a cost-effective processing route for superalloys. This manufacturing approach necessitates the development of new alloy compositions, optimised for the rapid and repeated thermal cycles specific to 3D printing and for reducing the influence of metallurgical defects such as porosity and cracking [39–42]. Section 5 is focused on additive manufacturing and its applicability to hydrogen gas turbines and material aspects, such as corrosion resistance, hydrogen embrittlement and dynamic embrittlement due to the particularities of AM parts.

2.4   Thermal barrier coating systems

Thermal barrier coatings (TBC), together with improved cooling technology, enable the operating temperature of gas turbines to be increased beyond the melting temperature of the structural alloy, with significant gains in the gas turbine efficiency. The TBC system comprises a ceramic top coat, a thermally grown oxide layer and a metallic bond coat, as illustrated in Figure 4. The ceramic top coat is based on low thermal conductivity materials and is usually quite thick (> 500 μm) to maximize the thermal resistance. The most common commercially used TBC material is ZrO_2 stabilized with 7 wt.% Y_2O_3 (7YSZ) [43]. This composition has a high melting point of 2700 °C and a low thermal conductivity of 2.3-4.2 W/mK (for a dense, sintered sample [44]). The thermal conductivity can be further reduced to 0.8-1.3 W/mK by tailoring the microstructure and porosity [45,46].

The metastable, non-transformable tetragonal phase (t') of YSZ is the desired state as this has a high bend strength, fracture toughness, and thermal shock resistance. When aged at temperatures above ca. 1200 °C, the t' phase undergoes a phase transformation into the cubic (c) and equilibrium, transformable tetragonal (t) phases [47,48]. Upon cooling, the t phase is transformed to a monoclinic phase, which is associated with a volume change that causes high stresses and thereby risk of coating spallation. Much of the development work on improving YSZ has focused on increasing the stability of the non-transformable tetragonal phase at higher temperatures by adding alternative stabilizers such as CeO_2, Sc_2O_3 and TiO_2 [49,50].

Figure 4 (a) Thermal barrier coating system (TBC); (b) Schematic general structures of TBC produced by (b) EB-PVD method, (c) APS method. Reprinted with permission from [51].

The TBC ceramic top coat is commercially fabricated using atmospheric plasma spraying (APS) or electron-beam physical vapor deposition (EB-PVD) while alternative deposition methods such as suspension plasma spraying (SPS) or plasma-spray physical vapor deposition (PS-PVD) are under development [50]. The different deposition techniques result in different coating microstructures (Figure 4), which can have a significant effect on the coating properties such as fracture toughness and thermal conductivity. Coatings fabricated by APS have horizontal splats that result in a lower thermal conductivity compared to the columnar structure formed by EB-PVD. On the other hand, coatings produced by EB-PVD have a higher strain tolerance and a smoother surface, providing better aerodynamics [52]. APS is cheaper and better suited for coating large components – it is therefore the preferred method for coating parts for large-scale land-based turbine parts while EB-PVD is usually reserved for the more demanding components, *e.g.* the leading edge of an air foil [19].

The adhesion between the sprayed YSZ layer and the alloy substrate is typically weak and the YSZ layer does not provide much protection against oxidation as the coating is porous and YSZ is a good oxide ion conductor. A bond coat, having high affinity for both the ceramic YSZ layer and the metallic substrate is therefore applied to improve the adhesion and oxidation resistance. The bond coat used with Ni-based superalloys is usually a thin metallic layer (*e.g.* NiAl) that forms an aluminide by interdiffusion with the alloy, or an overlay type coating based on NiCrAlY [53]. For both systems, Al is an essential component that forms a thermally grown oxide (TGO) of alpha-alumina during operation. The TGO is slow-growing and thereby protects the underlying alloy against high temperature oxidation. The YSZ top coat, the bond coat and TGO are commonly referred to as the TBC system (Figure 4).

The main challenges with current TBC systems are failure due to cracking, spallation or growth of undesired oxides between the top coat and the bond coat [54]. In the temperature range of RT-900 °C, the thermal expansion coefficient (TEC) of Ni-based superalloys ($14\text{-}16\times10^{-6}$ K^{-1} [55]) is similar to the TEC of NiCrAlY-type bond coats ($13\text{-}14\times10^{-6}$ K^{-1}[56]), while the TECs of the YSZ top coat (10×10^{-6} K^{-1} [57]) and the alpha-alumina TGO (9.6×10^{-6} K^{-1} [58]) are much lower. The mismatch in TEC between the alloy and different layers of the coating can lead to cracking and spallation during thermal cycling [54]. Martena et al. [59] used a finite element method to analyse the stress distribution in a TBC system due to growth of the TGO and thermal expansion misfits and showed that delamination of the TBC could be attributed to stresses normal to the top coat/TGO interface, which grew with increasing TGO

9

thickness. Even with relatively thin TGO layers, a tensile stress nearly equal to the tensile strength was imposed on the TGO during cooling and subsequent heating to the maximum peak temperature. One approach to reduce the stress due to thermal expansion mismatch is to intentionally introduce cracks and/or pores in the coating that can aid stopping a crack from propagating [50]. Ensuring a high roughness of the bond coat/top coat interface is another way to improve the top-coat adherence and the thermal fatigue resistance of the TBC [60]. The proposed explanation for this is that the compressive out-of-plane stress in the concave regions of the interface hinder crack propagation [61].

The temperature gradient across a coated and air-cooled gas turbine component can be as much as 200-300 °C. As mentioned in the introduction, a higher water vapour content resulting from fuelling with hydrogen will increase the heat transfer coefficient of the gas. If this is compensated by increasing the mass flow rate of the blade air cooling, the thermal gradient across the TBC will become even higher. The increased temperature gradient may accelerate some modes of cracking and degradation of the coating [96]. Dong et al. [62] showed experimentally and by modelling that an increasing temperature gradient decreases the cyclic lifetime of TBCs following a power function. These challenges necessitate the development of new TBCs with even lower thermal conductivity and/or higher fracture toughness, and alloys that retain the desired mechanical properties at a higher temperature.

Among the materials that have been researched as alternatives to replace the YSZ top coat are hexa-aluminates (*e.g.* $LaMgAl_{11}O_{19}$ [63]), perovskite oxides (*e.g.* doped $SrZrO_3$ [64]), Yttrium aluminium garnets (YAG)[65], and pyrochlores (*e.g.* $Gd_2Zr_2O_7$ [50,66]). The pyrochlores are considered to be one of the most promising candidates because of their high melting point, low thermal conductivity and greater resistance against calcium magnesium aluminosilicate (CMAS) attack compared to YSZ (see Section 4.1) [50]. However, the poor chemical compatibility between pyrochlores and the alumina TGO layer requires the use of YSZ as an intermediate diffusion-barrier layer [27], as illustrated in Figure 5. Alternative bond coats under consideration are Al_2O_3 forming MAX phases such as Cr_2AlC [108] and Ti_2AlC [109]. The MAX phases are polycrystalline nanolaminates of ternary carbides and nitrides, named from their general formula of $M_{n+1}AX_n$ (where M is a transition metal, A is an A group (mostly IIIA and IVA) element, X is C and/or N, and n = 1 to 3).These compounds are very oxidation resistant at temperatures up to 1300 °C, however, they are susceptible to volatilization in high pressure and high gas velocity environments [109], making them perhaps less suitable for the conditions of a hydrogen fuelled gas turbine.

Marra [37] reported on the development of various gas turbine coatings and alloys and their performance in natural gas and syngas with high hydrogen content, in a high heat flux rig. Bond coats derived from the state of the art (SoA) Siemens bond coat (Sicoat® 2464) with addition of 1.5wt.% of Nd, Ce and Hf and with increased roughness for improving the TBC adhesion were investigated. The Hf and Ce containing bond coats demonstrated increased oxidation and poor oxide scale adhesion of the TBC during isothermal furnace cycling at 1010, 1080 and 1121 °C in air. The Nd containing bond coat showed 30% longer life when compared to the baseline Re containing bond coat and improved the adhesion of the TBC but demonstrated poor strain-to-crack mechanical properties. Other bond coats based on MCrAlY, *i.e.* NiCrAlY (NI-1154) and NiCoCrAlY (Ni-1155) demonstrated superior oxidation resistance and similar or better mechanical properties. The NiCrAlY based bond coat enabled 100 °C increase in operating temperature compared to the baseline composition, evaluated based on the time before depletion of the alumina-rich phase.
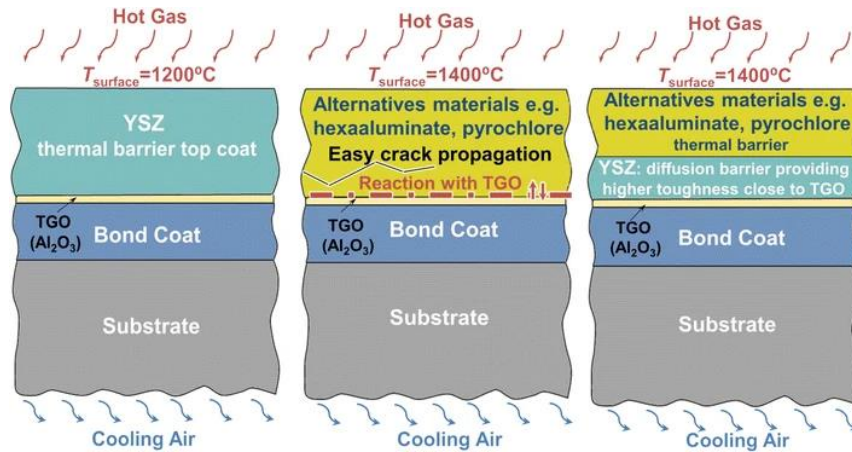
Figure 5 Double layer structure for TBCs working at higher temperatures, after [67].

The lifetime of the TBC system can in some cases be limited by the bond coat, either because of growth of the protective TGO layer beyond a critical thickness for spallation, or because of Al depletion from the bond coat below the level necessary to sustain the TGO formation [68]. Such depletion will allow other, less protective and faster-growing oxides of Cr and Ni to form. A sufficient reservoir of Al in the bond coat is thus essential for a long component lifetime. Evans and Taylor [69] introduced the concept of *diffusion cells* to explain the bond coat failure in plasma sprayed TBC systems. The diffusion cells were described as internal planes of alumina within the bond coat that are formed at splat boundaries within the bond coat due to faster oxidation in this relatively porous region. The diffusion cells block the supply of Al across the coating, thereby causing enhanced depletion of aluminium.

2.5 Environmental barrier coatings

Hot-section components made out of SiC-based CMC require a different coating system than the Ni-based superalloy as the coating in this case needs to prevent volatilization of Si-containing compounds (see Section 3.1.4). The coating systems applied onto CMC are typically dubbed environmental barrier coatings (EBC). The selection of materials is limited by the requirements of a close TEC match to SiC (3-5×10^{-6} K^{-1} in the temperature range RT– 1000 °C [70]). The most promising EBC candidates are celsian-phase silicates such as (Ba,Sr)O-SiO_2-Al_2O_3 (BSAS) and rare-earth (RE) mono- or disilicates (RE_2SiO_4 and $RE_2Si_2O_4$), which sometimes are combined with a Si bond coat layer to ensure better adherence to and compatibility with the SiC substrate (Figure 6) [52,71,72]. For the EBC system, SiO_2 is formed as the TGO instead of Al_2O_3.

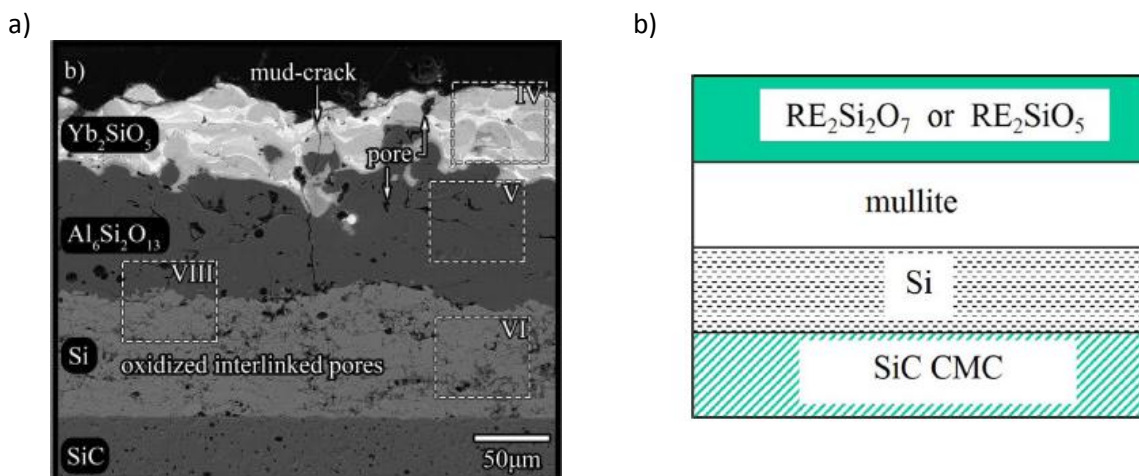a)   b)

Figure 6 a) EBC system fabricated by plasma spraying, after 20 h anneal at 1300 °C, from [73]. b) schematic of the EBC system, from [72]. Reprinted with permission from Elsevier.

11

Increasing the operating temperature of turbines with CMC components requires the addition of a low thermal conductivity TBC on top of the EBC. The current solution is to use conventional TBCs such as zirconate or hafnate to provide the extra thermal insulation, but the high TEC of these materials makes the solution sensitive to failure during thermal cycling, especially after long periods of operation when the strain tolerance of the TBC has been reduced due to sintering. Rare-earth pyrosilicate solid-solution ceramics (*e.g.* $Y_xYb_{(2-x)}Si_2O_7$) have been proposed as a promising "single-layer" alternative to replace both the EBC and the TBC [110]. But more work is needed to improve the APS of these coatings in order to achieve the desired microstructure and crystallinity. Further increase of operating temperatures may also require the replacement of the Si bond coat, which has a melting point of 1414 °C.
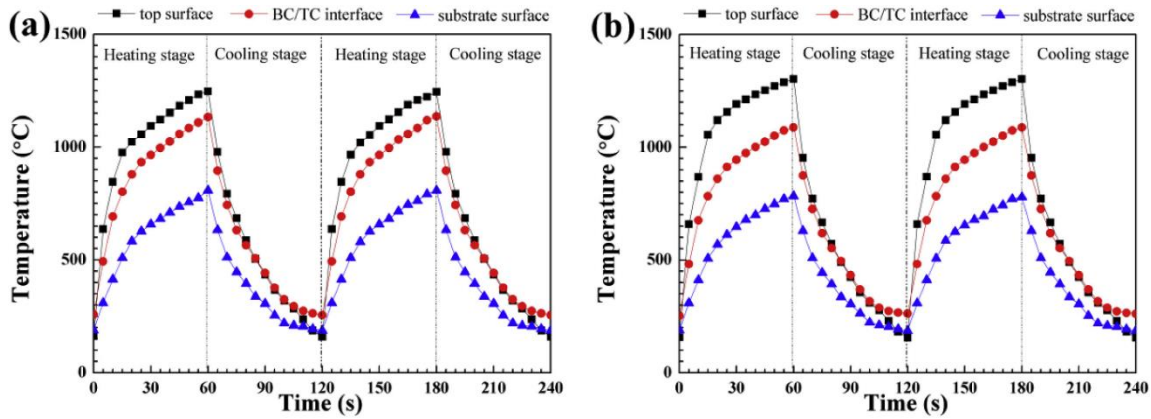
3   High temperature oxidation of gas turbine components

As already mentioned in the introduction, even assuming similar target flame temperatures in the transition from hydrocarbon fuels to hydrogen (in order to conserve cycle efficiency), hydrogen-firing of gas turbines can result in a significantly higher heat flux to the combustor's walls (due to lower quenching distance), in a higher flow velocity (to mitigate flashback), and in a higher steam content. The following sections will focus on how these changes to the operating conditions influence oxidation and other degradation mechanisms of the gas turbine components. The influence of additive manufacturing on the corrosion resistance and dynamic embrittlement of components for hydrogen gas turbine is discussed in Section 5.2.

The working conditions of a gas turbine are difficult to replicate in a laboratory setting; both in terms of the high temperatures, gas velocities and steam content, and in terms of the thermal gradient across a component resulting from the cooling applied on one side. There are only a few laboratories that have the capability of accurately replicating such conditions ex-situ, and different set-ups have been constructed to simulate as accurately as possible the gas turbine conditions. For example, some researchers have employed capillary tubes to impinge H_2O jets on the surface of a sample, achieving gas velocities up to 300 m/s [74,75]. However, most studies concerning the oxidation resistance of Ni-based superalloys and thermal barrier coatings employ even more simplified set-ups with modest gas velocities and no thermal gradients. It is important to interpret these results with care, as the "milder" conditions during an ex-situ test may give a false picture of how the components will perform during actual operation in a gas turbine.

One potential pitfall is to neglect the difference in gas velocity and how this influences the evaporation rate of volatile oxides. For example, Mumm et al. [76] pointed out that a volatilization-redeposition mechanism observed in a lab test utilizing modest gas flow rates of 40 ml/min is less likely to be present in an actual gas turbine where the much higher gas flow rate likely will carry away the volatilized species (preventing redeposition). Furthermore, the volatilization observed when studying the alloy, bond coat or TGO isolated may not be transferable to the volatilization from this component in an actual system where these components are overlayed by a YSZ top coat. The volatilization of elements from gas turbine materials will be discussed further in Section 3.1.

Another important difference between component tests and real operation in a gas turbine is the thermal gradient across a gas turbine component resulting from the internal air cooling. As illustrated in Figure 7 for aeroturbines, the temperature difference between the surface of the substrate and the top surface of the coating can be as much as 450 °C. This gradient results in a higher stress level and a different stress distribution in the gas turbine compared to an ex-situ test under isothermal conditions [77]. Thus, a component that survives several ex-situ thermal cycles without spallation may potentially fail when extra stress is imposed on it by the thermal gradient. The geometry of the component is also
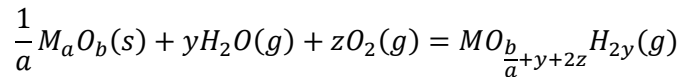
an important factor when evaluating the stresses experienced by the gas turbine blade, as pointed out in refs [78,79]. Even the more sophisticated set-ups such as the above mentioned capillary tube has potential pitfalls, *e.g.* the very small area of the sample that is corroded relative to the large inhomogeneities in the microstructure of a TBC. Nevertheless, the simplified studies are important to increase the fundamental understanding of the oxidation process and how this is influenced by singular factors such as the temperature, gas velocity and gas composition.

Figure 7 Temperature gradient profiles of the TBC layer: top surface (black), interface bond coat – top coat (red) and at the substrate surface (blue) for a) 100 µm and b) 200 µm TBC layer, Reprinted from [77] with permission from Elsevier.

3.1   Effect of increased steam content

It is well established that the presence of water vapor can increase the oxidation rate of alloys and the volatilization of many oxides [80,81]. The mechanism for the influence on the oxidation rate depends on the alloy, while the increased evaporation rate is related to the fact that many oxides volatilize in oxidizing and humid conditions according to the following reaction:

$$\frac{1}{a} M_a O_b(s) + y H_2 O(g) + z O_2(g) = M O_{\frac{b}{a}+y+2z} H_{2y}(g)$$

The following sections will discuss the role of steam in the oxidation and volatilization of various materials used in gas turbines.

3.1.1   Chromia-forming alloys

Many Fe-based alloys that under dry conditions form a slow-growing chromia scale exhibit rapid break-away oxidation when water vapor is present. This has been linked to the volatilization of the Cr_2O_3 scale by the formation of $CrO_2(OH)_2$, for which the rate of volatilization increases with increasing pH_2O and increasing gas velocity [82,83]. Break-away oxidation can take place either because the volatilization of the Cr_2O_3 proceeds faster than the re-growth by oxidation, or because of the alloy with time becomes depleted of Cr below the limit required to sustain re-growth of the chromia scale [83–85]. In extreme cases of a thin component and conditions promoting high evaporation rates, the Cr vaporization may lead to void formation within the alloy bulk, which severely degrades the mechanical properties of the component [85].

Since the volatilization of Cr_2O_3 requires oxygen to be present (cf. reaction above) it is usually insignificant in wet H_2-containing atmospheres. However, water vapor has been shown to influence the oxidation rate of chromia-forming Fe-based alloys under these conditions. For example, Hooshyar et al. [86] reported that the stainless steel 304L forms a duplex scale of inward-growing $(Fe,Cr)_3O_4$ and outward-growing Fe_3O_4 in a range of Ar-H_2-H_2O mixtures at 600 °C, whereas a thin Cr_2O_3 scale is formed

in 5%O_2-N_2. The rate of oxidation increased with increasing pH_2O, also when the activity of O_2 was kept constant. Based on oxidation studies of pure chromium, Henry et al. [87] proposed that an increased oxidation rate in steam is because of the faster diffusion of the smaller hydroxide ion compared to the oxygen ion, while Hultquist et al. attributed it to the uptake of hydrogen leading to faster cation diffusion through the scale [88].
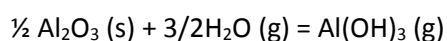
The effect of water vapor on the oxidation of Ni-based chromia forming alloys is more complicated. Some authors report that a wet H_2-containing atmosphere is more corrosive than oxygen [89], while others report slower growth of the oxide scale in wet oxygen/air compared to dry conditions [90]. This apparent discrepancy may be explained by the Cr evaporation kinetics of Ni-based alloys. Sand et al. [91] showed that the Cr vaporization rate from the alloy 690 decreases with time during exposure to humidified air, as the initial chromia-rich scale gradually is replaced by a Ni-rich and Cr-poor scale that mitigates further evaporation of Cr. It should be noted that the time needed to transition from a chromia-rich to a Ni-rich scale greatly varies with the exposure conditions, and that in the meantime the alloy may become depleted with Cr to a point where it has an influence on the mechanical properties [92]. For Ni-based alloys applied at very high temperatures, the volatilization of Ni should be considered. The evaporation rate of Ni from a $NiAl_2O_4$ spinel at 1125 °C and 200 sccm (standard cubic centimetres per minute) is in the range of 10^{-11}-10^{-10} kg/m²s, depending on the pH_2O [76], which is of the same order of magnitude as the evaporation rate of Cr from ferritic stainless steel at 850 °C.

3.1.2 Alumina-forming alloys and bond coats

Water vapor is reported to have an adverse effect on the ability to form protective α-alumina scales on both Ni-based and Fe-based alumina-forming alloys [93]. An oxidation study of Ni-Cr-Al model alloys found that a higher concentration of Al was required to form α-alumina when the alloy was oxidized in air with 30 vol.% H_2O compared to when it was oxidized in dry air [94]. The inability to form a protective α-alumina scale was linked to a change in the scaling morphology – fewer, but larger internal precipitates were formed in humid air compared to in dry air, making it more difficult to form a continuous α-alumina scale by lateral growth. In studies of Fe-based alumina formers, it was suggested that the adverse effect of water vapour is caused by a stabilization of the γ-alumina phase that is normally formed during the transient stage of oxidation [95,96]. In dry conditions, γ-alumina is converted to the slower growing α-phase, but in wet conditions this transition is hindered, likely due to hydroxylation of the γ-alumina surface. This theory is supported by fundamental investigations into the effect of water vapor on the formation and stability of alumina by Sohlberg et al. [97]. The authors described γ-alumina as a "reactive sponge" that can store and release water in the form of hydrogen, which is compensated by the expansion of the alumina spinel lattice and the formation of Al vacancies.

Another observed negative effect of water vapor is decreased scale adhesion, or increased tendency for scale spallation, particularly during thermal cycling [80,93,98]. Often, the spallation occurs at room temperature after the sample has been exposed to H_2O at higher temperatures. This so-called moisture-induced delayed spallation (MIDS) of alumina-forming alloys has been attributed to hydrogen embrittlement of the alloy-scale interface [99]. MIDS takes place even at ambient levels of humidity in the atmosphere and there are no studies known to us that have investigated whether the mechanism is promoted by higher concentrations of water vapour.

Volatilization of alumina may take place according to the following reaction:

$$\tfrac{1}{2}\,Al_2O_3\,(s) + 3/2H_2O\,(g) = Al(OH)_3\,(g)$$

There are reported observations of Al evaporation at 1100 °C [84], but the vapor pressure of $Al(OH)_3$ is so low below 1300 °C that the vaporization of alumina has been considered as negligible under most

conditions [93]. However, given the strong dependency of the $Al(OH)_3$ vapor pressure on the pH_2O, this reaction may become significant in hydrogen-fuelled gas turbines where both the water vapor content and temperature are higher compared to natural gas fuelled turbines. According to thermodynamics, the vapor pressure of $Al(OH)_3$ in 0.5 atm of water vapor and 0.5 atm of oxygen will increase by more than four orders of magnitude from 1000 to 1400 °C [100].
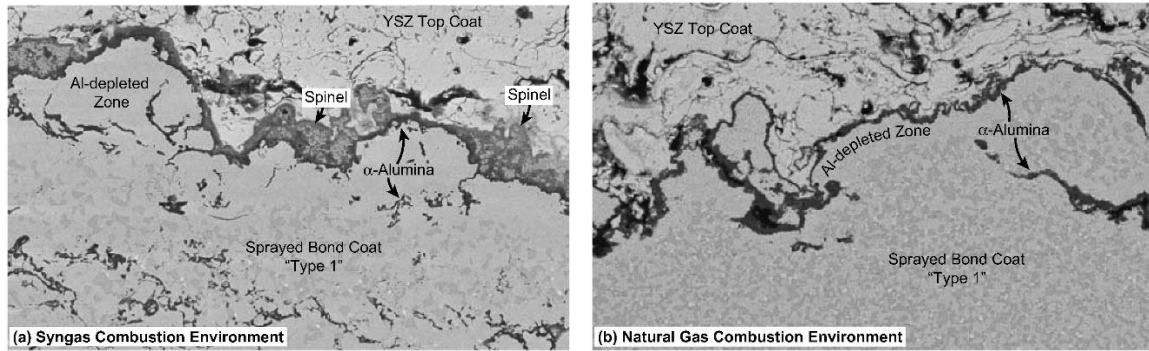
3.1.3   Thermal barrier coatings

Since the components exposed to the highest temperature will be coated with a TBC system, the stability of YSZ and the bond coat material at higher temperature and steam contents should be considered. There have been several studies to determine the durability of TBC and bond coats under various levels of water vapour content:

Sumner et al. [101] tested gas turbine blades in a simulated H_2-rich syngas composition with 20 vol% H_2O over 1000 h. The combustion temperature was up to 1440 °C, but air cooling was used to limit the blade surface temperature to 950-1050 °C. The blades were made of the Ni-based superalloy Rene 80 and coated with either a high velocity oxy fuel (HVOF) metallic coating (Sicoat® 2464, NiCoCrReYAl) or different combinations of a thermal barrier coating (YSZ-based) and a bond coat. After exposure, the TBC surface appeared with a red/brown coloration, suggesting the formation of Fe-rich oxide deposits, deriving from gaseous iron oxides/hydroxides present at higher gas temperatures in the hot gas flow, that condensed below ~1100 –1200°C. The TBC had delaminated at the leading edge of the blade, possibly due to erosion or imperfections in coating manufacturing.

Zhou et al. [102] studied the oxidation kinetics of nickel based superalloys in O_2 and O_2-5%H_2O at 1050 °C. The alloys were coated with a plasma sprayed NiCrAlY (Ni-28Cr-6Al-0.4Y wt.%) bond coat and a 7.5 wt.%Y_2O_3-ZrO_2 TBC. In dry O_2, parabolic oxidation kinetics were followed with a very low oxidation rate and the oxide formed on the bond coat layer was Al_2O_3. In O_2-5%H_2O, the oxidation kinetics were almost linear after long exposure times and the interfacial scale between the bond coat and the TBC was in this case composed of $Ni(Al,Cr)_2O_4$, NiO, Cr_2O_3 and Al_2O_3. An increase in Ni and Cr cation transport in the presence of water vapor was suggested as a possible explanation for the increased degradation rate.

Cernuschi et al. [103] evaluated the sintering kinetics and phase stability of 7YSZ, YSZ-GZO, and YAG coatings prepared by APS after aging as freestanding samples for 500 h in the temperature range of 1000-1250 °C. The authors found no clear evidence that the thermal diffusivity, thermal conductivity or phase composition of the coatings was different when aged in air with 20 vol.% H_2O compared to dry air. The morphology and density of the coatings was concluded as being more important for the thermo-physical properties than the aging environment.

Results from testing MCrAlY bond coats in industrial gas turbines show that fuelling with syngas (CO+H_2) instead of natural gas results in the formation of a thick (30 μm) non-protective spinel-alumina layer between the bond coat and a YSZ top coat instead of a thin (ca. 1 μm) protective α-alumina layer, see Figure 8 [104]. The spinel layer is susceptible to cracking and weakens the TGO/YSZ interface. Sullivan and Mumm [104] attributed the formation of the spinel phase to the higher water vapour content in the combustion gas when fuelling with syngas compared to natural gas. They performed a comprehensive series of tests with different bond coat materials in varying pH_2O and pO_2 environments, focusing on the transient stage (0-5 h) of oxidation. The surface coverage by a $(Ni,Co)(Al,Cr)_2O_4$ spinel was increased with increasing pH_2O up to ca. 15 vol.%, whereafter the coverage plateaued and slightly decreased. Interestingly, spinel formation was promoted at low pO_2 when water vapor was present. Sullivan and Mumm postulated that water vapor elongates the γ and δ alumina stages, which enables the diffusion of spinel forming cations across the normally protective TGO layer.

15

Figure 8 Cross sectional images of a TBC tested in an industrial gas turbine operated with syngas (a) and with natural gas (b). Reprinted from [104] with permission from Elsevier.

From the above results it is clear that water vapor has an adverse effect on the TBC lifetime. Whether the rate of degradation is increased by increasing the water vapor content beyond 10-20 vol.% is however less clear, as will be seen from the following summary of literature.

Haynes et al. [100] investigated the effect of water vapor on the oxidation behaviour of a TBC system comprising an APS YSZ top coat and a HVOF-deposited NiCoCrAlY bond coat deposited on a single crystal Ni-based superalloy. The average TBC lifetime (defined by onset of spallation) during thermal cycling was reduced by at least 20% in air with 10 vol.% H_2O compared to when cycling in dry O_2. Increasing the water vapor content to 50 vol.% did not lead to any further decrease in the lifetime compared to 10 vol.%.
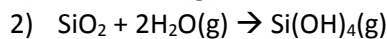
Pint et al. [105,106] reported that the lifetime of Pt diffusion coatings ($\gamma+\gamma'$ bond coats) was hardly affected by water vapor, while the lifetime of a Pt β-aluminide coating (β coating) was almost halfed in 10 % water vapor. This effect may be asociated with the orientation of the β aluminide, leading to formation of non-uniform, epitaxially oriented, cubic metastable alumina scales before the nucleation of an α-Al_2O_3 phase. Interestingly, the lifetime was seemingly less affected when the steam content increased further to 50 and 90 %. For both types of coatings, a thicker TGO layer was formed in humid conditions than in dry. Pint et al. [82] also evaluated the lifetime of NiCoCrAlYHfSi-coated X4 and 1483 substrates with an APS YSZ top coat in dry and humidified O_2 and air at 1100 °C. The lifetime, defined as the number of 1 h cycles before spallation of the YSZ top coat, decreased with the addition of water vapor. A shorter lifetime was obtained for the 1483 substrate compared to X4, which was attributed to the lower Al content in the former. Also in this case there was no increase in the adverse effect with increasing water vapor content.

Lance et al. [98] studied thermal cycling of the single-crystal nickel-based superalloy PWA 1483 and X4 with HVOF processed NiCoCrAlYHfSi bond coatings and an air plasma sprayed YSZ top coat. Alloy 1483 does not contain Re like many other single crystal superalloys, and is therefore less expensive, while alloy X4 is a second-generation alloy containing 3% Re. The oxidation and cycling resistance were studied in dry air, and air with 10 or 50 vol% H_2O at 1100 °C with cycles of either 1 h (simulating air jet) or 100 h (simulating land-based turbine). With 1 h cycles, the increased water content was reported to decrease the lifetime of the components, while for the 100 h cycles the behaviour was inconsistent with the pH_2O. Degradation during 1 h cycles was attributed to stresses in the YSZ top coat while the degradation during 100 h cycles was more dominated by diffusion processes. Samples based on X4 had an overall longer (30-40%) lifetime than samples based on 1483, which was attributed to the higher Al content and possibly the higher Ti content in the former.

Nowak [107] studied the oxidation behaviour of polycrystalline super-alloy Rene 80 at temperatures up to 1120 °C in Ar-O_2 and air with various water vapor contents up to 20 vol.%. No major effects of H_2O were observed with a MCrAlY coating and with slow heating rates (10 K/min), while for higher heating rates (90 K/min), water vapor promoted the formation of meta-stable alumina during initial exposure. With an APS-TBC coating on top, the addition of water vapor shortened the lifetime due to decreased TGO adherence. At temperatures below 400 °C, water vapor enhanced the transformation from tetragonal to monoclinic zirconia, which was suggested to be the cause of the observed increase in degradation. The results suggests that the degradation caused by water vapor is more relevant for gas turbines operated with heavy cycling, such as aeroturbines. This is consistent with the results from Pint, Haynes and others showing that the degradation due to water vapor is more pronounced with shorter thermal cycles. For stationary, more continuous operations, this degradation mechanism should be less relevant.

3.1.4 CMCs and EBCs

CMC are prone to Si volatilization when exposed to steam containing atmospheres. The loss of SiC proceeds by forming SiO_2 as an intermediate. The predominant reactions are:

1) $SiC + 3H_2O(g) \rightarrow SiO_2 + 2H_2(g) + CO(g)$
2) $SiO_2 + 2H_2O(g) \rightarrow Si(OH)_4(g)$

As suggested by the above reactions, the volatility of SiO_2 increases strongly with increasing partial pressure of water vapour ($\propto p_{H_2O}^2$) [108]. The loss of SiC is rapid, causing materials recession at order of 6-9 μm/h in high velocity steam jet [109]. The evaporation reaction has a weak temperature dependence, making evaporation of SiO_2 a challenge also at modest gas turbine operating temperatures [108]. For this reason, the SiC CMC applied in gas turbines are combined with environmental barrier coatings, as described in Section 2.5. Volatilization is not completely avoided as these coating materials also comprise Si, but it is greatly reduced compared to a non-coated SiC/SiO_2 surface. The evaporation rate from the coated material is proportional to the surface activity of Si, and for this reason RE_2SiO_4 is preferred over $RE_2Si_2O_4$, despite the latter having a better TEC match with the substrate [109,110].

4 Other types of degradation

4.1 Hot corrosion and CMAS attack

When low purity fuels containing sulphur and/or alkali metal contaminants are used, the hot gas components of the gas turbine are susceptible to a degradation form known as hot corrosion. This can for example be the formation of alkali sulphates (sulphidation) that degrade the TBC coating [50]. Due to the lower calorific value per mole of hydrogen compared to natural gas, the fuel/air ratio will be greater in a H_2 fuelled gas turbine. This implies that hot corrosion may become a challenge at lower levels of fuel impurities [20]. Hydrogen produced by electrolysis has typically a very high purity and is therefore less likely to cause hot corrosion, while by-product hydrogen may contain critical amounts of sulphur and other impurities.

Another "external" source of degradation is impurities such as sand, ash and dust in the combustion air, which can lead to so-called calcium-magnesium-alumino-silicate (CMAS) attack [111]. The CMAS deposits have an unfavourable microstructure and high TEC and thereby cause failure of the TBC or EBC. The CMAS degradation mechanism involves a number of thermally activated processes, making this degradation more critical for turbines operating at higher temperatures. On the other hand, as hydrogen turbines are operated with a relatively lower flow rate of air, impurities in the air are potentially less critical for hydrogen fuelled gas turbines compared to natural gas turbines.
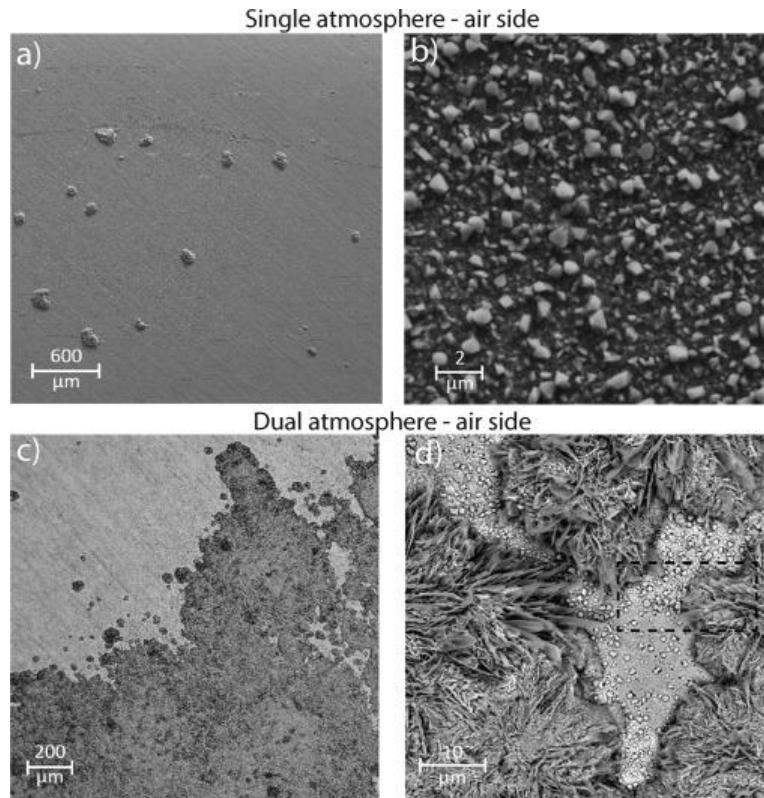
4.2   Dual atmosphere effect

High temperature corrosion of steel is typically studied in a single atmosphere replicating the service conditions. However, in some applications, the steel is simultaneously exposed to different atmospheres on each side of the specimen. An example is the gas turbine fuel injector, where the inner surface of the injector will be exposed to hydrogen, while the outer surface will be exposed to air. Such exposure to dual atmosphere can cause anomalous oxidation behaviour not observed when exposing the same steel specimen separately to the two atmospheres. The so-called dual atmosphere effect has been widely studied in the field of solid oxide fuel cells, where the steel interconnect is exposed to (humidified) hydrogen on one side and air on the other at temperatures between 600 and 900 °C [112–116]. In all cases, the anomalous oxidation behaviour is on the air side where formation of Fe-oxides is observed in dual atmosphere conditions on ferritic stainless steels that normally form stable Cr_2O_3 oxides under single air atmosphere conditions, see Figure 9. It has been suggested that steels having a lower Cr content are more susceptible to the dual atmosphere effect [112,116] and that the effect becomes more pronounced with decreasing temperature from 900 °C to 600 °C [115,117].

Several mechanisms have been proposed to explain the dual atmosphere effect. Hydrogen at the fuel side is believed to adsorb into the ferritic stainless steel (FSS) and migrate towards the air side. The presence of hydrogen defects is suggested to alter the defect structure near the alloy surface by the formation of metal vacancies, V_M''' [114,118]:
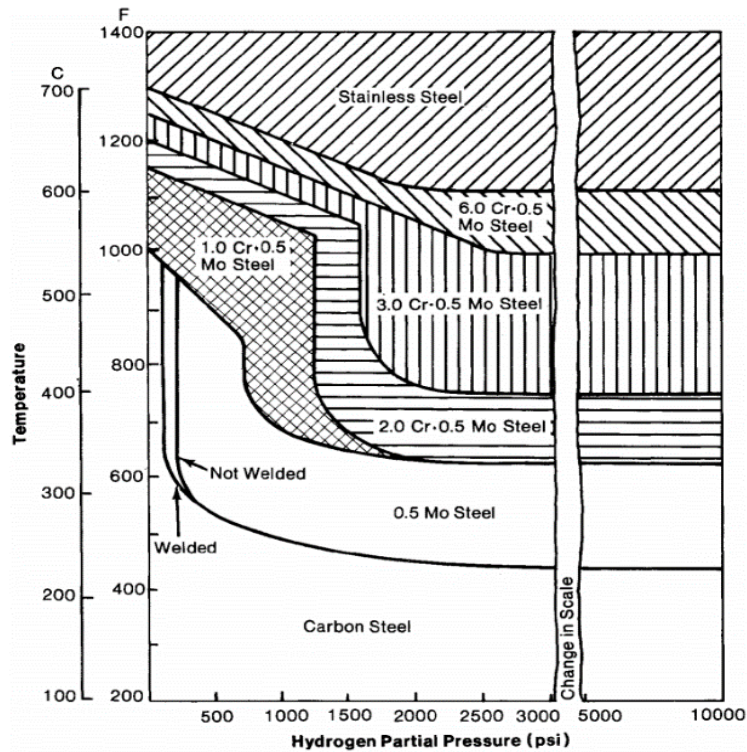
$$3[V_M'''] = p + [(OH)_O^{\cdot}]$$

where the hydrogen defects have been written in the form of OH-complexes on oxygen sites, p is the concentration of electron holes, and the metal is assumed to be 3-valent. The increased concentration of metal vacancies is expected to increase the diffusion of cations through the scale, thus increasing the likelihood of forming Fe-rich oxides on the surface [12]. This could explain why the Fe-rich nodules sometimes are reported to form along the grain boundaries of the alloy, seeing as these are typical high-diffusivity paths [119]. Another proposed explanation is that the presence of hydrogen depresses the p_{O_2} locally, thus promoting the formation of isolated Fe-rich nodules [120]. The presence of hydrogen could also lead to the formation of steam, resulting in porosity near the surface of the alloy [114,116]. The pores enhance inward oxygen transport, which typically leads to a faster oxidation rate and could even result in localized metal loss, which sometimes is observed in connection with the Fe-rich oxide nodules. Finally, it has also been suggested that the Fe-rich nodules are formed due to the surface on the air side having been made more acidic by the presence of hydrogen [121,122]. The higher acidity is believed to favour the formation of Fe_2O_3 relative to Cr_2O_3.

Figure 9 Surface SEM images of samples tested under single (air) or dual (air + H_2) atmosphere exposure, showing Cr_2O_3 oxide formation in air only and Fe-oxide formation under dual atmosphere conditions. Reprinted from [115] with permission under Creative Commons CC BY-NC-ND.

4.3   H-diffusion in alloys relevant for gas turbine application

Hydrogen embrittlement causes the loss of ductility, deterioration of material strength and mechanical properties of upon exposure to hydrogen. Hydrogen attack may occur by atomic hydrogen diffusing into the steel lattice. Inside the steel, the atomic hydrogen may accumulate at stress concentration regions such as vacancies, grain boundaries and other lattice defects and form molecular hydrogen resulting in a pressure built-up. The pressure may lead to voids and/or degradation of the ductility to a degree where the steel becomes brittle and cracks. Hydrogen may also react with dissolved carbon or oxygen in the steel to form methane or steam, respectively. In general, an increasing Cr-content in austenitic steels increases the maximum temperature and hydrogen partial pressure tolerated by the steel (Figure 10) [123,124].

Figure 10 Maximum temperature and hydrogen partial pressure for safe operation of steels in hydrogen service, reproduced from [124].
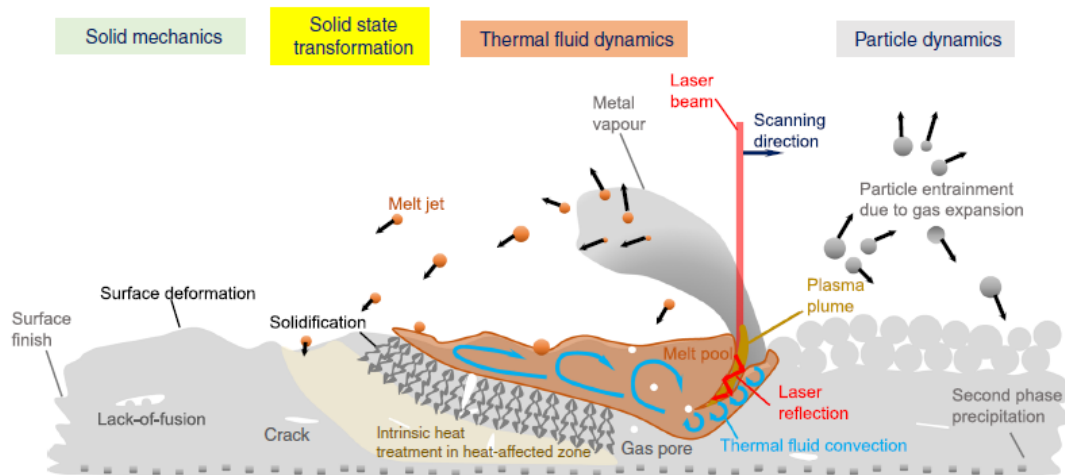
Ni based alloys are susceptible to hydrogen attack in a large temperature interval from -103 to 327 °C and Ti based alloys are susceptible to attach in the range of 0 to 93 °C [125]. An early work by Gray [126] reports on the embrittlement of several Ni-based superalloys such as Inconel 718, Udimet 700, Rene 41, Hastelloy X, and TD-NiCr after exposure to 0.1MPa gaseous hydrogen from 430 to 980 °C for 1000 h. All of the tested alloys absorbed substantial concentrations of hydrogen during the exposure, which was suggested to be interstitially dissolved and diffusible. The hydrogen could be removed and the ductility of the alloy regained by degassing at elevated temperatures. In more recent work, Balyts'kyi et al. [127] has studied the hydrogen embrittlement of gas turbine blade single crystal cast alloys such as SM-104-VI, SM-90-VI and SM-88U-VI at 30 MPa hydrogen pressure, at temperatures between 20 and 900 °C. The negative effect of hydrogen decreased with increasing temperature, but the authors reported a measurable decrease in strength and plasticity of the alloys even at 900 °C. The alloy SM-90-VI was reported as the least sensitive to hydrogen embrittlement. Hydrogen embrittlement of AM parts is discussed in Section 5.3.

5   Additive manufacturing

5.1   Additive manufacturing of materials relevant for gas turbine parts

Additive manufacturing is suitable for fabrication of gas turbine parts (blades, vanes, fuel injectors, impellers, swirlers, burners, combustion chambers, cladding, seals, housings) [128] and for the production of functionally integrated parts [129]. The technique can be used both for building new parts and for repairing damaged parts at worn areas, directly on the original parts [130]. Additive manufacturing is also used to address the challenges of fuelling gas turbines with hydrogen by the development of novel combustion technology with complex cooling profiles and fuel routing paths [131]. AM or 3D printing allows for the burner design to be adjusted on the inside without changing the exterior, which makes it easier to retrofit existing turbines to enable hydrogen operation. The method is currently limited by the available printing size [132].
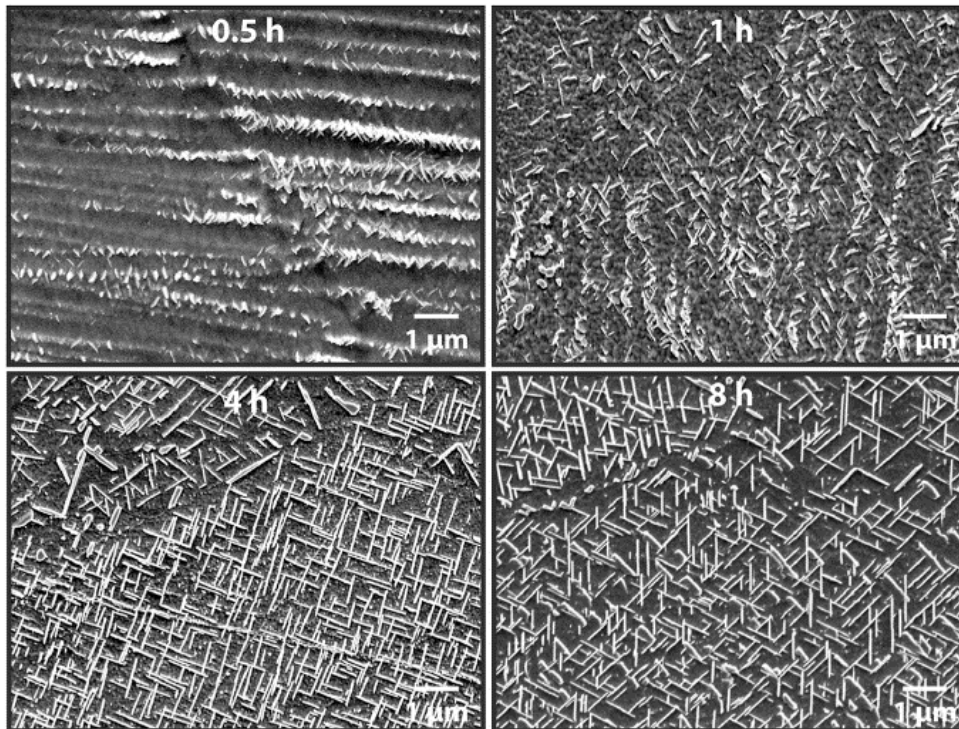
20

Nickel based superalloys are of particular interest for producing gas turbine parts by AM because of their excellent properties at elevated temperatures. However, the microstructure and grain structure are strongly influenced by the directional building, fast cooling and complex thermal cycles (reheating). The production of complex parts by additive manufacturing results in a non-equilibrium state of the processed material. An illustration of the physical phenomena describing the AM fabrication of metals by powder bed fusion is shown in Figure 11 [39]. The interaction of the laser with the metal powder generates the coexistence and interaction of solid, liquid, gas vapour and plasma. The rapid heating and cooling thermal cycles generate thermal gradients and determine the metastable nature of the chemical, structural and mechanical state of the system. Modelling of the physical phenomena is scarce, yet necessary to address the complexity of the system.

Figure 11 Physical effects that describe the AM of metals powders via the powder bed fusion (or SLM) fabrication method, Reprinted from [39] with permission under Creative Commons CC BY license.

Nickel-based superalloys rely on precipitation hardening and/or solid-solution-hardening while the precipitation of the γ' phase occurs upon cooling and is dependent on the cooling rate [30,133]. Ni-based superalloys like IN939, IN718, IN625 and Hastelloy X are commercially available for AM and have been studied to facilitate the understanding of processing, microstructure and properties. Fu et al. [131] described the microstructure resulting from selective laser melting (SLM) processing as characterised by fine, elongated grains that can recrystallize during heat treatment to form equiaxed and isotropic structures. In case recrystallization does not occur, the material remains anisotropic. Deng [133] studied microstructures and mechanical properties of electron beam melting (EBM) and SLM processed IN718. It was found that the EBM microstructure is characterized by columnar grains, elongated in the building direction while SLM resulted in a fine, dendritic microstructure. The as-built EBM microstructure was location-dependent with an irregular frame part having a weak texture. The strengthening phases γ'/γ'' precipitated during the AM processing and intermetallic phases with the AB_2 (laves phases) composition were observed. The mechanical properties of the fabricated samples were anisotropic, with higher tensile strength and lower elongation along the building direction. The strength was somewhat increased by heat treatment. The as-built SLM microstructure showed a weak texture, with fine laves phase in the interdendrites and no precipitation of the γ'/γ'' strengthening phases. The tensile properties and elongation showed anisotropy depending on the building direction. Homogenisation heat treatments demonstrated positive results in the segregation of the γ'/γ'' strengthening phases and for decreasing the anisotropy.

Zhang et al. [134] reported the formation of unwanted platelet-shaped δ phase precipitates (orthorhombic Nb and Mo rich phases, with a wide range of local compositions, *e.g.* Ni-20.20Nb-11.00Mo-8.70Nb-0.05C) upon stress relief thermal treatment of AM processed (by laser-sintering powder-bed fusion) Inconel 625 much faster than in wrought materials, in a matter of minutes instead of tens to hundreds of hours, as shown in Figure 12. Elemental segregation in AM materials was identified as the root cause for the δ phase precipitation. A subsequent homogenisation heat treatment was effective in removing the δ phase. It was concluded that alloy specific strategies should be developed to mitigate the effects of AM processing.

Figure 12 Surface micrographs of a 3D printed IN625 showing the formation of δ phase precipitates, initially at interdendritic regions, at 870°C after 0.5, 1, 4 and 8h, Reprinted from [134] with permission from Elsevier.

Shaikh [30] studied the effect of thermal treatments of IN939 Ni-based superalloy parts obtained by laser-powder bed fusion. Other Ni-based superalloys were as well reviewed. The results demonstrated notable differences in the fractions and morphologies of the γ' strengthening phases, in comparison with the conventional materials. The author specified that superalloys processed by laser-powder bed fusion are susceptible to cracking, with solidification cracking as the primary responsible mechanism. It was mentioned that post processing thermal treatments affect grain structure, morphology, distribution, and size of strengthening precipitates. IN939 could be produced free from defects and the thermal treatments applied resulted in excellent room temperature tensile properties.

Andersson et. al. [135] applied this approach for a burner repair in a specifically designed gas turbine via SLM indicating no defects on the surface of the 3D printed part. The porosity and inclusions levels were low in all examined parts with an average porosity of less than 0.09%. The presence of sulphur and some surface oxidation was observed up to 50 μm in the material after testing the 3D printed burner parts. Non-destructive and destructive tests showed that printed burners were in functional condition [135].

22

5.2 Corrosion resistance of steel manufactured by AM

The effect of microstructure of alloys produced by AM on corrosion resistance is discussed by Örnek [136] and Kong et al. [137]. Örnek characterised the microstructural features of additive manufactured metallic parts, such as porosity, structural gradients, chemical inhomogeneities, microstructural heterogeneities, texture, the formation of surface oxides, grain size, strain and stress, surface roughness and their influence on corrosion resistance. The author concludes that controlled microstructure has a significant importance for obtaining reproducible properties and that more systematic development of AM-materials should be made in parallel with corrosion studies to optimise corrosion properties. Kong et al. [137] also reviewed the influence of the internal microstructure, such as porosity, surface roughness, phase segregations, oxides, inclusions, and the corrosion properties. The authors point out the necessity of focusing on the optimisation of fabrication parameters and establishing a correspondence between key structural features and corrosion resistance. Laleh et al. [138] reviewed the corrosion behaviour of austenitic, precipitation-hardened, and duplex stainless steels processed by AM in comparison with the conventionally produced counter parts. The review addressed the corrosion resistance in acidic and NaCl solutions at room temperature. Important aspects that influence the corrosion resistance are the particularities of the AM manufacturing, such as the effects of porosity and defects, compositional differences generated by evaporation of alloying elements due to the high temperature laser, inclusions and interdendritic chemical segregation. The residual stress and non-homogeneous microstructure determine a more complex corrosion behaviour than for the conventionally processed steels.
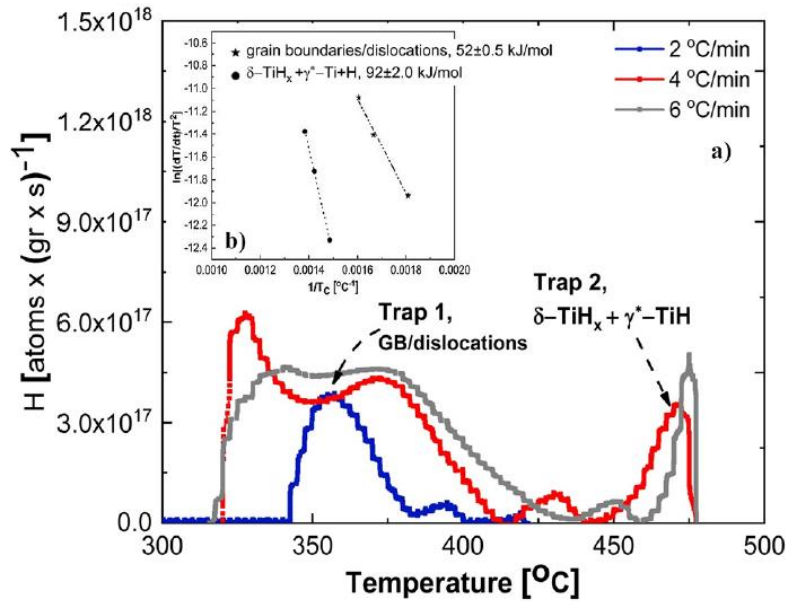
5.3 Hydrogen embrittlement of steel manufactured by AM

The susceptibility to hydrogen attack and other properties of metal parts obtained by additive manufacturing is the cumulated result of several factors like alloy design, microstructure, properties and AM processing conditions, describing the structure – property – processing – performance relationship. Several studies conducted on the hydrogen exposure effects on 3D printed specimens indicate optimised 3D printing manufacturing methods as suitable for producing metallic parts for hydrogen service and hydrogen infrastructure. The published literature in AM of austenitic stainless steels is focused mostly on 316L and 304L [139–143]. However, Seifi et al. [144] and Gorsse et al. [145] report on the technology readiness levels (TRL) in additive manufacturing for Ni-based superalloys (Hastelloy X, Inconel 625 and Inconel 718), Co-Cr alloys (Co28Cr6Mo) and Ti-based alloys (Ti-6Al-4V, Ti-6Al-4V ELI), with TRL 7-9. Other alloys are included such as tool steels (H13 and Maraging 300) with TRL 9, stainless steels (316L and 17–4PH) with TRL 7–8, Al-based alloys with TRL 4–8, Cu-based alloys, intermetallic (titanium aluminide), and low alloy steels (AISI 4140) with TRL 4–5 [146–149].
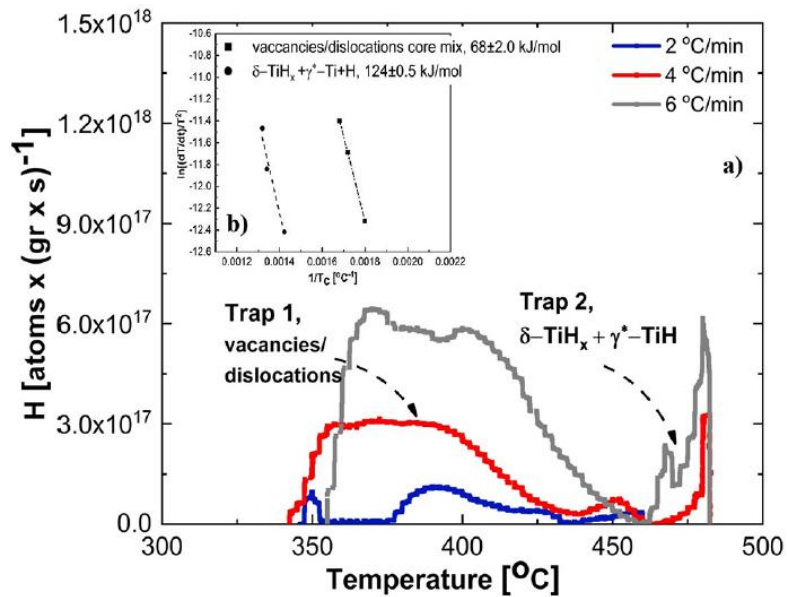
Another type of alloy used for advanced gas turbine engines is Ti-6Al-4V. Silverstein et al. [150] reported on the hydrogen embrittlement, trapping and desorption behaviour in 3D printed-Ti-6Al-4V by SLM method. Titanium alloys have reasonable resistance to chemical attack, but hydrogen attack causes severe problems, such as loss of ductility and decreased material strength. The processing of complex shaped alloy parts by additive manufacturing results in a complex, non-equilibrium state of the material. The hydrogen trapping characteristics were studied to determine the efficiency of hydrogen traps to bind hydrogen and preventing it from reaching cracking sites. Hydrogen embrittlement was studied by exposing samples to hydrogen atmosphere of 0.5 MPa hydrogen pressure at 500 °C for 10 h. Hydrogen evolution and hydrogen trapping interactions were evaluated via thermal desorption spectrometry (TDS), as illustrated in Figure 13. Samples 1 and 2, printed in direction X-Z and X-Y , were compared and it was shown that susceptibility to hydrogen embrittlement is influenced significantly by the printing direction. Sample 1 showed an increased susceptibility to hydrogen embrittlement, due to a higher content of Ti-hydrides and lower trapping energy of TiH compared to sample 2. The hydrogen desorption was considered as diffusion controlled for sample 1

23

and de-trapping controlled desorption for sample 2. The increased resistance to hydrogen embrittlement observed for sample 2 was associated with increased stress of the material in the printing direction [150].

a)

b)

Figure 13 Thermal desorption of hydrogen for: a) sample 1, with inset plot of activation energies for two fitted hydrogen desorption peaks and b) sample 2, with inset plot of the activation energies for two fitted hydrogen desorption peaks. Reprinted from [150] with permission from Elsevier.

Hydrogen embrittlement of AM parts produced for gas turbine applications is reported at low temperatures, from RT and up to 300°C. The 3D printed parts are generally reported with high resistance to hydrogen attack, correlated with the internal microstructure of the specimens [140,151]. Baek et al. [139] evaluated the effect of hydrogen attack for 3D printed metallic parts for 304L at 150°C to be used for manufacturing and repair of specialized parts such as blades and fuel nozzles for gas turbines [139]. The results indicated high resistance to hydrogen attack of the AM parts when compared with rolled plate specimens. Smith et al. [140] studied the effect of hydrogen corrosion on

tensile fracture and fatigue crack growth for 304L printed specimens at 300°C in comparison with wrought steel specimens. AM may induce defects such as microcracks, leading to reduction of ductility in hydrogen environment. The study concluded that 3D printed specimens can exhibit similar tensile and fatigue properties with wrought specimens in air and extreme hydrogen environment when manufacturing defects are avoided or effectively attenuated [140].

5.4 Dynamic embrittlement

The increased steam content in hydrogen fuelled gas turbines may act as an oxygen source to cause dynamic embrittlement of Ni based superalloys at intermediate temperatures. Ni based superalloys show ductility loss and intergranular cracking at intermediate temperatures. The embrittling behaviour is reported between 500 and 900 °C, with maximum of embrittlement around 600 °C [152]. The intergranular cracking of Ni based superalloys, caused by the diffusion of atomic oxygen at the grain boundaries (GB), is known as Oxidation Assisted Intergranular Cracking (OAIC) [153] or dynamic embrittlement [154]. A similar process of time-dependent decohesion at GB may occur under sustained or cyclic loading, determined by interactions with oxygen at the crack tip for Ni based superalloys [155]. Embrittling elements may be present in the alloy or oxygen from surrounding atmosphere may diffuse into the steel lattice and induce cracking along GB in the alloy. Ni based superalloy IN718 was designed for high temperature, but its application is limited to 650 °C due to the embrittlement occurring at higher temperatures [153]. For the Ni based superalloy U720Li no embrittlement was reported below 600 °C, with trans-granular failure observed. At temperatures of 600 to 850 °C, the ductility decreased significantly with quasibrittle intergranular failure, while above 850 °C the tensile ductility was recovered [156].

Chan [155] applied the grain boundary fracture model for Ni based superalloys, like IN718, to predict the onset of dynamic embrittlement and oxidation-induced crack growth and concluded that the model predicts correctly the decrease of tensile ductility of Ni-based superalloys with increasing oxygen content and temperatures. It was also concluded that dynamic embrittlement may occur prior to oxide formation, caused by the oxygen segregated GB, while oxide formation in the crack may have a strengthening effect on the crack-tip. It is mentioned that the heat of oxygen solution in Ni seems to be the activation energy for dynamic embrittlement. Deng et al. [157] studied the dwell-fatigue cracking at 550 °C of IN718 prepared by EBM AM technique, with focus on the anisotropic cracking resistance of the AM processed alloy. It was concluded that the loading parallel to the columnar GB demonstrated better dwell-fatigue cracking resistance than the loading perpendicular to the columnar GB. The AM processed specimens had superior dwell-fatigue cracking resistance in comparison with conventionally processed IN718 specimens both in parallel and perpendicular loaded specimens, resulted from the structure of the GB, grain size, low angle grain boundaries and the formation of the δ precipitate phase at GB.

6 Conclusions

Materials development for gas turbines has been focused on improving the gas turbine efficiency and profitability by increasing the maximum allowable service temperature and the long-term stability. Much of the advancement has been made in the area of thermal and environmental barrier coatings that can be utilized at higher operating temperatures and provide greater protection against oxidation. Alongside this, additive manufacturing is being explored and continuously improved as a promising method for fabricating new and complex combustor designs, intricate air cooling channels and other complex structures. The advancements made in these developments cover to some extent the new requirements arising from utilizing H_2 as fuel. However, this review has found that there are some potential challenges that require more attention.

Among the most critical challenges is the larger temperature gradients that emerge across air-cooled components in hydrogen-fired gas turbines, arising from the smaller flame-wall quenching distance, the potentially higher flame temperature and the larger heat transfer coefficient of the combustion products. This necessitates the development of thermal barrier coatings with even lower thermal conductivities and fracture toughness to withstand thermal stress induced cracking and spallation. Another potential challenge of hydrogen fired gas turbines is the increased steam content in the combustion products, which may have a significant negative effect on the corrosion resistance and lifetime of the barrier coatings and of the underlying metal component. Review of the available literature suggest that especially the combination of water vapor and heavy/fast cycling may be detrimental, meaning it will be more critical for aero applications than for stationary ones. There are few studies available that have investigated the degradation and lifetime as a function of the water vapor content. This is an area that should receive more attention in the development of materials specifically for hydrogen fired gas turbines. Other degradation phenomena such the dual atmosphere effect and hydrogen embrittlement require also more research in the context of gas turbines.

Additive manufacturing has excellent applicability for producing metallic parts with complex designs, for on-site building of new parts, and on-site repair of damaged/worn parts. Current development is focused on controlling the microstructure of the printed parts by optimizing printing parameters such as the laser scanning speed, intensity, layer thickness, etc. in order to melt the metal sufficiently to avoid porosity, while at the same time controlling evaporation of elements and segregation of secondary phases. The structure of the GB, the grain size and low angle grain boundaries is also of high importance. Control of microstructure is currently still a challenge with the conventional Ni-based alloys used in gas turbines, and progress in additive manufacturing may lead to the development of new gas turbine alloy compositions that are more optimised for the rapid and repeated thermal cycles specific to 3D printing. In cases where the printed parts contain pores, inclusions and similar defects, a greater susceptibility to hydrogen embrittlement and a lower high temperature corrosion resistance has been reported. On the other hand, parts fabricated with a more optimized microstructure are reported to be less susceptible to hydrogen embrittlement than conventionally processed parts.

7 Acknowledgements

8 Disclosure statement

No potential conflict of interest was reported by the author(s).

9 ORCID

Elena Stefan, https://orcid.org/0000-0002-8804-0597

Belma Talic, https://orcid.org/0000-0001-8148-6863

Yngve Larring, https://orcid.org/0000-0002-6600-9951

Andrea Gruber, https://orcid.org/0000-0003-2753-9690

Thijs A. Peters, https://orcid.org/0000-0002-1168-3455

10 List of abbreviations

AM   Additive manufacturing
APS   Atmospheric plasma spraying
CCS   Carbon capture and storage
CHP   Combined heat and power
CMAS   Calcium magnesium aluminosilicate
CMC   Ceramic matrix composites
CO_2 Carbon dioxide
DLE   Dry low emission
EB-PVD Electron-beam physical vapor deposition
EBC   Environmental barrier coatings
EBM   Electron beam melting
GB   Grain boundary
HVOF   High velocity oxy fuel
kWh   kilowatt hour
MAX $M_{n+1}AX_n$
NO_x Nitrogen oxide
OAIC   Oxidation assisted intergranular cracking
ODS   oxide-dispersion-strengthened
PS-PVD Plasma-spray physical vapor deposition
RT   Room temperature
Sccm   Standard cubic centimetres per minute
SLM   Selective laser melting
SoA   State of the art
SPS   Suspension plasma spraying
TBC   Thermal barrier coatings
TDS   Thermal desorption spectrometry
TEC   Thermal expansion coefficient
TGO   Thermally grown oxide
US   United States
YAG   Yttrium aluminium garnets
YSZ   Yttria stabilised zirconia

11 References

[1]   World's Most Efficient Combined-Cycle Power Plant | GE Power n.d. https://www.ge.com/power/about/insights/articles/2018/03/nishi-nagoya-efficiency-record (accessed May 25, 2020).

[2]   Spath PL, Mann MK. Life Cycle Assessment of a Natural Gas Combined Cycle Power Generation System. 2000. https://doi.org/10.2172/776930.

[3]   Kloess M, Zach K. Bulk electricity storage technologies for load-leveling operation – An economic assessment for the Austrian and German power market. International Journal of Electrical Power & Energy Systems 2014;59:111–22. https://doi.org/10.1016/j.ijepes.2014.02.002.

[4]   Santos S, Collodi G, Azzaro G, Ferrari N. Reference Data and Supporting Literature Reviews for SMR based Hydrogen Production with CCS. IEAGHG; 2017.

[5]   Energy Information Administration. The Impact of Increased Use of Hydrogen on Petroleum Consumption and Carbon Dioxide Emissions. 2008.

[6]   Langston LS. Hydrogen Fueled Gas Turbines. Mechanical Engineering 2019;141:52–4. https://doi.org/10.1115/1.2019-MAR-6.

[7]   Quarton CJ, Samsatli S. Power-to-gas for injection into the gas grid: What can we learn from real-life projects, economic assessments and systems modelling? Renewable and Sustainable Energy Reviews 2018;98:302–16. https://doi.org/10.1016/j.rser.2018.09.007.

[8]   White paper: Hydrogen power with Siemens gas turbines 2020.

[9]   du Toit MH, Avdeenkov AV, Bessarabov D. Reviewing H2 Combustion: A Case Study for Non-Fuel-Cell Power Systems and Safety in Passive Autocatalytic Recombiners. Energy Fuels 2018;32:6401–22. https://doi.org/10.1021/acs.energyfuels.8b00724.

[10]   ETN GLOBAL. The path towards a zero-carbon gas turbine. n.d.

[11]   World's First Successful Technology Verification of 100% Hydrogen-fueled Gas Turbine Operation with Dry Low NOx Combustion Technology | NEDO n.d. https://www.nedo.go.jp/english/news/AA5en_100427.html (accessed September 14, 2020).

[12]   Bothien MR, Ciani A, Wood JP, Fruechtel G. Toward Decarbonized Power Generation With Gas Turbines by Using Sequential Combustion for Burning Hydrogen. Journal of Engineering for Gas Turbines and Power 2019;141. https://doi.org/10.1115/1.4045256.

[13]   Griebel P. Gas Turbines and Hydrogen. Hydrogen Science and Engineering : Materials, Processes, Systems and Technology, John Wiley & Sons, Ltd; 2016, p. 1011–32. https://doi.org/10.1002/9783527674268.ch43.

[14]   Daniele S, Jansohn P, Mantzaras J, Boulouchos K. Turbulent flame speed for syngas at gas turbine relevant conditions. Proceedings of the Combustion Institute 2011;33:2937–44. https://doi.org/10.1016/j.proci.2010.05.057.

[15]   Dreizler A, Böhm B. Advanced laser diagnostics for an improved understanding of premixed flame-wall interactions. Proceedings of the Combustion Institute 2015;35:37–64. https://doi.org/10.1016/j.proci.2014.08.014.

[16]   Gruber A, Sankaran R, Hawkes ER, Chen JH. Turbulent flame–wall interaction: a direct numerical simulation study. Journal of Fluid Mechanics 2010;658:5–32. https://doi.org/10.1017/S0022112010001278.

[17]   Chiesa P, Lozza G, Mazzocchi L. Using Hydrogen as Gas Turbine Fuel. J Eng Gas Turbines Power 2005;127:73–80. https://doi.org/10.1115/1.1787513.

[18]   Alvin MA. Materials and Component Development for Advanced Turbine Systems. Volume 4: Cycle Innovations; Industrial and Cogeneration; Manufacturing Materials and Metallurgy; Marine, Orlando, Florida, USA: ASMEDC; 2009, p. 737–46. https://doi.org/10.1115/GT2009-59106.

[19]   Clarke DR, Oechsner M, Padture NP. Thermal-barrier coatings for more efficient gas-turbine engines. MRS Bulletin 2012;37:891–8. https://doi.org/10.1557/mrs.2012.232.

[20]   Wright IG, Gibbons TB. Recent developments in gas turbine materials and technology and their implications for syngas firing. International Journal of Hydrogen Energy 2007;32:3610–21. https://doi.org/10.1016/j.ijhydene.2006.08.049.

[21]   Singh K. Advanced Materials for Land Based Gas Turbines. Trans Indian Inst Met 2014;67:601–15. https://doi.org/10.1007/s12666-014-0398-3.

[22]   Pollock TM, Tin S. Nickel-Based Superalloys for Advanced Turbine Engines: Chemistry, Microstructure and Properties. Journal of Propulsion and Power 2006;22:361–74. https://doi.org/10.2514/1.18239.

[23]   Muktinutalapati NR. Materials for Gas Turbines – An Overview. Advances in Gas Turbine Technology 2011. https://doi.org/10.5772/20730.

[24]   SCHILKE P. Advanced Gas Turbine Materials and Coatings. GE Reference Library GER-3569G 2004:1–25.

[25]   Wee S, Do J, Kim K, Lee C, Seok C, Choi B-G, et al. Review on Mechanical Thermal Properties of Superalloys and Thermal Barrier Coating Used in Gas Turbines. Applied Sciences 2020;10:5476. https://doi.org/10.3390/app10165476.

[26] Lagow BW. Materials Selection in Gas Turbine Engine Design and the Role of Low Thermal Expansion Materials. JOM 2016;68:2770–5. https://doi.org/10.1007/s11837-016-2071-2.

[27] Bakan E, Mack DE, Mauer G, Vaßen R, Lamon J, Padture NP. High-temperature materials for power generation in gas turbines. Advanced Ceramics for Energy Conversion and Storage, Elsevier; 2020, p. 3–62. https://doi.org/10.1016/B978-0-08-102726-4.00001-6.

[28] Goldmeer DJ. GEA33861 Electrify Europe Whitepaper 2018. /paper/GEA33861-Electrify-Europe-Whitepaper-Goldmeer/ae2b78ad10651c1061918b9030951ac02c1256b5 (accessed July 27, 2020).

[29] Electrical Monitor :: Alstom GT24/GT26 gas turbines create record n.d. http://www.electricalmonitor.com/ArticleDetails.aspx?aid=481&sid=9 (accessed June 27, 2020).

[30] Shaikh AS. Development of a γ' Precipitation Hardening Ni-Base Superalloy for Additive Manufacturing. 2018. https://doi.org/10.13140/RG.2.2.11472.81921.

[31] Pauzi AA, Ghazali MJ, W. Zamri WFH, Rajabi A. Wear Characteristics of Superalloy and Hardface Coatings in Gas Turbine Applications–A Review. Metals 2020;10:1171. https://doi.org/10.3390/met10091171.

[32] Dorcheh AS, Galetz MC. Challenges in Developing Oxidation-Resistant Chromium-Based Alloys for Applications Above 900°C. JOM 2016;68:2793–802. https://doi.org/10.1007/s11837-016-2079-7.

[33] Gu YF, Harada H, Ro Y. Chromium and chromium-based alloys: Problems and possibilities for high-temperature service. JOM 2004;56:28–33. https://doi.org/10.1007/s11837-004-0197-0.

[34] Michalik M, Tobing SL, Hänsel M, Shemet V, Quadakkers WJ, Young DJ. Effects of water vapour on the high temperature nitridation of chromium. Materials and Corrosion 2014;65:260–6. https://doi.org/10.1002/maco.201307160.

[35] Szweda A, Butner S, Ruffoni J, Bacalski C, Lane J, Morrison J, et al. Development and Evaluation of Hybrid Oxide/Oxide Ceramic Matrix Composite Combustor Liners, American Society of Mechanical Engineers Digital Collection; 2008, p. 315–21. https://doi.org/10.1115/GT2005-68496.

[36] Pimentel G, Capdevila C, Bartolome M, Chao J, Serrano M, García-Junceda A, et al. Advanced FeCrAl ODS steels for high-temperature structural applications in energy generation systems. Revista de Metalurgia 2012;48:303. https://doi.org/10.3989/revmetalm.1165.

[37] Furrer D, Fecht H. Ni-based superalloys for turbine discs. JOM 1999;51:14–7. https://doi.org/10.1007/s11837-999-0005-y.

[38] Smith TM, Esser BD, Antolin N, Carlsson A, Williams REA, Wessman A, et al. Phase transformation strengthening of high-temperature superalloys. Nature Communications 2016;7:13434. https://doi.org/10.1038/ncomms13434.

[39] Panwisawas C, Tang YT, Reed RC. Metal 3D printing as a disruptive technology for superalloys. Nature Communications 2020;11:2327. https://doi.org/10.1038/s41467-020-16188-7.

[40] Basoalto HC, Panwisawas C, Sovani Y, Anderson MJ, Turner RP, Saunders B, et al. A computational study on the three-dimensional printability of precipitate-strengthened nickel-based superalloys. Proceedings of the Royal Society A: Mathematical, Physical and Engineering Sciences 2018;474:20180295. https://doi.org/10.1098/rspa.2018.0295.

[41] Chauvet E, Kontis P, Jägle E, Gault B, Raabe D, TASSIN C, et al. Hot cracking mechanism affecting a non-weldable Ni-based superalloy produced by selective electron Beam Melting. Acta Materialia 2018;142:82–94. https://doi.org/10.1016/j.actamat.2017.09.047.

[42] Hojjatzadeh SMH, Parab ND, Yan W, Guo Q, Xiong L, Zhao C, et al. Pore elimination mechanisms during 3D printing of metals. Nature Communications 2019;10:3088. https://doi.org/10.1038/s41467-019-10973-9.

[43] Smialek JL, Miller RA. Revisiting the Birth of 7YSZ Thermal Barrier Coatings: Stephan Stecura †. Coatings 2018;8:255. https://doi.org/10.3390/coatings8070255.

[44] Hasselman DPH, Johnson LF, Bentsen LD, Syed R, Lee HL, Swain MV. Thermal Diffusivity and Conductivity of Dense Polycrystalline Zr02 Ceramics: A Survey 1987;66:9.

[45] Pawlowski L, Lombard D, Fauchais P. Structure-thermal properties—relationship in plasma sprayed zirconia coatings. Journal of Vacuum Science & Technology A: Vacuum, Surfaces, and Films 1985;3:2494–500. https://doi.org/10.1116/1.572865.

[46] Marra J. Advanced Hydrogen Turbine Development. Siemens Energy, Inc., Orlando, FL (United States); 2015. https://doi.org/10.2172/1261639.

[47] Schulz U. Phase Transformation in EB-PVD Yttria Partially Stabilized Zirconia Thermal Barrier Coatings during Annealing. Journal of the American Ceramic Society 2000;83:904–10. https://doi.org/10.1111/j.1151-2916.2000.tb01292.x.

[48] Witz G, Shklover V, Steurer W, Bachegowda S, Bossmann H-P. Phase Evolution in Yttria-Stabilized Zirconia Thermal Barrier Coatings Studied by Rietveld Refinement of X-Ray Powder Diffraction Patterns. Journal of the American Ceramic Society 2007;90:2935–40. https://doi.org/10.1111/j.1551-2916.2007.01785.x.

[49] Liu B, Liu Y, Zhu C, Xiang H, Chen H, Sun L, et al. Advances on strategies for searching for next generation thermal barrier coating materials. Journal of Materials Science & Technology 2019;35:833–51. https://doi.org/10.1016/j.jmst.2018.11.016.

[50] Bakan E, Vaßen R. Ceramic Top Coats of Plasma-Sprayed Thermal Barrier Coatings: Materials, Processes, and Properties. J Therm Spray Tech 2017;26:992–1010. https://doi.org/10.1007/s11666-017-0597-7.

[51] Gok MG, Goller G. State of the Art of Gadolinium Zirconate Based Thermal Barrier Coatings: Design, Processing and Characterization. Methods for Film Synthesis and Coating Procedures 2019. https://doi.org/10.5772/intechopen.85451.

[52] Padture NP, Gell M, Jordan EH. Thermal Barrier Coatings for Gas-Turbine Engine Applications. Science 2002;296:280–4. https://doi.org/10.1126/science.1068609.

[53] Naumenko D, Pillai R, Chyrkin A, Quadakkers WJ. Overview on Recent Developments of Bondcoats for Plasma-Sprayed Thermal Barrier Coatings. J Therm Spray Tech 2017;26:1743–57. https://doi.org/10.1007/s11666-017-0649-z.

[54] Evans AG, Mumm DR, Hutchinson JW, Meier GH, Pettit FS. Mechanisms controlling the durability of thermal barrier coatings. Progress in Materials Science 2001;46:505–53. https://doi.org/10.1016/S0079-6425(00)00020-7.

[55] Quested PN, Brooks RF, Chapman L, Morrell R, Youssef Y, Mills KC. Measurement and estimation of thermophysical properties of nickel based superalloys. Materials Science and Technology 2009;25:154–62. https://doi.org/10.1179/174328408X361454.

[56] Taylor TA, Walsh PN. Thermal expansion of MCrAlY alloys. Surface and Coatings Technology 2004;177–178:24–31. https://doi.org/10.1016/j.surfcoat.2003.05.001.

[57] Taylor TA. Thermal properties and microstructure of two thermal barrier coatings. In: Sartwell BD, McGUIRE GE, Hofmann S, editors. Metallurgical Coatings and Thin Films 1992, Amsterdam: Elsevier; 1992, p. 53–7. https://doi.org/10.1016/B978-0-444-89900-2.50015-4.

[58] Touloukian YS. Thermal Expansion: Nonmetallic Solids. Springer US; 1977.

[59] Martena M, Botto D, Fino P, Sabbadini S, Gola MM, Badini C. Modelling of TBC system failure: Stress distribution as a function of TGO thickness and thermal expansion mismatch. Engineering Failure Analysis 2006;13:409–26. https://doi.org/10.1016/j.engfailanal.2004.12.027.

[60] Eriksson R, Sjöström S, Brodin H, Johansson S, Östergren L, Li X-H. TBC bond coat–top coat interface roughness: Influence on fatigue life and modelling aspects. Surface and Coatings Technology 2013;236:230–8. https://doi.org/10.1016/j.surfcoat.2013.09.051.

[61] Ahrens M, Vaßen R, Stöver D. Stress distributions in plasma-sprayed thermal barrier coatings as a function of interface roughness and oxide scale thickness. Surface and Coatings Technology 2002;161:26–35. https://doi.org/10.1016/S0257-8972(02)00359-6.

[62] Dong H, Yang G-J, Cai H-N, Ding H, Li C-X, Li C-J. The influence of temperature gradient across YSZ on thermal cyclic lifetime of plasma-sprayed thermal barrier coatings. Ceramics International 2015;41:11046–56. https://doi.org/10.1016/j.ceramint.2015.05.049.

[63] Sun J, Wang J, Zhang H, Yuan J, Dong S, Jiang J, et al. Preparation, structure, mechanical properties and thermal cycling behavior of porous LaMgAl11O19 coating. Journal of Alloys and Compounds 2018;750:1007–16. https://doi.org/10.1016/j.jallcom.2018.04.097.

[64] Zhang J, Bai Y, Li E, Dong H, Ma W. Yb2O3-Gd2O3 codoped strontium zirconate composite ceramics for potential thermal barrier coating applications. International Journal of Applied Ceramic Technology 2020;17:1608–18. https://doi.org/10.1111/ijac.13500.

[65] Gell M, Wang J, Kumar R, Roth J, Jiang C, Jordan EH. Higher Temperature Thermal Barrier Coatings with the Combined Use of Yttrium Aluminum Garnet and the Solution Precursor Plasma Spray Process. J Therm Spray Tech 2018;27:543–55. https://doi.org/10.1007/s11666-018-0701-7.

[66] Doleker KM, Karaoglanli AC. Comparison of oxidation behavior of YSZ and Gd2Zr2O7 thermal barrier coatings (TBCs). Surface and Coatings Technology 2017;318:198–207. https://doi.org/10.1016/j.surfcoat.2016.12.078.

[67] Bakan E. Yttria-stabilized zirconia/gadolinium zirconate double-layer plasma-sprayed thermal barrier coating systems (TBCs). Jülich: Forschungszentrum Jülich; 2015.

[68] Pint BA. High-Temperature Corrosion in Fossil Fuel Power Generation: Present and Future. JOM 2013;65:1024–32. https://doi.org/10.1007/s11837-013-0642-z.

[69] Evans HE, Taylor MP. Diffusion Cells and Chemical Failure of MCrAlY Bond Coats in Thermal-Barrier Coating Systems. Oxidation of Metals 2001;55:17–34. https://doi.org/10.1023/A:1010369024142.

[70] Li Z, Bradt RC. Thermal expansion of the cubic (3C) polytype of SiC. J Mater Sci 1986;21:4366–8. https://doi.org/10.1007/BF01106557.

[71] Eaton HE, Linsey GD. Accelerated oxidation of SiC CMC's by water vapor and protection via environmental barrier coating approach. Journal of the European Ceramic Society 2002;22:2741–7. https://doi.org/10.1016/S0955-2219(02)00141-3.

[72] Xu Y, Hu X, Xu F, Li K. Rare earth silicate environmental barrier coatings: Present status and prospective. Ceramics International 2017;43:5847–55. https://doi.org/10.1016/j.ceramint.2017.01.153.

[73] Richards BT, Wadley HNG. Plasma spray deposition of tri-layer environmental barrier coatings. Journal of the European Ceramic Society 2014;34:3069–83. https://doi.org/10.1016/j.jeurceramsoc.2014.04.027.

[74] Lucato SL dos S e, Sudre OH, Marshall DB. A Method for Assessing Reactions of Water Vapor with Materials in High-Speed, High-Temperature Flow. Journal of the American Ceramic Society 2011;94:s186–95. https://doi.org/10.1111/j.1551-2916.2011.04556.x.

[75] Golden RA, Opila EJ. A method for assessing the volatility of oxides in high-temperature high-velocity water vapor. Journal of the European Ceramic Society 2016;36:1135–47. https://doi.org/10.1016/j.jeurceramsoc.2015.11.016.

[76] Mumm D. Mechanisms Underpinning Degradation of Protective Oxides and Thermal Barrier Coatings in High Hydrogen Content (HHC) - Fueled Turbines. 2013. https://doi.org/10.2172/1149472.

[77] Yu CT, Liu H, Zhang J, Ullah A, Bao ZB, Jiang CY, et al. Gradient thermal cycling behavior of a thermal barrier coating system constituted by NiCoCrAlY bond coat and pure metastable tetragonal nano-4YSZ top coat. Ceramics International 2019;45:15281–9. https://doi.org/10.1016/j.ceramint.2019.05.018.

[78] Ziaei-Asl A, Ramezanlou MT. Thermo-mechanical behavior of gas turbine blade equipped with cooling ducts and protective coating with different thicknesses. International Journal of Mechanical Sciences 2019;150:656–64. https://doi.org/10.1016/j.ijmecsci.2018.10.070.

[79] Vaßen R, Kerkhoff G, Stöver D. Development of a micromechanical life prediction model for plasma sprayed thermal barrier coatings. Materials Science and Engineering: A 2001;303:100–9. https://doi.org/10.1016/S0921-5093(00)01853-0.

[80]	Saunders SRJ, Monteiro M, Rizzo F. The oxidation behaviour of metals and alloys at high temperatures in atmospheres containing water vapour: A review. Progress in Materials Science 2008;53:775–837. https://doi.org/10.1016/j.pmatsci.2007.11.001.

[81]	Meschter PJ, Opila EJ, Jacobson NS. Water Vapor–Mediated Volatilization of High-Temperature Materials. Annual Review of Materials Research 2013;43:559–88. https://doi.org/10.1146/annurev-matsci-071312-121636.

[82]	Opila EJ, Myers DL, Jacobson NS, Nielsen IMB, Johnson DF, Olminsky JK, et al. Theoretical and Experimental Investigation of the Thermochemistry of $CrO_2(OH)_2$(g). J Phys Chem A 2007;111:1971–80. https://doi.org/10.1021/jp0647380.

[83]	Asteman H, Svensson J-E, Norell M, Johansson L-G. Influence of Water Vapor and Flow Rate on the High-Temperature Oxidation of 304L; Effect of Chromium Oxide Hydroxide Evaporation. Oxidation of Metals 2000;54:11–26. https://doi.org/10.1023/A:1004642310974.

[84]	Tedmon CS. The Effect of Oxide Volatilization on the Oxidation Kinetics of Cr and Fe-Cr Alloys. J Electrochem Soc 1966;113:766–8. https://doi.org/10.1149/1.2424115.

[85]	Sachitanand R, Svensson J-E, Froitzheim J. The Influence of Cr Evaporation on Long Term Cr Depletion Rates in Ferritic Stainless Steels. Oxid Met 2015;84:241–57. https://doi.org/10.1007/s11085-015-9552-5.

[86]	Hooshyar H, Jonsson T, Hall J, Svensson J-E, Johansson LG, Liske J. The Effect of H2 and H2O on the Oxidation of 304L-Stainless Steel at 600 °C: General Behaviour (Part I). Oxid Met 2016;85:321–42. https://doi.org/10.1007/s11085-015-9597-5.

[87]	Henry S, Mougin J, Wouters Y, Petit J-P, Galerie A. Characterization of Chromia Scales Grown on Pure Chromium in Different Oxidizing Atmospheres. Materials at High Temperatures 2000;17:231–4. https://doi.org/10.1179/mht.2000.17.2.008.

[88]	Hultquist G, Tveten B, Hörnlund E. Hydrogen in Chromium: Influence on the High-Temperature Oxidation Kinetics in H2O, Oxide-Growth Mechanisms, and Scale Adherence. Oxidation of Metals 2000;54:1–10. https://doi.org/10.1023/A:1004610626903.

[89]	Zurek J, Young DJ, Essuman E, Hänsel M, Penkalla HJ, Niewolak L, et al. Growth and adherence of chromia based surface scales on Ni-base alloys in high- and low-pO2 gases. Materials Science and Engineering: A 2008;477:259–70. https://doi.org/10.1016/j.msea.2007.05.035.

[90]	Simon D, Gorr B, Christ HJ. Effect of Atmosphere and Sample Thickness on Kinetics, Microstructure, and Compressive Stresses of Chromia Scale Grown on Ni–25Cr. Oxid Met 2017;87:417–29. https://doi.org/10.1007/s11085-016-9702-4.

[91]	Sand T, Geers C, Cao Y, Svensson JE, Johansson LG. Effective Reduction of Chromium-oxy-hydroxide Evaporation from Ni-Base Alloy 690. Oxid Met 2019;92:259–79. https://doi.org/10.1007/s11085-019-09935-9.

[92]	Pint BA, Dryepondt S, Unocic KA. Oxidation of Superalloys in Extreme Environments. Superalloy 718 and Derivatives, John Wiley & Sons, Ltd; 2012, p. 859–75. https://doi.org/10.1002/9781118495223.ch66.

[93]	Maris-Sida MC, Meier GH, Pettit FS. Some Water Vapor Effects during the Oxidation of Alloys that are ⎵-Al2O3 Formers. METALLURGICAL AND MATERIALS TRANSACTIONS A 2003:11.

[94]	Zhao W, Gleeson B. Assessment of the Detrimental Effects of Steam on Al2O3-Scale Establishment. Oxid Met 2015;83:607–27. https://doi.org/10.1007/s11085-015-9541-8.

[95]	Liu F, Josefsson H, Svensson J-E, Johansson L-G, Halvarsson M. TEM investigation of the oxide scales formed on a FeCrAlRE alloy (Kanthal AF) at 900°C in dry O2 and O2 with 40% H2O. Materials at High Temperatures 2005;22:521–6. https://doi.org/10.1179/mht.2005.062.

[96]	Götlind H, Liu F, Svensson J-E, Halvarsson M, Johansson L-G. The Effect of Water Vapor on the Initial Stages of Oxidation of the FeCrAl Alloy Kanthal AF at 900 °C. Oxid Met 2007;67:251–66. https://doi.org/10.1007/s11085-007-9055-0.

[97]	Sohlberg K, Pennycook SJ, Pantelides ST. Hydrogen and the Structure of the Transition Aluminas. J Am Chem Soc 1999;121:7493–9. https://doi.org/10.1021/ja991098o.

[98] Pint BA, Haynes JA, Zhang Y, More KL, Wright IG. The effect of water vapor on the oxidation behavior of Ni–Pt–Al coatings and alloys. Surface and Coatings Technology 2006;201:3852–6. https://doi.org/10.1016/j.surfcoat.2006.07.244.

[99] Smialek JL. Moisture-Induced TBC Spallation on Turbine Blade Samples. Surface and Coatings Technology 2011;206:1577–85. https://doi.org/10.1016/j.surfcoat.2011.07.015.

[100] Opila EJ, Myers DL. Alumina Volatility in Water Vapor at Elevated Temperatures. Journal of the American Ceramic Society 2004;87:1701–5. https://doi.org/10.1111/j.1551-2916.2004.01701.x.

[101] Sumner J, Simms NJ, Stamm W, Oakey JE. Simulating novel gas turbine conditions for materials assessment: cascade design and operation. Materials Science and Technology 2017;33:1090–9. https://doi.org/10.1080/02670836.2017.1310492.

[102] Zhou C, Yu J, Gong S, Xu H. Influence of water vapor on the high temperature oxidation behavior of thermal barrier coatings. Materials Science and Engineering: A 2003;348:327–32. https://doi.org/10.1016/S0921-5093(02)00742-6.

[103] Cernuschi F, Bison P, Mack DE, Merlini M, Boldrini S, Marchionna S, et al. Thermo-physical properties of as deposited and aged thermal barrier coatings (TBC) for gas turbines: State-of-the art and advanced TBCs. Journal of the European Ceramic Society 2018;38:3945–61. https://doi.org/10.1016/j.jeurceramsoc.2018.04.044.

[104] Sullivan MH, Mumm DR. Transient stage oxidation of MCrAlY bond coat alloys in high temperature, high water vapor content environments. Surface and Coatings Technology 2014;258:963–72. https://doi.org/10.1016/j.surfcoat.2014.07.048.

[105] Unocic KA, Pint BA. Effect of water vapor on thermally grown alumina scales on bond coatings. Surface and Coatings Technology 2013;215:30–8. https://doi.org/10.1016/j.surfcoat.2012.08.100.

[106] Pint BA, Garner GW, Lowe TM, Haynes JA, Zhang Y. Effect of increased water vapor levels on TBC lifetime with Pt-containing bond coatings. Surface and Coatings Technology 2011;206:1566–70. https://doi.org/10.1016/j.surfcoat.2011.06.008.

[107] Nowak W. High Temperature Corrosion of Alloys and Coatings in Gas-Turbines Fired with Hydrogen-Rich Syngas Fuels. 2014.

[108] Opila EJ, Smialek JL, Robinson RC, Fox DS, Jacobson NS. SiC Recession Caused by SiO2 Scale Volatility under Combustion Conditions: II, Thermodynamics and Gaseous-Diffusion Model. Journal of the American Ceramic Society 1999;82:1826–34. https://doi.org/10.1111/j.1151-2916.1999.tb02005.x.

[109] Parker CG, Opila EJ. Stability of the Y2O3–SiO2 system in high-temperature, high-velocity water vapor. Journal of the American Ceramic Society 2020;103:2715–26. https://doi.org/10.1111/jace.16915.

[110] Padture NP. Environmental degradation of high-temperature protective coatings for ceramic-matrix composites in gas-turbine engines. Npj Materials Degradation 2019;3:1–6. https://doi.org/10.1038/s41529-019-0075-4.

[111] Li L, Hitchman N, Knapp J. Failure of Thermal Barrier Coatings Subjected to CMAS Attack. J Therm Spray Tech 2010;19:148–55. https://doi.org/10.1007/s11666-009-9356-8.

[112] Yang Z, Walker MS, Singh P, Stevenson JW. Anomalous Corrosion Behavior of Stainless Steels under SOFC Interconnect Exposure Conditions. Electrochem Solid-State Lett 2003;6:B35–7. https://doi.org/10.1149/1.1603012.

[113] Kurokawa H, Kawamura K, Maruyama T. Oxidation behavior of Fe–16Cr alloy interconnect for SOFC under hydrogen potential gradient. Solid State Ionics 2004;168:13–21. https://doi.org/10.1016/j.ssi.2004.02.008.

[114] Holcomb GR, Ziomek-Moroz M, Cramer SD, Jr BSC, Bullard SJ. Dual-environment effects on the oxidation of metallic interconnects. J of Materi Eng and Perform 2006;15:404–9. https://doi.org/10.1361/105994906X117198.

[115] Alnegren P, Sattari M, Svensson J-E, Froitzheim J. Severe dual atmosphere effect at 600 °C for stainless steel 441. Journal of Power Sources 2016;301:170–8. https://doi.org/10.1016/j.jpowsour.2015.10.001.

[116] Gannon P, Amendola R. High-Temperature, Dual-Atmosphere Corrosion of Solid-Oxide Fuel Cell Interconnects. JOM 2012;64:1470–6. https://doi.org/10.1007/s11837-012-0473-3.

[117] Goebel C, Alnegren P, Faust R, Svensson J-E, Froitzheim J. The effect of pre-oxidation parameters on the corrosion behavior of AISI 441 in dual atmosphere. International Journal of Hydrogen Energy 2018;43:14665–74. https://doi.org/10.1016/j.ijhydene.2018.05.165.

[118] Yang Z, Walker MS, Singh P, Stevenson JW, Norby T. Oxidation Behavior of Ferritic Stainless Steels under SOFC Interconnect Exposure Conditions. J Electrochem Soc 2004;151:B669–78. https://doi.org/10.1149/1.1810393.

[119] Zhao Y, Fergus JW. Oxidation Behavior of Stainless Steel 441 and 430 in Dual Atmosphere: Effects of Alloy Grain Boundaries. J Electrochem Soc 2014;161:C69–76. https://doi.org/10.1149/2.076401jes.

[120] Rufner J, Gannon P, White P, Deibert M, Teintze S, Smith R, et al. Oxidation behavior of stainless steel 430 and 441 at 800 °C in single (air/air) and dual atmosphere (air/hydrogen) exposures. International Journal of Hydrogen Energy 2008;33:1392–8. https://doi.org/10.1016/j.ijhydene.2007.12.067.

[121] Galerie A, Henry S, Wouters Y, Mermoux M, Petit J-P, Antoni L. Mechanisms of chromia scale failure during the course of 15–18Cr ferritic stainless steel oxidation in water vapour. Materials at High Temperatures 2005;22:105–12. https://doi.org/10.1179/mht.2005.012.

[122] Zhao Y, Fergus JW. Oxidation of Alloys 430 and 441 in SOFC Dual Atmospheres: Effects of Flow Rate and Humidity. J Electrochem Soc 2012;159:C109–13. https://doi.org/10.1149/2.013203jes.

[123] Nickel institute: High temperature characteristics of stainless steels n.d.

[124] Nelson GA, Effinger RT. BLISTERING AND EMBRITTLEMENT OF PRESSURE VESSEL STEELS BY HYDROGEN. Welding J (NY) 1955;Vol: 34.

[125] Nibur KA, Somerday BP. 7 - Fracture and fatigue test methods in hydrogen gas. In: Gangloff RP, Somerday BP, editors. Gaseous Hydrogen Embrittlement of Materials in Energy Technologies, vol. 2, Woodhead Publishing; 2012, p. 195–236. https://doi.org/10.1533/9780857093899.2.195.

[126] Gray HR. Embrittlement of nickel-, cobalt-, and iron-base superalloys by exposure to hydrogen. 1975.

[127] Balyts'kyi AI, Kvasnyts'ka YuH, Ivas'kevich LM, Myal'nitsa HP. Corrosion- and Hydrogen-Resistance of Heat-Resistant Blade Nickel-Cobalt Alloys. Mater Sci 2018;54:230–9. https://doi.org/10.1007/s11003-018-0178-z.

[128] Owen D, Tokmo F, Hickey J, Phillips L, Jenkins S, Zhang J. Gas Turbine Engine Components Manufactured via Additive Manufacturing Process. ASTM Project Grant Final Report n.d.:10.

[129] Kellner T. Fired Up: GE Successfully Tested Its Advanced Turboprop Engine With 3D-Printed Parts | GE News n.d. https://www.ge.com/news/reports/ge-fired-its-3d-printed-advanced-turboprop-engine (accessed June 30, 2020).

[130] Additive Manufacturing for Turbomachinery & Turbines | EOS n.d. https://www.eos.info/en/3d-printing-examples-applications/production-and-industry/turbomachinery-turbines (accessed June 24, 2020).

[131] Fu W, Haberland C, Klapdor EV, Rule D, Piegert S. Streamlined frameworks for advancing metal based additive manufacturing technologies. J Glob Power Propuls Soc 2018;2:317–28. https://doi.org/10.22261/JGPPS.QJLS4L.

[132] Gebisa AW, Lemu HG. Additive Manufacturing for the Manufacture of Gas Turbine Engine Components: Literature Review and Future Perspectives, American Society of Mechanical Engineers Digital Collection; 2018. https://doi.org/10.1115/GT2018-76686.

[133] Deng D. Additively Manufactured Inconel 718 : Microstructures and Mechanical Properties 2018.

[134] Zhang F, Levine LE, Allen AJ, Stoudt MR, Lindwall G, Lass EA, et al. Effect of heat treatment on the microstructural evolution of a nickel-based superalloy additive-manufactured by laser powder bed fusion. Acta Materialia 2018;152:200–14. https://doi.org/10.1016/j.actamat.2018.03.017.

[135] Andersson O, Graichen A, Brodin H, Navrotsky V. Developing Additive Manufacturing Technology for Burner Repair. J Eng Gas Turbines Power 2017;139. https://doi.org/10.1115/1.4034235.

[136] Örnek C. Additive manufacturing – a general corrosion perspective. Corrosion Engineering, Science and Technology 2018;53:531–5. https://doi.org/10.1080/1478422X.2018.1511327.

[137] Kong D, Dong C, Ni X, Li X. Corrosion of metallic materials fabricated by selective laser melting. Npj Materials Degradation 2019;3:1–14. https://doi.org/10.1038/s41529-019-0086-1.

[138] Laleh M, Hughes AE, Xu W, Gibson I, Tan MY. A critical review of corrosion characteristics of additively manufactured stainless steels. International Materials Reviews 2020;0:1–37. https://doi.org/10.1080/09506608.2020.1855381.

[139] Baek S-W, Song EJ, Kim JH, Jung M, Baek UB, Nahm SH. Hydrogen embrittlement of 3-D printing manufactured austenitic stainless steel part for hydrogen service. Scripta Materialia 2017;130:87–90. https://doi.org/10.1016/j.scriptamat.2016.11.020.

[140] Smith TR, San Marchi C, Sugar JD, Balch DK. Effects of Extreme Hydrogen Environments on the Fracture and Fatigue Behavior of Additively Manufactured Stainless Steels, American Society of Mechanical Engineers Digital Collection; 2019. https://doi.org/10.1115/PVP2019-93903.

[141] Kong D, Dong C, Ni X, Zhang L, Luo H, Li R, et al. Superior resistance to hydrogen damage for selective laser melted 316L stainless steel in a proton exchange membrane fuel cell environment. Corrosion Science 2020;166:108425. https://doi.org/10.1016/j.corsci.2019.108425.

[142] Kulkarni A. Additive Manufacturing of Nickel Based Superalloy. ArXiv:180511664 [Physics] 2018.

[143] Xu J, Gruber H, Boyd R, Jiang S, Peng RL, Moverare JJ. On the strengthening and embrittlement mechanisms of an additively manufactured Nickel-base superalloy. Materialia 2020;10:100657. https://doi.org/10.1016/j.mtla.2020.100657.

[144] Seifi M, Salem A, Beuth J, Harrysson O, Lewandowski JJ. Overview of Materials Qualification Needs for Metal Additive Manufacturing. JOM 2016;68:747–64. https://doi.org/10.1007/s11837-015-1810-0.

[145] Gorsse S, Hutchinson C, Gouné M, Banerjee R. Additive manufacturing of metals: a brief review of the characteristic microstructures and properties of steels, Ti-6Al-4V and high-entropy alloys. Science and Technology of Advanced Materials 2017;18:584–610. https://doi.org/10.1080/14686996.2017.1361305.

[146] How Mature Are Metal 3D Printing Technologies? AMFG 2019. https://amfg.ai/2019/09/03/how-mature-are-metal-3d-printing-technologies/ (accessed August 7, 2020).

[147] Norsk Titanium Completes TRL 8 Certification: 3D Printed RPD Components Pass Stringent Testing. 3DPrintCom | The Voice of 3D Printing / Additive Manufacturing 2015. https://3dprint.com/112084/norsk-titanium-trl8/ (accessed August 7, 2020).

[148] Metal Materials for 3D printing | EOS GmbH n.d. https://www.eos.info/en/additive-manufacturing/3d-printing-metal/dmls-metal-materials (accessed August 7, 2020).

[149] TRLs Promise Quality in 3D Printing | EOS GmbH n.d. https://www.eos.info/en/additive-manufacturing/3d-printing-metal/trl (accessed August 7, 2020).

[150] Silverstein R, Eliezer D. Hydrogen trapping in 3D-printed (additive manufactured) Ti-6Al-4V. Materials Characterization 2018;144:297–304. https://doi.org/10.1016/j.matchar.2018.07.029.

[151] Hong Y, Zhou C, Zheng Y, Zhang L, Zheng J, Chen X, et al. Formation of strain-induced martensite in selective laser melting austenitic stainless steel. Materials Science and Engineering: A 2019;740–741:420–6. https://doi.org/10.1016/j.msea.2018.10.121.

[152] Zheng L, Schmitz G, Meng Y, Chellali M, Schlesiger R. Mechanism of Intermediate Temperature Embrittlement of Ni and Ni-based Superalloys. Critical Reviews in Solid State and Material Sciences 2012;37:181–214. https://doi.org/10.1080/10408436.2011.613492.

[153] Varela A de V, de Deus HD, de Siqueira MC, Rezende MC, de Almeida LH. Oxidation assisted intergranular cracking in 718 Nickel Superalloy: on the mechanism of dynamic embrittlement. Journal of Materials Research and Technology 2018;7:319–25. https://doi.org/10.1016/j.jmrt.2018.02.008.

[154] Saarimäki J. Cracks in superalloys. 2018. https://doi.org/10.3384/diss.diva-144397.

[155] Chan K. A Grain Boundary Fracture Model for Predicting Dynamic Embrittlement and Oxidation-Induced Cracking in Superalloys. Metallurgical and Materials Transactions A 2015;46. https://doi.org/10.1007/s11661-015-2860-1.

[156] Németh AAN, Crudden DJ, Armstrong DEJ, Collins DM, Li K, Wilkinson AJ, et al. Environmentally-assisted grain boundary attack as a mechanism of embrittlement in a nickel-based superalloy. Acta Materialia 2017;126:361–71. https://doi.org/10.1016/j.actamat.2016.12.039.

[157] Deng D, Peng RL, Moverare J. On the dwell-fatigue crack propagation behavior of a high strength superalloy manufactured by electron beam melting. Materials Science and Engineering: A 2019;760:448–57. https://doi.org/10.1016/j.msea.2019.06.013.

Materials challenges in hydrogen-fuelled gas turbines

Elena Stefan*[1], Belma Talic*[1], Yngve Larring[1], Andrea Gruber[2], Thijs A. Peters[1]@

[1] SINTEF Industry, P.O. Box 124 Blindern, N-0314, Oslo, Norway

[2] SINTEF Energy Research, Thermal Energy Department, Trondheim, Norway

*These authors contributed equally to this work.

@Corresponding author email: thijs.peters@sintef.no

Contents

Abstract

With the increased pressure to decarbonize the power generation sector several gas turbine manufacturers are working towards increasing the hydrogen-firing capabilities of their engines towards 100%. In this review, we discuss the potential materials challenges of gas turbines fuelled with hydrogen, provide an updated overview of the most promising alloys and coatings for this application, and highlight topics requiring further research and development. Particular focus is given to the high-temperature oxidation of gas turbine materials exposed to hydrogen and steam at elevated temperatures and to the corrosion challenges of parts fabricated by additive manufacturing. Other degradation mechanisms such as hot corrosion, the dual atmosphere effect and hydrogen diffusion in the base alloys are also discussed.

1   Introduction

Gas turbines are among the most widely used power-generation technologies today. Their theoretical basic principle, the Brayton thermodynamic cycle, relies on thermal energy conversion of a chemically reactive fuel and leverages on an abundantly available gas (air) as working fluid to generate electric power or to mechanically drive rotating equipment (*e.g.* in compressor stations). State-of-the-art combined cycle gas turbines offer the advantages of a high total efficiency (>60 % [1]), low NO_x and SO_x emissions, and high fuel flexibility. However, despite being considered the cleanest of the conventional fossil-fuel power generation technologies, gas turbines fuelled with hydrocarbon-based fuels inevitably lead to considerable CO_2 emissions (ca. 440 gCO_2/kWh for natural gas [2]). These CO_2 emissions could be greatly reduced or even eliminated if the gas turbine instead is fuelled with hydrogen produced using either renewable energy [3] or natural gas reforming combined with carbon capture and storage (CCS) schemes [4]. Gas turbines are complementary to other hydrogen-conversion technologies such as fuel cells as they currently are more cost-efficient at large scale and can utilize lower-purity hydrogen, for example produced during the synthesis of aromatics and olefins or hydrogen from chlor-alkali plants. The hydrogen available from these sources amounts to > 10 000 metric tons per year in the US alone [5].

A jet engine powered by hydrogen was demonstrated already in 1937, which shows that the hydrogen-fuelling of gas turbines is not novel [6]. However, practical considerations and the historically lower price of natural gas compared to hydrogen favoured the development of gas turbines highly tuned for operation with natural gas. With the increased pressure to decarbonize the power generation sector in order to limit global warming, the industry is re-considering hydrogen as a viable fuel. In a few countries such as the Netherlands, small amounts (<20 vol.%) of hydrogen are being mixed into the natural gas grid and used to fuel conventional gas turbines [7]. While this is an important step in the right direction, adding hydrogen to natural gas has only a minor effect on the CO_2 emissions because of the low volumetric energy density of hydrogen relative to methane. For example, adding 10 vol.% hydrogen to methane will only reduce CO_2 emissions by 2.7 % [8]. For a completely CO_2-emission free operation, gas turbines capable of operating on 100 % hydrogen are hence required.

As illustrated in Figure 1, several commercially-available gas turbines based on diffusion-flame combustion systems can already be operated with 100 % hydrogen [9]. However, these systems require the addition of large quantities of treated water (or nitrogen) in order to adequately decrease the flame temperature and NO_x emissions in wet low emission (WLE) combustors, which results in a more complex, bulkier, and expensive system with a lower overall efficiency. Therefore, recent research and development efforts have focused on hydrogen-firing of state-of-the-art dry low-

2

emission (DLE) combustion systems that have greater potential to simultaneously ensure high efficiencies and emissions-compliant operation. In DLE combustors the flame temperature is typically moderated by ensuring that fuel-lean conditions are achieved before combustion occurs, thereby avoiding any significant production of NO_x. This is achieved through an highly-optimized injection and mixing of the fuel with the oxidant (air) before the resulting burnable mixture enters the combustion chamber.

None of the commercially available DLE combustion systems today, however, can be operated with more than 30-60 vol.% of hydrogen [10]. While the Japanese company Kawasaki reported in July 2020 the world's first demonstration of a 100% hydrogen-fuelled gas turbine using a DLE combustion system [11], this achievement was obtained in the context of a small combined heat and power (CHP) application featuring relatively low electrical efficiency (~28%) and, therefore, requiring a relatively low firing temperature. Significant outstanding issues remain if 100 % hydrogen DLE operation has to be implemented in gas turbines capable of state-of-the-art electrical efficiencies that reach ~43% in open cycles configurations (~63% in combined cycles) and require high firing temperatures [12]. The gas turbine industry in Europe is targeting to achieve this by 2030 [10].

The main challenges encountered in the operation of DLE systems with 100 % hydrogen are related to the combustion characteristics of hydrogen [9,13] that become increasingly difficult to handle, from the combustion system's design point of view, for higher flame temperatures. This is a significant issue since the flame temperature is the single most important quantity controlling the turbine inlet temperature, the power output and the efficiency of the gas turbine, *i.e.* its ability to produce work (electricity or mechanical drive). Among the most important characteristics that differentiate hydrogen from conventional hydrocarbon fuels (*e.g.* natural gas) is the combustion burning rate, *i.e.* the rate at which the flame is able to consume the combustible mixture, increasing the working fluid's temperature to accelerate it towards the turbine stage. The burning rate (flame speed) in laminar hydrogen flames is nominally three to seven times higher compared to methane (the main component of natural gas) at equal flame temperature because of hydrogen's fast reaction and diffusion rates [8,13]. Even larger differences are observed in the highly turbulent flames found in the combustion system of modern gas turbines [14]. The augmented burning rate can lead to flame instability issues, increasing the risk of unwanted flame displacement into the upstream mixing section of the burner (flashback) and resulting in early combustion of a sub-optimal (still fuel-rich) mixture of fuel and oxidant. In turn, this causes very high local flame temperatures that promote pollutants formation (NO_x) and exposure above the melting point of the stainless-steel alloy construction materials.
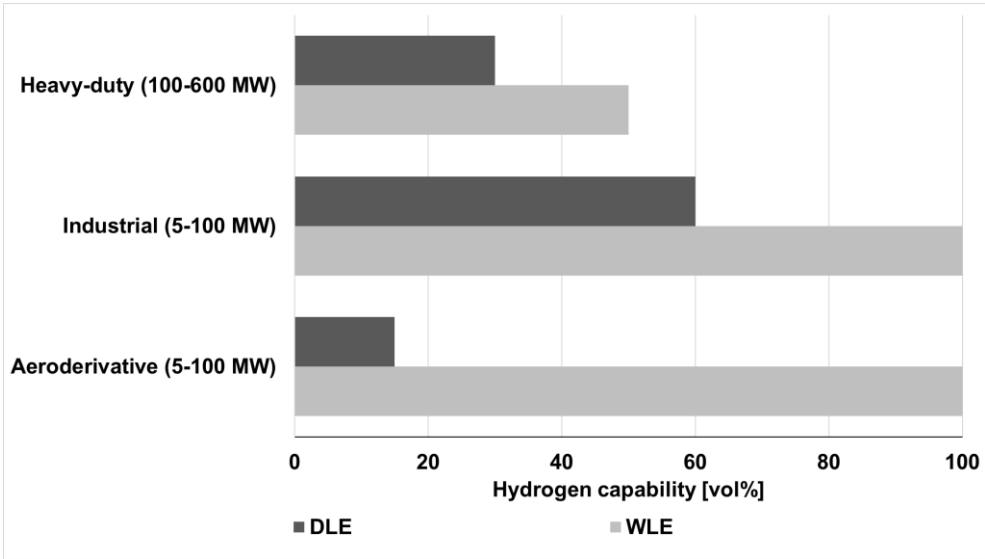
An additional important challenge introduced by hydrogen combustion that is of specific relevance to the material-science aspect of the technology development is related to the flame characteristic quenching distance (δ_q). This quantity defines the minimal distance between a hot flame and a (relatively) cold solid surface at which quenching nominally occurs. Both fundamental modelling and experimental investigations have indicated that δ_q is significantly smaller (by a factor of 1/2) for hydrogen flames compared to hydrocarbon flames [15], implying the possibility of a greatly enhanced heat-flux to the solid surfaces that are in vicinity of the hydrogen flame stabilization location. The quenching heat-flux from the flame to the combustor walls is further amplified in the presence of characteristic near-wall turbulence structures [16], establishing an unsteady spatial pattern with peaks exceeding 1 MW/m^2 that, when opportunely modulated by the controlling time and length scale of the turbulent flow, can result in severe thermal stress of the solid material.

While many of the above-mentioned challenges related to the combustion of hydrogen can be handled through modifications to the design of the burner, factors such as an increased temperature and steam content may also require the development of new materials. One potential challenge from the materials' perspective is that hydrogen combustion results in a higher steam concentration in the
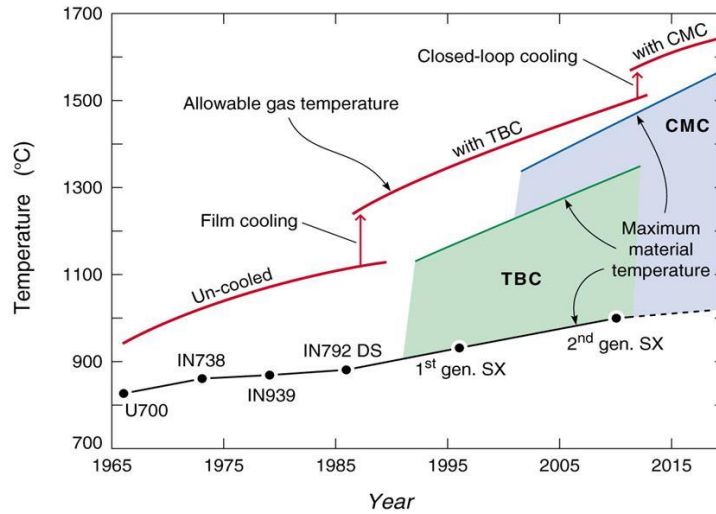
3

exhaust gas relative to natural gas combustion. The exhaust from natural gas fired land-based turbines typically contains 10 vol.% steam and 5 vol.% CO_2. State-of-the-art DLE operation with pure hydrogen (yet to be achieved) would theoretically increase the steam fraction in the combustion products to 16 vol.%, while legacy technologies utilizing steam dilution or water injection result in exhaust steam content up to 85 vol.% [17,18]. One of the impacts of increased water content in the combustion products is that the heat transfer coefficient between the hot gas and all solid surfaces exposed to it is increased, resulting in higher temperatures of the metal blades in the first, critical turbine stages that are subjected to the largest heat load [13]. This effect can be compensated by decreasing the flame and the turbine inlet temperatures, but at the expense of a lower efficiency [19].

There are several reviews available that provide an overview of the latest developments in materials for gas turbines [20–27]. Most of these discuss the possible challenges with using natural gas as the fuel, while less literature is available regarding the possible materials challenges with using hydrogen. To our own knowledge, only the 2007 review by Wright and Gibbons [20] considered the suitability of applying state-of-the-art materials developed for "conventional" gas turbines in gas turbines burning coal-derived syngas or hydrogen. They concluded that the combustion environment with coal derived hydrogen or syngas was possibly more corrosive than natural gas, because of the greater level of impurities such as sulphur, water vapour and particulates that affect the durability of some components. The development of materials for gas turbines has significantly progressed since Wright and Gibbons [20] published their review. The most important trend is the development of new materials enabling a higher operating temperature, and thus higher turbine efficiency, as shown in Figure 2. Another trend is the increased application of additive manufacturing or 3D printing to fabricate complex gas turbine combustor designs, such as those currently being developed for hydrogen-fuelled gas turbines. The time is therefore mature to review the current state-of-the art materials and their suitability for application in hydrogen-fuelled gas turbines.

In this review, we aim to present an overview of the materials challenges in gas turbines fuelled with 100 % hydrogen, provide an updated overview of the most promising alloys and coatings for this application, and highlight topics requiring further research and development. Particular focus is given to the high-temperature oxidation of gas turbine materials exposed to hydrogen and steam at elevated temperatures and the potential corrosion issues for gas turbine components made by additive manufacturing.
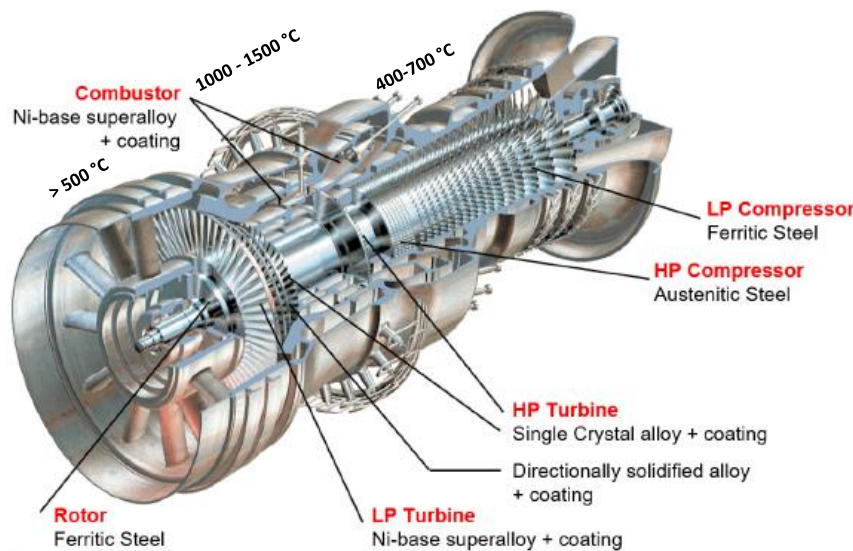
Figure 2 Material improvements with firing temperature capability of industrial gas turbines (TBC – thermal barrier coatings, CMC – ceramic matrix composites), after [19].

2   Materials used in gas turbines

The materials used in the different parts of a gas turbine must meet a demanding set of requirements in terms of mechanical and thermal properties, manufacturability into complex geometries, and stability under the working conditions. Figure 3 illustrates the range of exposure conditions for different parts of the gas turbine and highlights commonly employed materials. Since a single material in most cases cannot provide the necessary combination of mechanical robustness/strength and sufficient oxidization resistance, some of the gas turbine components are coated and/or internally cooled.

Figure 3 Main parts of an Alstom gas turbine, exposure conditions and materials used in different sections, after [29,30].

The following sections contain a description of the exposure conditions in the different parts of the gas turbine and how these may be influenced when the gas turbine is fuelled with hydrogen instead of natural gas. An overview of the most commonly used turbine materials and the most promising new developments is presented. In the previous two decades, several companies and research programs focused on developing syngas (*i.e.* CO + H$_2$) fuelled gas turbines, which has given some experience with use of hydrogen containing fuels [13]. Much of the more general materials development has otherwise been driven by the development of aeroturbines, as these operate at harsher conditions and have stricter requirements for high efficiency and low weight. Industrial-scale land-based turbines have tougher requirements of low cost that, alongside challenges with upscaling certain manufacturing methods, imposes restrictions on which materials that can be adopted. For example, single crystal alloys are attractive because of their high temperature tolerance, but difficult to manufacture without defects in the large size required for industrial scale gas turbines [12,19,21].

2.1 Materials for the compressor section

The temperature in the air compressor part of the turbine is typically limited to 400-500 °C, making it possible to use relatively inexpensive alloys such as martensitic stainless steels, *e.g.* AISI 403 or AISI 403 Nb [23]. In small and intermediate scale gas turbines operated with relatively clean air, these alloys do not suffer from any significant materials challenges [21]. The materials requirements are harsher for gas turbines installed in industrial settings where the air is contaminated by acids and/or salts. In these situations, alloys such as the precipitation hardened martensitic stainless steel GTD-450 is a good alternative [23]. This alloy has a higher Cr and Mo content compared to AISI 403, which provides corrosion resistance to moisture containing acids and salts [23,24].

Hydrogen fuelling does not have any intrinsic requirements for higher or lower compressor output compared to natural gas fuelling of gas turbines. Thus, no changes are expected for this part of the gas turbine when switching to hydrogen.

2.2 Materials for combustor parts

State-of-art DLE combustion systems for stationary gas turbines are based on a lean premixed combustion approach and typically consists of a mixing section where fuel is injected and mixed into the oxidant stream and a combustion chamber. In stationary applications, longitudinal or radial (co-axial) fuel staging designs are often adopted in order to optimize the combustion process and limit pollutants formation. However, footprint and weight constraints severely limit the adoption of staged combustion systems in aero-applications which, because of flame stability and high-altitude relight requirements, traditionally employ a non-premixed combustion approach with important consequences on emissions from the diffusion-type flame. The combustion chamber is the hottest part of the gas turbine where temperatures can reach 1600 °C or even higher [20]. The materials used for some specific parts of the combustion system must therefore meet a series of strong requirements including high temperature creep rupture strength, good oxidation resistance, and endurance against thermal and cycle fatigue. The materials should also have good formability and weldability to enable fabrication of complex shapes [20,21].

Commonly applied materials able to meet the mechanical requirements are wrought Ni base superalloys such as Hastelloy X, IN617, Nimonic 263, Haynes 188 or Haynes 230 and SS309 [21,23,24,31]. In order to keep the surface of these alloys sufficiently below their melting point, internal air cooling and thermal barrier coatings (see Section 2.4) or ceramic tiles are applied as the combustor lining.

Land-based gas turbines are striving to reduce costs by exchanging the low-Re (Rhenium) second generation superalloys to Re-free first-generation alloys such as 1483, or to directionally solidified

6

superalloys such as 247. Other research, motivated by cost reductions, is to replace the relatively expensive Ni-based superalloys in parts of the gas turbine with cheaper Cr-based alloys. Cr-based alloys have other advantages besides a low cost, such as a 400-500 °C higher melting temperature and 2-4 times higher thermal conductivity. However, challenges such as decreased high temperature strength and ductility, and lower oxidation and corrosion resistance compared to Ni-based superalloys need to be overcome before the Cr-based alloys can be applied in gas turbines. Dorcheh and Galetz [32] have reviewed the challenges with using Cr-based alloys with focus on their oxidation resistance and reported volatilization and nitridation to be the major obstacles for the use of these alloys in air above 900 °C. Gu et al. [33] also pointed out embrittlement resulting from nitridation during high temperature air exposure as a major problem for Cr-based alloys and reviewed various strategies for improving the high temperature strength and other mechanical properties. It is worth noting that the addition of water vapour to a N_2-1%O_2 atmosphere has been found to decrease and even completely supress the nitridation of high purity chromia [34]. Thus, in this respect, fuelling with hydrogen (and the resulting increase in water vapour) may actually prove to be beneficial.

The desire to operate gas turbines at higher efficiencies and with hydrogen as the fuel puts even stronger requirements on the combustor materials due to the increase in temperature and steam content. Alternative alloys such as oxide-dispersion-strengthened (ODS) superalloys, ferritic alloys (*e.g.* PM2000 and Incoloy MA956) and ceramic matrix composites such as SiC/SiC based composites are therefore being considered [20,21,35]. ODS superalloys are advanced high temperature materials able to retain strength up a high fraction of their melting point and are therefore attractive to use for the hot gas path components [36]. However, high costs and a brittle nature limiting how large the ODS components can be made, restricts the use of ODS superalloys mostly to aircraft turbine vanes.

SiC/SiC ceramic matrix composites (CMC) have been used as an alternative to Ni-based superalloys in the hot section of commercial aircraft turbine engines for the last few years. Compared to Ni-based superalloys, the CMCs offer a lower weight and better resistance to higher operating temperatures. This reduces some of the need for internal cooling, which improves the turbine efficiency. During service, the SiC will form a slow growing, dense layer of SiO_2 on the surface, which greatly slows down further oxidation. Because of the high volatility of SiO_2 in humid conditions (see Section 3.1.4) the CMCs have to be coated with environmental barrier coatings such as rare earth (Yb, Y, Mo - Yb_2SiO_5 and $MoSiO_2$) disilicates. As will be further discussed in Section 3.1.4, hydrogen-fuelling of the gas turbine will likely strengthen the need for coatings with a low Si-volatility due to the higher steam content in the combustion gas.

2.3   Turbine components

In the turbine expansion stage, the hot exhaust gasses from the combustor are passed through a series of discs and vanes connected to a drive shaft that transmits the generated power. The temperature of the turbine inlet can be up to 1300-1600 °C and decreases towards the outlet. The turbine discs have to tolerate the axial loadings from the blades attached to it and the thermal, vibrational and centrifugal stresses during operation. This requires the turbine discs materials to have superior tensile strength, creep and high fatigue strength, as well as resistance to oxidation and corrosion attack. For turbine discs operating at the highest temperatures, Ni-based superalloys are preferred [21]. Cast and wrought processing is commonly applied for Ni-based alloys like IN718, IN706, Waspaloy and U720Li [21]. To mitigate some of the challenges with obtaining large forgings of segregation-free Ni-based superalloys by forging, machining and welding, the alloy Udimet 720Li has been developed specifically for land based gas turbines [23,37].

Turbine blades and vanes are exposed to elevated temperatures, rotational and gas bending stress and thermo-mechanical loading cycles during start-up and shut down. The gas temperature at the turbine

7

entry can exceed 1350 °C. The elevated temperatures and stress may lead to creep, requiring alloys with excellent creep strength, tensile strength and toughness. In the colder end of the turbine (< 800 °C), bare Ni-based superalloys can be used, while air cooling and thermal barrier coatings are used in the hotter end to avoid severe corrosion and erosion (see Section 2.4).
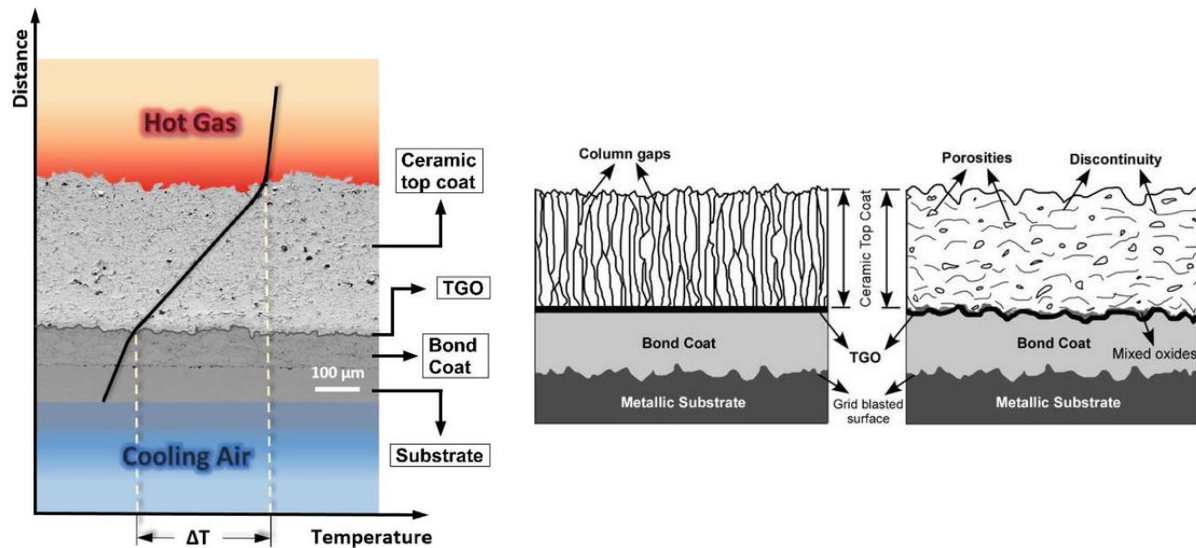
The alloys and processing methods for this application have evolved from conventionally cast Ni-base superalloys, to directionally solidified alloys, followed by the single crystal technology development. The single crystal alloys are categorised into generations based on the Re and Ru content. Re-free (CMSX-7) and low Re (CMSX-8) content alloys have been developed as 6th generation of single crystal alloys, but 2nd generation alloys, such as CMSX-4, René N5 and PWA 1484 with 3% Re are still commonly used [25]. The alloy development has enabled an increased temperature tolerance, from around 800 °C for the first generation of polycrystalline superalloys up to ca. 1100 °C for the newest single-crystal superalloys. In parallel, the creep strength has been improved by higher levels of alloying (Al, Ti, Ta, Re, W, Ru) to increase the content of the γ' strengthening phase [38]. Higher levels of alloying by addition of refractory elements such as Mo, W, Re and Ru also increase the thermal stability [39]. However, while this approach provides an excellent creep resistance, it reduces the corrosion resistance, thereby putting stronger requirements on the thermal barrier coatings [20,21,23,24]. Like the combustion parts, the components in the turbine expansion stage will be exposed to higher temperature and a greater steam content with the switch from natural gas to hydrogen fuelling. The impact this may have on the durability of these components is discussed in Section 3.

Material development for turbine blades and vanes is lately directed towards additive manufacturing (AM), which is a cost-effective processing route for superalloys. This manufacturing approach necessitates the development of new alloy compositions, optimised for the rapid and repeated thermal cycles specific to 3D printing and for reducing the influence of metallurgical defects such as porosity and cracking [39–42]. Section 5 is focused on additive manufacturing and its applicability to hydrogen gas turbines and material aspects, such as corrosion resistance, hydrogen embrittlement and dynamic embrittlement due to the particularities of AM parts.

2.4 Thermal barrier coating systems

Thermal barrier coatings (TBC), together with improved cooling technology, enable the operating temperature of gas turbines to be increased beyond the melting temperature of the structural alloy, with significant gains in the gas turbine efficiency. The TBC system comprises a ceramic top coat, a thermally grown oxide layer and a metallic bond coat, as illustrated in Figure 4. The ceramic top coat is based on low thermal conductivity materials and is usually quite thick (> 500 μm) to maximize the thermal resistance. The most common commercially used TBC material is ZrO_2 stabilized with 7 wt.% Y_2O_3 (7YSZ) [43]. This composition has a high melting point of 2700 °C and a low thermal conductivity of 2.3-4.2 W/mK (for a dense, sintered sample [44]). The thermal conductivity can be further reduced to 0.8-1.3 W/mK by tailoring the microstructure and porosity [45,46].

The metastable, non-transformable tetragonal phase (t') of YSZ is the desired state as this has a high bend strength, fracture toughness, and thermal shock resistance. When aged at temperatures above ca. 1200 °C, the t' phase undergoes a phase transformation into the cubic (c) and equilibrium, transformable tetragonal (t) phases [47,48]. Upon cooling, the t phase is transformed to a monoclinic phase, which is associated with a volume change that causes high stresses and thereby risk of coating spallation. Much of the development work on improving YSZ has focused on increasing the stability of the non-transformable tetragonal phase at higher temperatures by adding alternative stabilizers such as CeO_2, Sc_2O_3 and TiO_2 [49,50].

Figure 4 (a) Thermal barrier coating system (TBC); (b) Schematic general structures of TBC produced by (b) EB-PVD method, (c) APS method. Reprinted with permission from [51].

The TBC ceramic top coat is commercially fabricated using atmospheric plasma spraying (APS) or electron-beam physical vapor deposition (EB-PVD) while alternative deposition methods such as suspension plasma spraying (SPS) or plasma-spray physical vapor deposition (PS-PVD) are under development [50]. The different deposition techniques result in different coating microstructures (Figure 4), which can have a significant effect on the coating properties such as fracture toughness and thermal conductivity. Coatings fabricated by APS have horizontal splats that result in a lower thermal conductivity compared to the columnar structure formed by EB-PVD. On the other hand, coatings produced by EB-PVD have a higher strain tolerance and a smoother surface, providing better aerodynamics [52]. APS is cheaper and better suited for coating large components – it is therefore the preferred method for coating parts for large-scale land-based turbine parts while EB-PVD is usually reserved for the more demanding components, *e.g.* the leading edge of an air foil [19].

The adhesion between the sprayed YSZ layer and the alloy substrate is typically weak and the YSZ layer does not provide much protection against oxidation as the coating is porous and YSZ is a good oxide ion conductor. A bond coat, having high affinity for both the ceramic YSZ layer and the metallic substrate is therefore applied to improve the adhesion and oxidation resistance. The bond coat used with Ni-based superalloys is usually a thin metallic layer (*e.g.* NiAl) that forms an aluminide by interdiffusion with the alloy, or an overlay type coating based on NiCrAlY [53]. For both systems, Al is an essential component that forms a thermally grown oxide (TGO) of alpha-alumina during operation. The TGO is slow-growing and thereby protects the underlying alloy against high temperature oxidation. The YSZ top coat, the bond coat and TGO are commonly referred to as the TBC system (Figure 4).

The main challenges with current TBC systems are failure due to cracking, spallation or growth of undesired oxides between the top coat and the bond coat [54]. In the temperature range of RT-900 °C, the thermal expansion coefficient (TEC) of Ni-based superalloys ($14-16 \times 10^{-6}$ K^{-1} [55]) is similar to the TEC of NiCrAlY-type bond coats ($13-14 \times 10^{-6}$ K^{-1}[56]), while the TECs of the YSZ top coat (10×10^{-6} K^{-1} [57]) and the alpha-alumina TGO (9.6×10^{-6} K^{-1} [58]) are much lower. The mismatch in TEC between the alloy and different layers of the coating can lead to cracking and spallation during thermal cycling [54]. Martena et al. [59] used a finite element method to analyse the stress distribution in a TBC system due to growth of the TGO and thermal expansion misfits and showed that delamination of the TBC could be attributed to stresses normal to the top coat/TGO interface, which grew with increasing TGO

9

thickness. Even with relatively thin TGO layers, a tensile stress nearly equal to the tensile strength was imposed on the TGO during cooling and subsequent heating to the maximum peak temperature. One approach to reduce the stress due to thermal expansion mismatch is to intentionally introduce cracks and/or pores in the coating that can aid stopping a crack from propagating [50]. Ensuring a high roughness of the bond coat/top coat interface is another way to improve the top-coat adherence and the thermal fatigue resistance of the TBC [60]. The proposed explanation for this is that the compressive out-of-plane stress in the concave regions of the interface hinder crack propagation [61].

The temperature gradient across a coated and air-cooled gas turbine component can be as much as 200-300 °C. As mentioned in the introduction, a higher water vapour content resulting from fuelling with hydrogen will increase the heat transfer coefficient of the gas. If this is compensated by increasing the mass flow rate of the blade air cooling, the thermal gradient across the TBC will become even higher. The increased temperature gradient may accelerate some modes of cracking and degradation of the coating [96]. Dong et al. [62] showed experimentally and by modelling that an increasing temperature gradient decreases the cyclic lifetime of TBCs following a power function. These challenges necessitate the development of new TBCs with even lower thermal conductivity and/or higher fracture toughness, and alloys that retain the desired mechanical properties at a higher temperature.

Among the materials that have been researched as alternatives to replace the YSZ top coat are hexa-aluminates (*e.g.* $LaMgAl_{11}O_{19}$ [63]), perovskite oxides (*e.g.* doped $SrZrO_3$ [64]), Yttrium aluminium garnets (YAG)[65], and pyrochlores (*e.g.* $Gd_2Zr_2O_7$ [50,66]). The pyrochlores are considered to be one of the most promising candidates because of their high melting point, low thermal conductivity and greater resistance against calcium magnesium aluminosilicate (CMAS) attack compared to YSZ (see Section 4.1) [50]. However, the poor chemical compatibility between pyrochlores and the alumina TGO layer requires the use of YSZ as an intermediate diffusion-barrier layer [27], as illustrated in Figure 5. Alternative bond coats under consideration are Al_2O_3 forming MAX phases such as Cr_2AlC [108] and Ti_2AlC [109]. The MAX phases are polycrystalline nanolaminates of ternary carbides and nitrides, named from their general formula of $M_{n+1}AX_n$ (where M is a transition metal, A is an A group (mostly IIIA and IVA) element, X is C and/or N, and n = 1 to 3).These compounds are very oxidation resistant at temperatures up to 1300 °C, however, they are susceptible to volatilization in high pressure and high gas velocity environments [109], making them perhaps less suitable for the conditions of a hydrogen fuelled gas turbine.

Marra [37] reported on the development of various gas turbine coatings and alloys and their performance in natural gas and syngas with high hydrogen content, in a high heat flux rig. Bond coats derived from the state of the art (SoA) Siemens bond coat (Sicoat® 2464) with addition of 1.5wt.% of Nd, Ce and Hf and with increased roughness for improving the TBC adhesion were investigated. The Hf and Ce containing bond coats demonstrated increased oxidation and poor oxide scale adhesion of the TBC during isothermal furnace cycling at 1010, 1080 and 1121 °C in air. The Nd containing bond coat showed 30% longer life when compared to the baseline Re containing bond coat and improved the adhesion of the TBC but demonstrated poor strain-to-crack mechanical properties. Other bond coats based on MCrAlY, *i.e.* NiCrAlY (NI-1154) and NiCoCrAlY (Ni-1155) demonstrated superior oxidation resistance and similar or better mechanical properties. The NiCrAlY based bond coat enabled 100 °C increase in operating temperature compared to the baseline composition, evaluated based on the time before depletion of the alumina-rich phase.
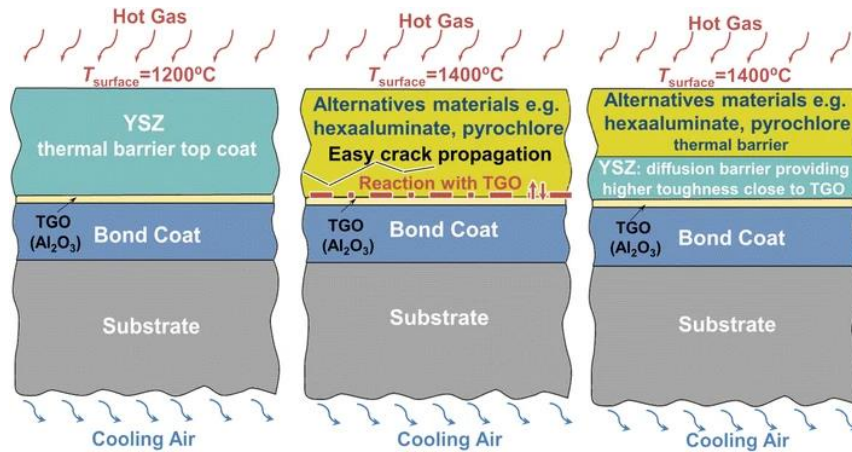
Figure 5 Double layer structure for TBCs working at higher temperatures, after [67].

The lifetime of the TBC system can in some cases be limited by the bond coat, either because of growth of the protective TGO layer beyond a critical thickness for spallation, or because of Al depletion from the bond coat below the level necessary to sustain the TGO formation [68]. Such depletion will allow other, less protective and faster-growing oxides of Cr and Ni to form. A sufficient reservoir of Al in the bond coat is thus essential for a long component lifetime. Evans and Taylor [69] introduced the concept of *diffusion cells* to explain the bond coat failure in plasma sprayed TBC systems. The diffusion cells were described as internal planes of alumina within the bond coat that are formed at splat boundaries within the bond coat due to faster oxidation in this relatively porous region. The diffusion cells block the supply of Al across the coating, thereby causing enhanced depletion of aluminium.

2.5 Environmental barrier coatings

Hot-section components made out of SiC-based CMC require a different coating system than the Ni-based superalloy as the coating in this case needs to prevent volatilization of Si-containing compounds (see Section 3.1.4). The coating systems applied onto CMC are typically dubbed environmental barrier coatings (EBC). The selection of materials is limited by the requirements of a close TEC match to SiC (3-5×10^{-6} K^{-1} in the temperature range RT– 1000 °C [70]). The most promising EBC candidates are celsian-phase silicates such as (Ba,Sr)O-SiO_2-Al_2O_3 (BSAS) and rare-earth (RE) mono- or disilicates (RE_2SiO_4 and $RE_2Si_2O_4$), which sometimes are combined with a Si bond coat layer to ensure better adherence to and compatibility with the SiC substrate (Figure 6) [52,71,72]. For the EBC system, SiO_2 is formed as the TGO instead of Al_2O_3.

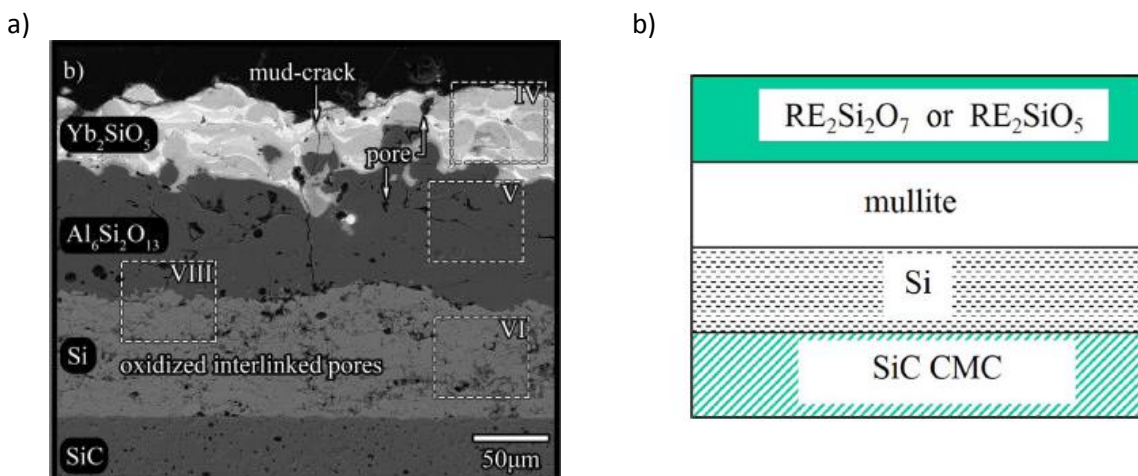a)   b)

Figure 6 a) EBC system fabricated by plasma spraying, after 20 h anneal at 1300 °C, from [73]. b) schematic of the EBC system, from [72]. Reprinted with permission from Elsevier.

Increasing the operating temperature of turbines with CMC components requires the addition of a low thermal conductivity TBC on top of the EBC. The current solution is to use conventional TBCs such as zirconate or hafnate to provide the extra thermal insulation, but the high TEC of these materials makes the solution sensitive to failure during thermal cycling, especially after long periods of operation when the strain tolerance of the TBC has been reduced due to sintering. Rare-earth pyrosilicate solid-solution ceramics (*e.g.* $Y_xYb_{(2-x)}Si_2O_7$) have been proposed as a promising "single-layer" alternative to replace both the EBC and the TBC [110]. But more work is needed to improve the APS of these coatings in order to achieve the desired microstructure and crystallinity. Further increase of operating temperatures may also require the replacement of the Si bond coat, which has a melting point of 1414 °C.
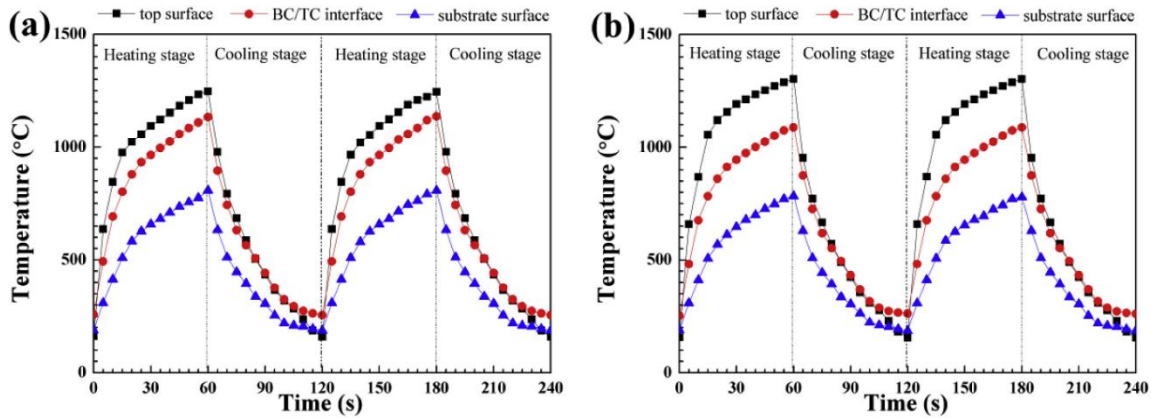
3   High temperature oxidation of gas turbine components

As already mentioned in the introduction, even assuming similar target flame temperatures in the transition from hydrocarbon fuels to hydrogen (in order to conserve cycle efficiency), hydrogen-firing of gas turbines can result in a significantly higher heat flux to the combustor's walls (due to lower quenching distance), in a higher flow velocity (to mitigate flashback), and in a higher steam content. The following sections will focus on how these changes to the operating conditions influence oxidation and other degradation mechanisms of the gas turbine components. The influence of additive manufacturing on the corrosion resistance and dynamic embrittlement of components for hydrogen gas turbine is discussed in Section 5.2.

The working conditions of a gas turbine are difficult to replicate in a laboratory setting; both in terms of the high temperatures, gas velocities and steam content, and in terms of the thermal gradient across a component resulting from the cooling applied on one side. There are only a few laboratories that have the capability of accurately replicating such conditions ex-situ, and different set-ups have been constructed to simulate as accurately as possible the gas turbine conditions. For example, some researchers have employed capillary tubes to impinge H_2O jets on the surface of a sample, achieving gas velocities up to 300 m/s [74,75]. However, most studies concerning the oxidation resistance of Ni-based superalloys and thermal barrier coatings employ even more simplified set-ups with modest gas velocities and no thermal gradients. It is important to interpret these results with care, as the "milder" conditions during an ex-situ test may give a false picture of how the components will perform during actual operation in a gas turbine.

One potential pitfall is to neglect the difference in gas velocity and how this influences the evaporation rate of volatile oxides. For example, Mumm et al. [76] pointed out that a volatilization-redeposition mechanism observed in a lab test utilizing modest gas flow rates of 40 ml/min is less likely to be present in an actual gas turbine where the much higher gas flow rate likely will carry away the volatilized species (preventing redeposition). Furthermore, the volatilization observed when studying the alloy, bond coat or TGO isolated may not be transferable to the volatilization from this component in an actual system where these components are overlayed by a YSZ top coat. The volatilization of elements from gas turbine materials will be discussed further in Section 3.1.

Another important difference between component tests and real operation in a gas turbine is the thermal gradient across a gas turbine component resulting from the internal air cooling. As illustrated in Figure 7 for aeroturbines, the temperature difference between the surface of the substrate and the top surface of the coating can be as much as 450 °C. This gradient results in a higher stress level and a different stress distribution in the gas turbine compared to an ex-situ test under isothermal conditions [77]. Thus, a component that survives several ex-situ thermal cycles without spallation may potentially fail when extra stress is imposed on it by the thermal gradient. The geometry of the component is also
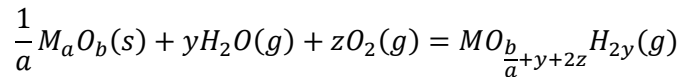
an important factor when evaluating the stresses experienced by the gas turbine blade, as pointed out in refs [78,79]. Even the more sophisticated set-ups such as the above mentioned capillary tube has potential pitfalls, *e.g.* the very small area of the sample that is corroded relative to the large inhomogeneities in the microstructure of a TBC. Nevertheless, the simplified studies are important to increase the fundamental understanding of the oxidation process and how this is influenced by singular factors such as the temperature, gas velocity and gas composition.

Figure 7 Temperature gradient profiles of the TBC layer: top surface (black), interface bond coat – top coat (red) and at the substrate surface (blue) for a) 100 µm and b) 200 µm TBC layer, Reprinted from [77] with permission from Elsevier.

3.1 Effect of increased steam content

It is well established that the presence of water vapor can increase the oxidation rate of alloys and the volatilization of many oxides [80,81]. The mechanism for the influence on the oxidation rate depends on the alloy, while the increased evaporation rate is related to the fact that many oxides volatilize in oxidizing and humid conditions according to the following reaction:

$$\frac{1}{a} M_a O_b(s) + y H_2 O(g) + z O_2(g) = M O_{\frac{b}{a}+y+2z} H_{2y}(g)$$

The following sections will discuss the role of steam in the oxidation and volatilization of various materials used in gas turbines.

3.1.1 Chromia-forming alloys

Many Fe-based alloys that under dry conditions form a slow-growing chromia scale exhibit rapid break-away oxidation when water vapor is present. This has been linked to the volatilization of the Cr_2O_3 scale by the formation of $CrO_2(OH)_2$, for which the rate of volatilization increases with increasing pH_2O and increasing gas velocity [82,83]. Break-away oxidation can take place either because the volatilization of the Cr_2O_3 proceeds faster than the re-growth by oxidation, or because of the alloy with time becomes depleted of Cr below the limit required to sustain re-growth of the chromia scale [83–85]. In extreme cases of a thin component and conditions promoting high evaporation rates, the Cr vaporization may lead to void formation within the alloy bulk, which severely degrades the mechanical properties of the component [85].

Since the volatilization of Cr_2O_3 requires oxygen to be present (cf. reaction above) it is usually insignificant in wet H_2-containing atmospheres. However, water vapor has been shown to influence the oxidation rate of chromia-forming Fe-based alloys under these conditions. For example, Hooshyar et al. [86] reported that the stainless steel 304L forms a duplex scale of inward-growing $(Fe,Cr)_3O_4$ and outward-growing Fe_3O_4 in a range of Ar-H_2-H_2O mixtures at 600 °C, whereas a thin Cr_2O_3 scale is formed

13

in 5%O_2-N_2. The rate of oxidation increased with increasing pH_2O, also when the activity of O_2 was kept constant. Based on oxidation studies of pure chromium, Henry et al. [87] proposed that an increased oxidation rate in steam is because of the faster diffusion of the smaller hydroxide ion compared to the oxygen ion, while Hultquist et al. attributed it to the uptake of hydrogen leading to faster cation diffusion through the scale [88].
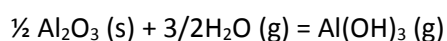
The effect of water vapor on the oxidation of Ni-based chromia forming alloys is more complicated. Some authors report that a wet H_2-containing atmosphere is more corrosive than oxygen [89], while others report slower growth of the oxide scale in wet oxygen/air compared to dry conditions [90]. This apparent discrepancy may be explained by the Cr evaporation kinetics of Ni-based alloys. Sand et al. [91] showed that the Cr vaporization rate from the alloy 690 decreases with time during exposure to humidified air, as the initial chromia-rich scale gradually is replaced by a Ni-rich and Cr-poor scale that mitigates further evaporation of Cr. It should be noted that the time needed to transition from a chromia-rich to a Ni-rich scale greatly varies with the exposure conditions, and that in the meantime the alloy may become depleted with Cr to a point where it has an influence on the mechanical properties [92]. For Ni-based alloys applied at very high temperatures, the volatilization of Ni should be considered. The evaporation rate of Ni from a NiAl$_2$O$_4$ spinel at 1125 °C and 200 sccm (standard cubic centimetres per minute) is in the range of 10^{-11}-10^{-10} kg/m^{2}s, depending on the pH_2O [76], which is of the same order of magnitude as the evaporation rate of Cr from ferritic stainless steel at 850 °C.

3.1.2 Alumina-forming alloys and bond coats

Water vapor is reported to have an adverse effect on the ability to form protective α-alumina scales on both Ni-based and Fe-based alumina-forming alloys [93]. An oxidation study of Ni-Cr-Al model alloys found that a higher concentration of Al was required to form α-alumina when the alloy was oxidized in air with 30 vol.% H_2O compared to when it was oxidized in dry air [94]. The inability to form a protective α-alumina scale was linked to a change in the scaling morphology – fewer, but larger internal precipitates were formed in humid air compared to in dry air, making it more difficult to form a continuous α-alumina scale by lateral growth. In studies of Fe-based alumina formers, it was suggested that the adverse effect of water vapour is caused by a stabilization of the γ-alumina phase that is normally formed during the transient stage of oxidation [95,96]. In dry conditions, γ-alumina is converted to the slower growing α-phase, but in wet conditions this transition is hindered, likely due to hydroxylation of the γ-alumina surface. This theory is supported by fundamental investigations into the effect of water vapor on the formation and stability of alumina by Sohlberg et al. [97]. The authors described γ-alumina as a "reactive sponge" that can store and release water in the form of hydrogen, which is compensated by the expansion of the alumina spinel lattice and the formation of Al vacancies.

Another observed negative effect of water vapor is decreased scale adhesion, or increased tendency for scale spallation, particularly during thermal cycling [80,93,98]. Often, the spallation occurs at room temperature after the sample has been exposed to H_2O at higher temperatures. This so-called moisture-induced delayed spallation (MIDS) of alumina-forming alloys has been attributed to hydrogen embrittlement of the alloy-scale interface [99]. MIDS takes place even at ambient levels of humidity in the atmosphere and there are no studies known to us that have investigated whether the mechanism is promoted by higher concentrations of water vapour.

Volatilization of alumina may take place according to the following reaction:

$$\tfrac{1}{2}\,Al_2O_3\,(s) + 3/2H_2O\,(g) = Al(OH)_3\,(g)$$

There are reported observations of Al evaporation at 1100 °C [84], but the vapor pressure of Al(OH)$_3$ is so low below 1300 °C that the vaporization of alumina has been considered as negligible under most

conditions [93]. However, given the strong dependency of the $Al(OH)_3$ vapor pressure on the pH_2O, this reaction may become significant in hydrogen-fuelled gas turbines where both the water vapor content and temperature are higher compared to natural gas fuelled turbines. According to thermodynamics, the vapor pressure of $Al(OH)_3$ in 0.5 atm of water vapor and 0.5 atm of oxygen will increase by more than four orders of magnitude from 1000 to 1400 °C [100].
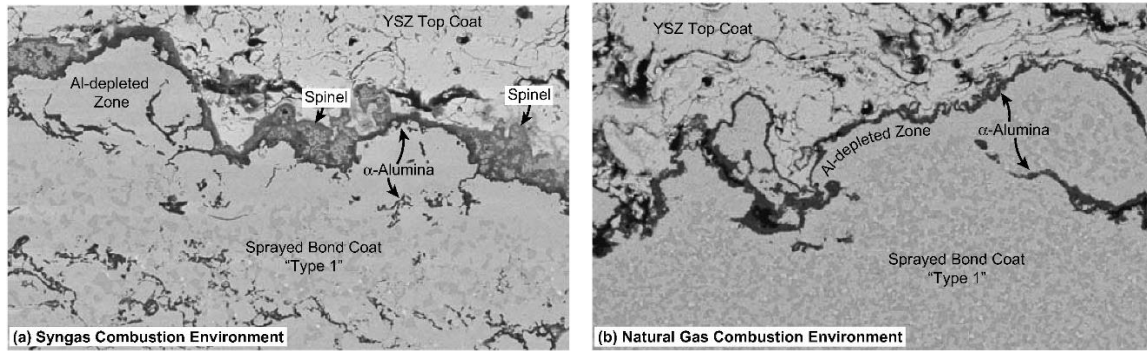
3.1.3 Thermal barrier coatings

Since the components exposed to the highest temperature will be coated with a TBC system, the stability of YSZ and the bond coat material at higher temperature and steam contents should be considered. There have been several studies to determine the durability of TBC and bond coats under various levels of water vapour content:

Sumner et al. [101] tested gas turbine blades in a simulated H_2-rich syngas composition with 20 vol% H_2O over 1000 h. The combustion temperature was up to 1440 °C, but air cooling was used to limit the blade surface temperature to 950-1050 °C. The blades were made of the Ni-based superalloy Rene 80 and coated with either a high velocity oxy fuel (HVOF) metallic coating (Sicoat® 2464, NiCoCrReYAl) or different combinations of a thermal barrier coating (YSZ-based) and a bond coat. After exposure, the TBC surface appeared with a red/brown coloration, suggesting the formation of Fe-rich oxide deposits, deriving from gaseous iron oxides/hydroxides present at higher gas temperatures in the hot gas flow, that condensed below ~1100 –1200°C. The TBC had delaminated at the leading edge of the blade, possibly due to erosion or imperfections in coating manufacturing.

Zhou et al. [102] studied the oxidation kinetics of nickel based superalloys in O_2 and O_2-5%H_2O at 1050 °C. The alloys were coated with a plasma sprayed NiCrAlY (Ni-28Cr-6Al-0.4Y wt.%) bond coat and a 7.5 wt.%Y_2O_3-ZrO_2 TBC. In dry O_2, parabolic oxidation kinetics were followed with a very low oxidation rate and the oxide formed on the bond coat layer was Al_2O_3. In O_2-5%H_2O, the oxidation kinetics were almost linear after long exposure times and the interfacial scale between the bond coat and the TBC was in this case composed of $Ni(Al,Cr)_2O_4$, NiO, Cr_2O_3 and Al_2O_3. An increase in Ni and Cr cation transport in the presence of water vapor was suggested as a possible explanation for the increased degradation rate.

Cernuschi et al. [103] evaluated the sintering kinetics and phase stability of 7YSZ, YSZ-GZO, and YAG coatings prepared by APS after aging as freestanding samples for 500 h in the temperature range of 1000-1250 °C. The authors found no clear evidence that the thermal diffusivity, thermal conductivity or phase composition of the coatings was different when aged in air with 20 vol.% H_2O compared to dry air. The morphology and density of the coatings was concluded as being more important for the thermo-physical properties than the aging environment.

Results from testing MCrAlY bond coats in industrial gas turbines show that fuelling with syngas (CO+H_2) instead of natural gas results in the formation of a thick (30 µm) non-protective spinel-alumina layer between the bond coat and a YSZ top coat instead of a thin (ca. 1 µm) protective α-alumina layer, see Figure 8 [104]. The spinel layer is susceptible to cracking and weakens the TGO/YSZ interface. Sullivan and Mumm [104] attributed the formation of the spinel phase to the higher water vapour content in the combustion gas when fuelling with syngas compared to natural gas. They performed a comprehensive series of tests with different bond coat materials in varying pH_2O and pO_2 environments, focusing on the transient stage (0-5 h) of oxidation. The surface coverage by a $(Ni,Co)(Al,Cr)_2O_4$ spinel was increased with increasing pH_2O up to ca. 15 vol.%, whereafter the coverage plateaued and slightly decreased. Interestingly, spinel formation was promoted at low pO_2 when water vapor was present. Sullivan and Mumm postulated that water vapor elongates the γ and δ alumina stages, which enables the diffusion of spinel forming cations across the normally protective TGO layer.

Figure 8 Cross sectional images of a TBC tested in an industrial gas turbine operated with syngas (a) and with natural gas (b). Reprinted from [104] with permission from Elsevier.

From the above results it is clear that water vapor has an adverse effect on the TBC lifetime. Whether the rate of degradation is increased by increasing the water vapor content beyond 10-20 vol.% is however less clear, as will be seen from the following summary of literature.

Haynes et al. [100] investigated the effect of water vapor on the oxidation behaviour of a TBC system comprising an APS YSZ top coat and a HVOF-deposited NiCoCrAlY bond coat deposited on a single crystal Ni-based superalloy. The average TBC lifetime (defined by onset of spallation) during thermal cycling was reduced by at least 20% in air with 10 vol.% H_2O compared to when cycling in dry O_2. Increasing the water vapor content to 50 vol.% did not lead to any further decrease in the lifetime compared to 10 vol.%.
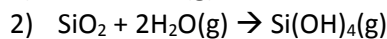
Pint et al. [105,106] reported that the lifetime of Pt diffusion coatings (γ+γ' bond coats) was hardly affected by water vapor, while the lifetime of a Pt β-aluminide coating (β coating) was almost halfed in 10 % water vapor. This effect may be asociated with the orientation of the β aluminide, leading to formation of non-uniform, epitaxially oriented, cubic metastable alumina scales before the nucleation of an α-Al_2O_3 phase. Interestingly, the lifetime was seemingly less affected when the steam content increased further to 50 and 90 %. For both types of coatings, a thicker TGO layer was formed in humid conditions than in dry. Pint et al. [82] also evaluated the lifetime of NiCoCrAlYHfSi-coated X4 and 1483 substrates with an APS YSZ top coat in dry and humidified O_2 and air at 1100 °C. The lifetime, defined as the number of 1 h cycles before spallation of the YSZ top coat, decreased with the addition of water vapor. A shorter lifetime was obtained for the 1483 substrate compared to X4, which was attributed to the lower Al content in the former. Also in this case there was no increase in the adverse effect with increasing water vapor content.

Lance et al. [98] studied thermal cycling of the single-crystal nickel-based superalloy PWA 1483 and X4 with HVOF processed NiCoCrAlYHfSi bond coatings and an air plasma sprayed YSZ top coat. Alloy 1483 does not contain Re like many other single crystal superalloys, and is therefore less expensive, while alloy X4 is a second-generation alloy containing 3% Re. The oxidation and cycling resistance were studied in dry air, and air with 10 or 50 vol% H_2O at 1100 °C with cycles of either 1 h (simulating air jet) or 100 h (simulating land-based turbine). With 1 h cycles, the increased water content was reported to decrease the lifetime of the components, while for the 100 h cycles the behaviour was inconsistent with the pH_2O. Degradation during 1 h cycles was attributed to stresses in the YSZ top coat while the degradation during 100 h cycles was more dominated by diffusion processes. Samples based on X4 had an overall longer (30-40%) lifetime than samples based on 1483, which was attributed to the higher Al content and possibly the higher Ti content in the former.

Nowak [107] studied the oxidation behaviour of polycrystalline super-alloy Rene 80 at temperatures up to 1120 °C in Ar-O_2 and air with various water vapor contents up to 20 vol.%. No major effects of H_2O were observed with a MCrAlY coating and with slow heating rates (10 K/min), while for higher heating rates (90 K/min), water vapor promoted the formation of meta-stable alumina during initial exposure. With an APS-TBC coating on top, the addition of water vapor shortened the lifetime due to decreased TGO adherence. At temperatures below 400 °C, water vapor enhanced the transformation from tetragonal to monoclinic zirconia, which was suggested to be the cause of the observed increase in degradation. The results suggests that the degradation caused by water vapor is more relevant for gas turbines operated with heavy cycling, such as aeroturbines. This is consistent with the results from Pint, Haynes and others showing that the degradation due to water vapor is more pronounced with shorter thermal cycles. For stationary, more continuous operations, this degradation mechanism should be less relevant.

3.1.4   CMCs and EBCs

CMC are prone to Si volatilization when exposed to steam containing atmospheres. The loss of SiC proceeds by forming SiO_2 as an intermediate. The predominant reactions are:

1) $SiC + 3H_2O(g) \rightarrow SiO_2 + 2H_2 (g) + CO(g)$
2) $SiO_2 + 2H_2O(g) \rightarrow Si(OH)_4(g)$

As suggested by the above reactions, the volatility of SiO_2 increases strongly with increasing partial pressure of water vapour ($\propto p_{H_2O}^2$) [108]. The loss of SiC is rapid, causing materials recession at order of 6-9 μm/h in high velocity steam jet [109]. The evaporation reaction has a weak temperature dependence, making evaporation of SiO_2 a challenge also at modest gas turbine operating temperatures [108]. For this reason, the SiC CMC applied in gas turbines are combined with environmental barrier coatings, as described in Section 2.5. Volatilization is not completely avoided as these coating materials also comprise Si, but it is greatly reduced compared to a non-coated SiC/SiO_2 surface. The evaporation rate from the coated material is proportional to the surface activity of Si, and for this reason RE_2SiO_4 is preferred over $RE_2Si_2O_4$, despite the latter having a better TEC match with the substrate [109,110].

4   Other types of degradation

4.1   Hot corrosion and CMAS attack

When low purity fuels containing sulphur and/or alkali metal contaminants are used, the hot gas components of the gas turbine are susceptible to a degradation form known as hot corrosion. This can for example be the formation of alkali sulphates (sulphidation) that degrade the TBC coating [50]. Due to the lower calorific value per mole of hydrogen compared to natural gas, the fuel/air ratio will be greater in a H_2 fuelled gas turbine. This implies that hot corrosion may become a challenge at lower levels of fuel impurities [20]. Hydrogen produced by electrolysis has typically a very high purity and is therefore less likely to cause hot corrosion, while by-product hydrogen may contain critical amounts of sulphur and other impurities.

Another "external" source of degradation is impurities such as sand, ash and dust in the combustion air, which can lead to so-called calcium-magnesium-alumino-silicate (CMAS) attack [111]. The CMAS deposits have an unfavourable microstructure and high TEC and thereby cause failure of the TBC or EBC. The CMAS degradation mechanism involves a number of thermally activated processes, making this degradation more critical for turbines operating at higher temperatures. On the other hand, as hydrogen turbines are operated with a relatively lower flow rate of air, impurities in the air are potentially less critical for hydrogen fuelled gas turbines compared to natural gas turbines.
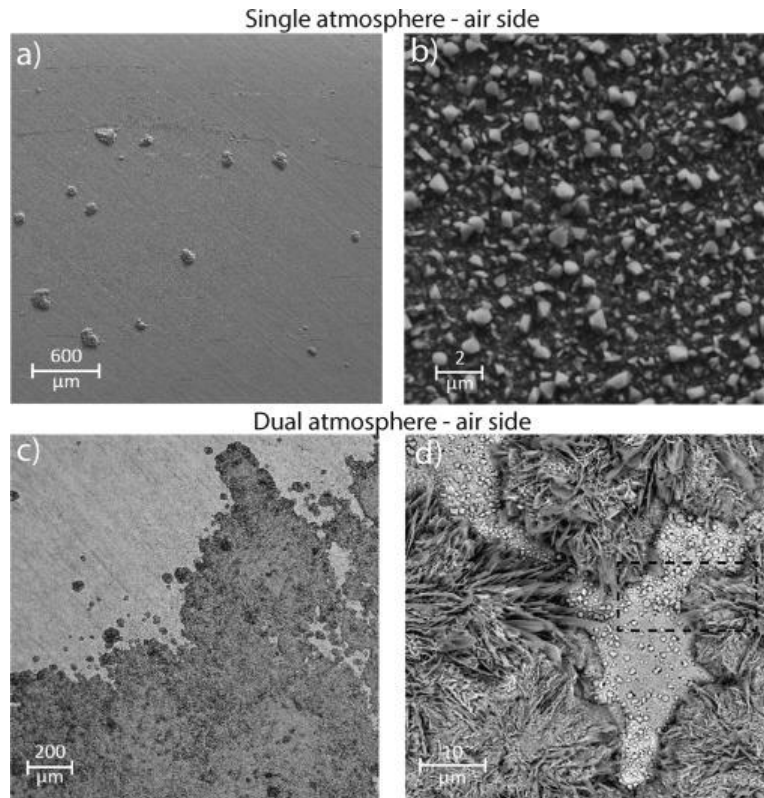
4.2 Dual atmosphere effect

High temperature corrosion of steel is typically studied in a single atmosphere replicating the service conditions. However, in some applications, the steel is simultaneously exposed to different atmospheres on each side of the specimen. An example is the gas turbine fuel injector, where the inner surface of the injector will be exposed to hydrogen, while the outer surface will be exposed to air. Such exposure to dual atmosphere can cause anomalous oxidation behaviour not observed when exposing the same steel specimen separately to the two atmospheres. The so-called dual atmosphere effect has been widely studied in the field of solid oxide fuel cells, where the steel interconnect is exposed to (humidified) hydrogen on one side and air on the other at temperatures between 600 and 900 °C [112–116]. In all cases, the anomalous oxidation behaviour is on the air side where formation of Fe-oxides is observed in dual atmosphere conditions on ferritic stainless steels that normally form stable Cr_2O_3 oxides under single air atmosphere conditions, see Figure 9. It has been suggested that steels having a lower Cr content are more susceptible to the dual atmosphere effect [112,116] and that the effect becomes more pronounced with decreasing temperature from 900 °C to 600 °C [115,117].

Several mechanisms have been proposed to explain the dual atmosphere effect. Hydrogen at the fuel side is believed to adsorb into the ferritic stainless steel (FSS) and migrate towards the air side. The presence of hydrogen defects is suggested to alter the defect structure near the alloy surface by the formation of metal vacancies, V_M''' [114,118]:
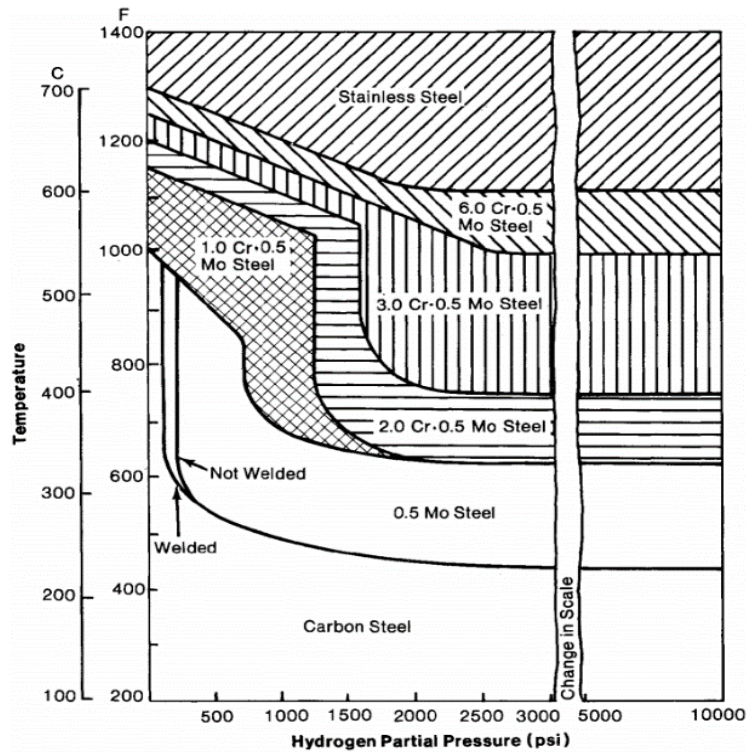
$$3[V_M'''] = p + [(OH)_O^{\cdot}]$$

where the hydrogen defects have been written in the form of OH-complexes on oxygen sites, p is the concentration of electron holes, and the metal is assumed to be 3-valent. The increased concentration of metal vacancies is expected to increase the diffusion of cations through the scale, thus increasing the likelihood of forming Fe-rich oxides on the surface [12]. This could explain why the Fe-rich nodules sometimes are reported to form along the grain boundaries of the alloy, seeing as these are typical high-diffusivity paths [119]. Another proposed explanation is that the presence of hydrogen depresses the p_{O_2} locally, thus promoting the formation of isolated Fe-rich nodules [120]. The presence of hydrogen could also lead to the formation of steam, resulting in porosity near the surface of the alloy [114,116]. The pores enhance inward oxygen transport, which typically leads to a faster oxidation rate and could even result in localized metal loss, which sometimes is observed in connection with the Fe-rich oxide nodules. Finally, it has also been suggested that the Fe-rich nodules are formed due to the surface on the air side having been made more acidic by the presence of hydrogen [121,122]. The higher acidity is believed to favour the formation of Fe_2O_3 relative to Cr_2O_3.

Figure 9 Surface SEM images of samples tested under single (air) or dual (air + H_2) atmosphere exposure, showing Cr_2O_3 oxide formation in air only and Fe-oxide formation under dual atmosphere conditions. Reprinted from [115] with permission under Creative Commons CC BY-NC-ND.

4.3 H-diffusion in alloys relevant for gas turbine application

Hydrogen embrittlement causes the loss of ductility, deterioration of material strength and mechanical properties of upon exposure to hydrogen. Hydrogen attack may occur by atomic hydrogen diffusing into the steel lattice. Inside the steel, the atomic hydrogen may accumulate at stress concentration regions such as vacancies, grain boundaries and other lattice defects and form molecular hydrogen resulting in a pressure built-up. The pressure may lead to voids and/or degradation of the ductility to a degree where the steel becomes brittle and cracks. Hydrogen may also react with dissolved carbon or oxygen in the steel to form methane or steam, respectively. In general, an increasing Cr-content in austenitic steels increases the maximum temperature and hydrogen partial pressure tolerated by the steel (Figure 10) [123,124].

Figure 10 Maximum temperature and hydrogen partial pressure for safe operation of steels in hydrogen service, reproduced from [124].
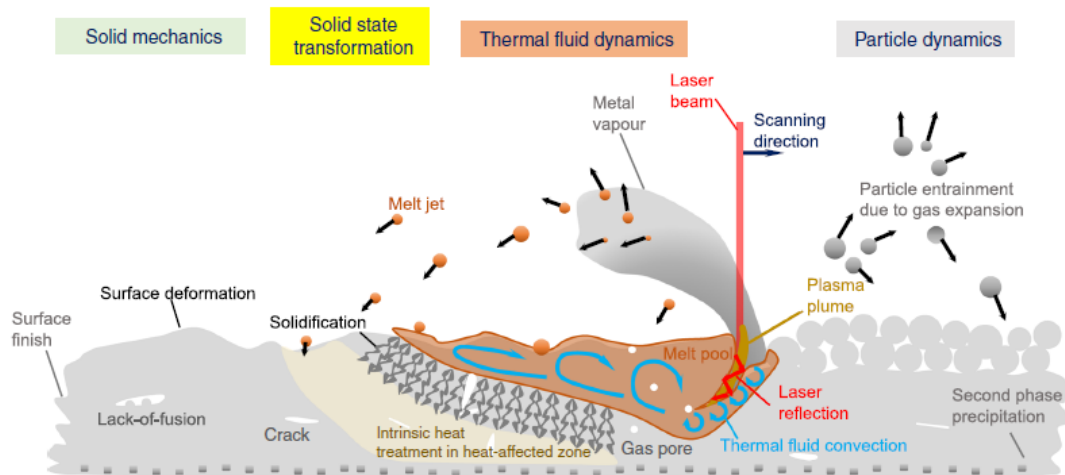
Ni based alloys are susceptible to hydrogen attack in a large temperature interval from -103 to 327 °C and Ti based alloys are susceptible to attach in the range of 0 to 93 °C [125]. An early work by Gray [126] reports on the embrittlement of several Ni-based superalloys such as Inconel 718, Udimet 700, Rene 41, Hastelloy X, and TD-NiCr after exposure to 0.1MPa gaseous hydrogen from 430 to 980 °C for 1000 h. All of the tested alloys absorbed substantial concentrations of hydrogen during the exposure, which was suggested to be interstitially dissolved and diffusible. The hydrogen could be removed and the ductility of the alloy regained by degassing at elevated temperatures. In more recent work, Balyts'kyi et al. [127] has studied the hydrogen embrittlement of gas turbine blade single crystal cast alloys such as SM-104-VI, SM-90-VI and SM-88U-VI at 30 MPa hydrogen pressure, at temperatures between 20 and 900 °C. The negative effect of hydrogen decreased with increasing temperature, but the authors reported a measurable decrease in strength and plasticity of the alloys even at 900 °C. The alloy SM-90-VI was reported as the least sensitive to hydrogen embrittlement. Hydrogen embrittlement of AM parts is discussed in Section 5.3.

5 Additive manufacturing

5.1 Additive manufacturing of materials relevant for gas turbine parts

Additive manufacturing is suitable for fabrication of gas turbine parts (blades, vanes, fuel injectors, impellers, swirlers, burners, combustion chambers, cladding, seals, housings) [128] and for the production of functionally integrated parts [129]. The technique can be used both for building new parts and for repairing damaged parts at worn areas, directly on the original parts [130]. Additive manufacturing is also used to address the challenges of fuelling gas turbines with hydrogen by the development of novel combustion technology with complex cooling profiles and fuel routing paths [131]. AM or 3D printing allows for the burner design to be adjusted on the inside without changing the exterior, which makes it easier to retrofit existing turbines to enable hydrogen operation. The method is currently limited by the available printing size [132].
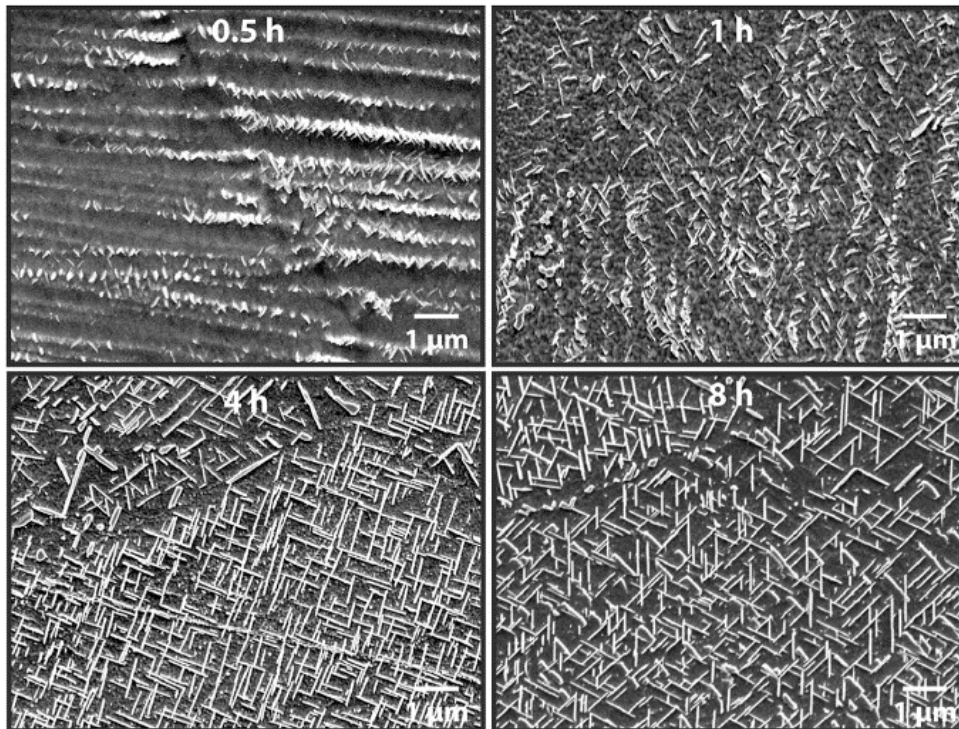
20

Nickel based superalloys are of particular interest for producing gas turbine parts by AM because of their excellent properties at elevated temperatures. However, the microstructure and grain structure are strongly influenced by the directional building, fast cooling and complex thermal cycles (reheating). The production of complex parts by additive manufacturing results in a non-equilibrium state of the processed material. An illustration of the physical phenomena describing the AM fabrication of metals by powder bed fusion is shown in Figure 11 [39]. The interaction of the laser with the metal powder generates the coexistence and interaction of solid, liquid, gas vapour and plasma. The rapid heating and cooling thermal cycles generate thermal gradients and determine the metastable nature of the chemical, structural and mechanical state of the system. Modelling of the physical phenomena is scarce, yet necessary to address the complexity of the system.

Figure 11 Physical effects that describe the AM of metals powders via the powder bed fusion (or SLM) fabrication method, Reprinted from [39] with permission under Creative Commons CC BY license.

Nickel-based superalloys rely on precipitation hardening and/or solid-solution-hardening while the precipitation of the γ' phase occurs upon cooling and is dependent on the cooling rate [30,133]. Ni-based superalloys like IN939, IN718, IN625 and Hastelloy X are commercially available for AM and have been studied to facilitate the understanding of processing, microstructure and properties. Fu et al. [131] described the microstructure resulting from selective laser melting (SLM) processing as characterised by fine, elongated grains that can recrystallize during heat treatment to form equiaxed and isotropic structures. In case recrystallization does not occur, the material remains anisotropic. Deng [133] studied microstructures and mechanical properties of electron beam melting (EBM) and SLM processed IN718. It was found that the EBM microstructure is characterized by columnar grains, elongated in the building direction while SLM resulted in a fine, dendritic microstructure. The as-built EBM microstructure was location-dependent with an irregular frame part having a weak texture. The strengthening phases γ'/γ'' precipitated during the AM processing and intermetallic phases with the AB_2 (laves phases) composition were observed. The mechanical properties of the fabricated samples were anisotropic, with higher tensile strength and lower elongation along the building direction. The strength was somewhat increased by heat treatment. The as-built SLM microstructure showed a weak texture, with fine laves phase in the interdendrites and no precipitation of the γ'/γ'' strengthening phases. The tensile properties and elongation showed anisotropy depending on the building direction. Homogenisation heat treatments demonstrated positive results in the segregation of the γ'/γ'' strengthening phases and for decreasing the anisotropy.

Zhang et al. [134] reported the formation of unwanted platelet-shaped δ phase precipitates (orthorhombic Nb and Mo rich phases, with a wide range of local compositions, *e.g.* Ni-20.20Nb-11.00Mo-8.70Nb-0.05C) upon stress relief thermal treatment of AM processed (by laser-sintering powder-bed fusion) Inconel 625 much faster than in wrought materials, in a matter of minutes instead of tens to hundreds of hours, as shown in Figure 12. Elemental segregation in AM materials was identified as the root cause for the δ phase precipitation. A subsequent homogenisation heat treatment was effective in removing the δ phase. It was concluded that alloy specific strategies should be developed to mitigate the effects of AM processing.

Figure 12 Surface micrographs of a 3D printed IN625 showing the formation of δ phase precipitates, initially at interdendritic regions, at 870°C after 0.5, 1, 4 and 8h, Reprinted from [134] with permission from Elsevier.

Shaikh [30] studied the effect of thermal treatments of IN939 Ni-based superalloy parts obtained by laser-powder bed fusion. Other Ni-based superalloys were as well reviewed. The results demonstrated notable differences in the fractions and morphologies of the γ' strengthening phases, in comparison with the conventional materials. The author specified that superalloys processed by laser-powder bed fusion are susceptible to cracking, with solidification cracking as the primary responsible mechanism. It was mentioned that post processing thermal treatments affect grain structure, morphology, distribution, and size of strengthening precipitates. IN939 could be produced free from defects and the thermal treatments applied resulted in excellent room temperature tensile properties.

Andersson et. al. [135] applied this approach for a burner repair in a specifically designed gas turbine via SLM indicating no defects on the surface of the 3D printed part. The porosity and inclusions levels were low in all examined parts with an average porosity of less than 0.09%. The presence of sulphur and some surface oxidation was observed up to 50 μm in the material after testing the 3D printed burner parts. Non-destructive and destructive tests showed that printed burners were in functional condition [135].

5.2   Corrosion resistance of steel manufactured by AM

The effect of microstructure of alloys produced by AM on corrosion resistance is discussed by Örnek [136] and Kong et al. [137]. Örnek characterised the microstructural features of additive manufactured metallic parts, such as porosity, structural gradients, chemical inhomogeneities, microstructural heterogeneities, texture, the formation of surface oxides, grain size, strain and stress, surface roughness and their influence on corrosion resistance. The author concludes that controlled microstructure has a significant importance for obtaining reproducible properties and that more systematic development of AM-materials should be made in parallel with corrosion studies to optimise corrosion properties. Kong et al. [137] also reviewed the influence of the internal microstructure, such as porosity, surface roughness, phase segregations, oxides, inclusions, and the corrosion properties. The authors point out the necessity of focusing on the optimisation of fabrication parameters and establishing a correspondence between key structural features and corrosion resistance. Laleh et al. [138] reviewed the corrosion behaviour of austenitic, precipitation-hardened, and duplex stainless steels processed by AM in comparison with the conventionally produced counter parts. The review addressed the corrosion resistance in acidic and NaCl solutions at room temperature. Important aspects that influence the corrosion resistance are the particularities of the AM manufacturing, such as the effects of porosity and defects, compositional differences generated by evaporation of alloying elements due to the high temperature laser, inclusions and interdendritic chemical segregation. The residual stress and non-homogeneous microstructure determine a more complex corrosion behaviour than for the conventionally processed steels.
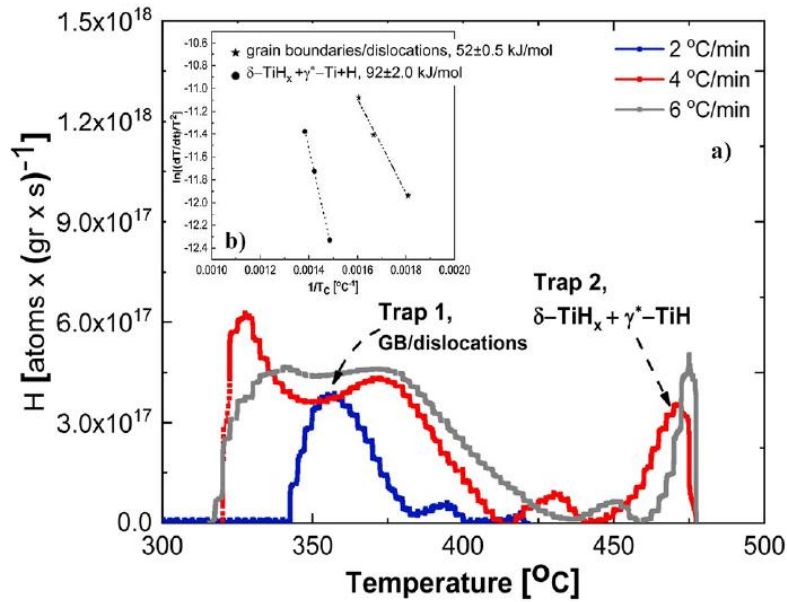
5.3   Hydrogen embrittlement of steel manufactured by AM

The susceptibility to hydrogen attack and other properties of metal parts obtained by additive manufacturing is the cumulated result of several factors like alloy design, microstructure, properties and AM processing conditions, describing the structure – property – processing – performance relationship. Several studies conducted on the hydrogen exposure effects on 3D printed specimens indicate optimised 3D printing manufacturing methods as suitable for producing metallic parts for hydrogen service and hydrogen infrastructure. The published literature in AM of austenitic stainless steels is focused mostly on 316L and 304L [139–143]. However, Seifi et al. [144] and Gorsse et al. [145] report on the technology readiness levels (TRL) in additive manufacturing for Ni-based superalloys (Hastelloy X, Inconel 625 and Inconel 718), Co-Cr alloys (Co28Cr6Mo) and Ti-based alloys (Ti-6Al-4V, Ti-6Al-4V ELI), with TRL 7-9. Other alloys are included such as tool steels (H13 and Maraging 300) with TRL 9, stainless steels (316L and 17–4PH) with TRL 7–8, Al-based alloys with TRL 4–8, Cu-based alloys, intermetallic (titanium aluminide), and low alloy steels (AISI 4140) with TRL 4–5 [146–149].
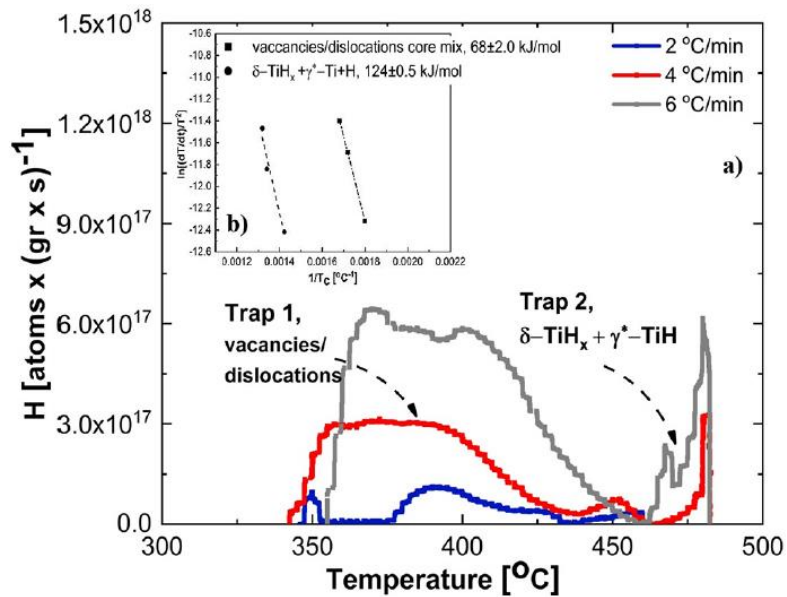
Another type of alloy used for advanced gas turbine engines is Ti-6Al-4V. Silverstein et al. [150] reported on the hydrogen embrittlement, trapping and desorption behaviour in 3D printed-Ti-6Al-4V by SLM method. Titanium alloys have reasonable resistance to chemical attack, but hydrogen attack causes severe problems, such as loss of ductility and decreased material strength. The processing of complex shaped alloy parts by additive manufacturing results in a complex, non-equilibrium state of the material. The hydrogen trapping characteristics were studied to determine the efficiency of hydrogen traps to bind hydrogen and preventing it from reaching cracking sites. Hydrogen embrittlement was studied by exposing samples to hydrogen atmosphere of 0.5 MPa hydrogen pressure at 500 °C for 10 h. Hydrogen evolution and hydrogen trapping interactions were evaluated via thermal desorption spectrometry (TDS), as illustrated in Figure 13. Samples 1 and 2, printed in direction X-Z and X-Y , were compared and it was shown that susceptibility to hydrogen embrittlement is influenced significantly by the printing direction. Sample 1 showed an increased susceptibility to hydrogen embrittlement, due to a higher content of Ti-hydrides and lower trapping energy of TiH compared to sample 2. The hydrogen desorption was considered as diffusion controlled for sample 1

and de-trapping controlled desorption for sample 2. The increased resistance to hydrogen embrittlement observed for sample 2 was associated with increased stress of the material in the printing direction [150].

a)

b)

Figure 13 Thermal desorption of hydrogen for: a) sample 1, with inset plot of activation energies for two fitted hydrogen desorption peaks and b) sample 2, with inset plot of the activation energies for two fitted hydrogen desorption peaks. Reprinted from [150] with permission from Elsevier.

Hydrogen embrittlement of AM parts produced for gas turbine applications is reported at low temperatures, from RT and up to 300°C. The 3D printed parts are generally reported with high resistance to hydrogen attack, correlated with the internal microstructure of the specimens [140,151]. Baek et al. [139] evaluated the effect of hydrogen attack for 3D printed metallic parts for 304L at 150°C to be used for manufacturing and repair of specialized parts such as blades and fuel nozzles for gas turbines [139]. The results indicated high resistance to hydrogen attack of the AM parts when compared with rolled plate specimens. Smith et al. [140] studied the effect of hydrogen corrosion on

tensile fracture and fatigue crack growth for 304L printed specimens at 300°C in comparison with wrought steel specimens. AM may induce defects such as microcracks, leading to reduction of ductility in hydrogen environment. The study concluded that 3D printed specimens can exhibit similar tensile and fatigue properties with wrought specimens in air and extreme hydrogen environment when manufacturing defects are avoided or effectively attenuated [140].

5.4   Dynamic embrittlement

The increased steam content in hydrogen fuelled gas turbines may act as an oxygen source to cause dynamic embrittlement of Ni based superalloys at intermediate temperatures. Ni based superalloys show ductility loss and intergranular cracking at intermediate temperatures. The embrittling behaviour is reported between 500 and 900 °C, with maximum of embrittlement around 600 °C [152]. The intergranular cracking of Ni based superalloys, caused by the diffusion of atomic oxygen at the grain boundaries (GB), is known as Oxidation Assisted Intergranular Cracking (OAIC) [153] or dynamic embrittlement [154]. A similar process of time-dependent decohesion at GB may occur under sustained or cyclic loading, determined by interactions with oxygen at the crack tip for Ni based superalloys [155]. Embrittling elements may be present in the alloy or oxygen from surrounding atmosphere may diffuse into the steel lattice and induce cracking along GB in the alloy. Ni based superalloy IN718 was designed for high temperature, but its application is limited to 650 °C due to the embrittlement occurring at higher temperatures [153]. For the Ni based superalloy U720Li no embrittlement was reported below 600 °C, with trans-granular failure observed. At temperatures of 600 to 850 °C, the ductility decreased significantly with quasibrittle intergranular failure, while above 850 °C the tensile ductility was recovered [156].

Chan [155] applied the grain boundary fracture model for Ni based superalloys, like IN718, to predict the onset of dynamic embrittlement and oxidation-induced crack growth and concluded that the model predicts correctly the decrease of tensile ductility of Ni-based superalloys with increasing oxygen content and temperatures. It was also concluded that dynamic embrittlement may occur prior to oxide formation, caused by the oxygen segregated GB, while oxide formation in the crack may have a strengthening effect on the crack-tip. It is mentioned that the heat of oxygen solution in Ni seems to be the activation energy for dynamic embrittlement. Deng et al. [157] studied the dwell-fatigue cracking at 550 °C of IN718 prepared by EBM AM technique, with focus on the anisotropic cracking resistance of the AM processed alloy. It was concluded that the loading parallel to the columnar GB demonstrated better dwell-fatigue cracking resistance than the loading perpendicular to the columnar GB. The AM processed specimens had superior dwell-fatigue cracking resistance in comparison with conventionally processed IN718 specimens both in parallel and perpendicular loaded specimens, resulted from the structure of the GB, grain size, low angle grain boundaries and the formation of the δ precipitate phase at GB.

6   Conclusions

Materials development for gas turbines has been focused on improving the gas turbine efficiency and profitability by increasing the maximum allowable service temperature and the long-term stability. Much of the advancement has been made in the area of thermal and environmental barrier coatings that can be utilized at higher operating temperatures and provide greater protection against oxidation. Alongside this, additive manufacturing is being explored and continuously improved as a promising method for fabricating new and complex combustor designs, intricate air cooling channels and other complex structures. The advancements made in these developments cover to some extent the new requirements arising from utilizing H_2 as fuel. However, this review has found that there are some potential challenges that require more attention.

Among the most critical challenges is the larger temperature gradients that emerge across air-cooled components in hydrogen-fired gas turbines, arising from the smaller flame-wall quenching distance, the potentially higher flame temperature and the larger heat transfer coefficient of the combustion products. This necessitates the development of thermal barrier coatings with even lower thermal conductivities and fracture toughness to withstand thermal stress induced cracking and spallation. Another potential challenge of hydrogen fired gas turbines is the increased steam content in the combustion products, which may have a significant negative effect on the corrosion resistance and lifetime of the barrier coatings and of the underlying metal component. Review of the available literature suggest that especially the combination of water vapor and heavy/fast cycling may be detrimental, meaning it will be more critical for aero applications than for stationary ones. There are few studies available that have investigated the degradation and lifetime as a function of the water vapor content. This is an area that should receive more attention in the development of materials specifically for hydrogen fired gas turbines. Other degradation phenomena such the dual atmosphere effect and hydrogen embrittlement require also more research in the context of gas turbines.

Additive manufacturing has excellent applicability for producing metallic parts with complex designs, for on-site building of new parts, and on-site repair of damaged/worn parts. Current development is focused on controlling the microstructure of the printed parts by optimizing printing parameters such as the laser scanning speed, intensity, layer thickness, etc. in order to melt the metal sufficiently to avoid porosity, while at the same time controlling evaporation of elements and segregation of secondary phases. The structure of the GB, the grain size and low angle grain boundaries is also of high importance. Control of microstructure is currently still a challenge with the conventional Ni-based alloys used in gas turbines, and progress in additive manufacturing may lead to the development of new gas turbine alloy compositions that are more optimised for the rapid and repeated thermal cycles specific to 3D printing. In cases where the printed parts contain pores, inclusions and similar defects, a greater susceptibility to hydrogen embrittlement and a lower high temperature corrosion resistance has been reported. On the other hand, parts fabricated with a more optimized microstructure are reported to be less susceptible to hydrogen embrittlement than conventionally processed parts.

7 Acknowledgements

8 Disclosure statement

No potential conflict of interest was reported by the author(s).

9 ORCID

Elena Stefan, https://orcid.org/0000-0002-8804-0597

Belma Talic, https://orcid.org/0000-0001-8148-6863

Yngve Larring, https://orcid.org/0000-0002-6600-9951

Andrea Gruber, https://orcid.org/0000-0003-2753-9690

Thijs A. Peters, https://orcid.org/0000-0002-1168-3455

10 List of abbreviations

AM	Additive manufacturing
APS	Atmospheric plasma spraying
CCS	Carbon capture and storage
CHP	Combined heat and power
CMAS	Calcium magnesium aluminosilicate
CMC	Ceramic matrix composites
CO_2	Carbon dioxide
DLE	Dry low emission
EB-PVD	Electron-beam physical vapor deposition
EBC	Environmental barrier coatings
EBM	Electron beam melting
GB	Grain boundary
HVOF	High velocity oxy fuel
kWh	kilowatt hour
MAX	$M_{n+1}AX_n$
NO_x	Nitrogen oxide
OAIC	Oxidation assisted intergranular cracking
ODS	oxide-dispersion-strengthened
PS-PVD	Plasma-spray physical vapor deposition
RT	Room temperature
Sccm	Standard cubic centimetres per minute
SLM	Selective laser melting
SoA	State of the art
SPS	Suspension plasma spraying
TBC	Thermal barrier coatings
TDS	Thermal desorption spectrometry
TEC	Thermal expansion coefficient
TGO	Thermally grown oxide
US	United States
YAG	Yttrium aluminium garnets
YSZ	Yttria stabilised zirconia

11 References

[1] World's Most Efficient Combined-Cycle Power Plant | GE Power n.d. https://www.ge.com/power/about/insights/articles/2018/03/nishi-nagoya-efficiency-record (accessed May 25, 2020).

[2] Spath PL, Mann MK. Life Cycle Assessment of a Natural Gas Combined Cycle Power Generation System. 2000. https://doi.org/10.2172/776930.

[3] Kloess M, Zach K. Bulk electricity storage technologies for load-leveling operation – An economic assessment for the Austrian and German power market. International Journal of Electrical Power & Energy Systems 2014;59:111–22. https://doi.org/10.1016/j.ijepes.2014.02.002.

[4] Santos S, Collodi G, Azzaro G, Ferrari N. Reference Data and Supporting Literature Reviews for SMR based Hydrogen Production with CCS. IEAGHG; 2017.

[5] Energy Information Administration. The Impact of Increased Use of Hydrogen on Petroleum Consumption and Carbon Dioxide Emissions. 2008.

[6] Langston LS. Hydrogen Fueled Gas Turbines. Mechanical Engineering 2019;141:52–4. https://doi.org/10.1115/1.2019-MAR-6.

[7] Quarton CJ, Samsatli S. Power-to-gas for injection into the gas grid: What can we learn from real-life projects, economic assessments and systems modelling? Renewable and Sustainable Energy Reviews 2018;98:302–16. https://doi.org/10.1016/j.rser.2018.09.007.

[8] White paper: Hydrogen power with Siemens gas turbines 2020.

[9] du Toit MH, Avdeenkov AV, Bessarabov D. Reviewing H2 Combustion: A Case Study for Non-Fuel-Cell Power Systems and Safety in Passive Autocatalytic Recombiners. Energy Fuels 2018;32:6401–22. https://doi.org/10.1021/acs.energyfuels.8b00724.

[10] ETN GLOBAL. The path towards a zero-carbon gas turbine. n.d.

[11] World's First Successful Technology Verification of 100% Hydrogen-fueled Gas Turbine Operation with Dry Low NOx Combustion Technology | NEDO n.d. https://www.nedo.go.jp/english/news/AA5en_100427.html (accessed September 14, 2020).

[12] Bothien MR, Ciani A, Wood JP, Fruechtel G. Toward Decarbonized Power Generation With Gas Turbines by Using Sequential Combustion for Burning Hydrogen. Journal of Engineering for Gas Turbines and Power 2019;141. https://doi.org/10.1115/1.4045256.

[13] Griebel P. Gas Turbines and Hydrogen. Hydrogen Science and Engineering : Materials, Processes, Systems and Technology, John Wiley & Sons, Ltd; 2016, p. 1011–32. https://doi.org/10.1002/9783527674268.ch43.

[14] Daniele S, Jansohn P, Mantzaras J, Boulouchos K. Turbulent flame speed for syngas at gas turbine relevant conditions. Proceedings of the Combustion Institute 2011;33:2937–44. https://doi.org/10.1016/j.proci.2010.05.057.

[15] Dreizler A, Böhm B. Advanced laser diagnostics for an improved understanding of premixed flame-wall interactions. Proceedings of the Combustion Institute 2015;35:37–64. https://doi.org/10.1016/j.proci.2014.08.014.

[16] Gruber A, Sankaran R, Hawkes ER, Chen JH. Turbulent flame–wall interaction: a direct numerical simulation study. Journal of Fluid Mechanics 2010;658:5–32. https://doi.org/10.1017/S0022112010001278.

[17] Chiesa P, Lozza G, Mazzocchi L. Using Hydrogen as Gas Turbine Fuel. J Eng Gas Turbines Power 2005;127:73–80. https://doi.org/10.1115/1.1787513.

[18] Alvin MA. Materials and Component Development for Advanced Turbine Systems. Volume 4: Cycle Innovations; Industrial and Cogeneration; Manufacturing Materials and Metallurgy; Marine, Orlando, Florida, USA: ASMEDC; 2009, p. 737–46. https://doi.org/10.1115/GT2009-59106.

[19] Clarke DR, Oechsner M, Padture NP. Thermal-barrier coatings for more efficient gas-turbine engines. MRS Bulletin 2012;37:891–8. https://doi.org/10.1557/mrs.2012.232.

[20] Wright IG, Gibbons TB. Recent developments in gas turbine materials and technology and their implications for syngas firing. International Journal of Hydrogen Energy 2007;32:3610–21. https://doi.org/10.1016/j.ijhydene.2006.08.049.

[21] Singh K. Advanced Materials for Land Based Gas Turbines. Trans Indian Inst Met 2014;67:601–15. https://doi.org/10.1007/s12666-014-0398-3.

[22] Pollock TM, Tin S. Nickel-Based Superalloys for Advanced Turbine Engines: Chemistry, Microstructure and Properties. Journal of Propulsion and Power 2006;22:361–74. https://doi.org/10.2514/1.18239.

[23] Muktinutalapati NR. Materials for Gas Turbines – An Overview. Advances in Gas Turbine Technology 2011. https://doi.org/10.5772/20730.

[24] SCHILKE P. Advanced Gas Turbine Materials and Coatings. GE Reference Library GER-3569G 2004:1–25.

[25] Wee S, Do J, Kim K, Lee C, Seok C, Choi B-G, et al. Review on Mechanical Thermal Properties of Superalloys and Thermal Barrier Coating Used in Gas Turbines. Applied Sciences 2020;10:5476. https://doi.org/10.3390/app10165476.

[26] Lagow BW. Materials Selection in Gas Turbine Engine Design and the Role of Low Thermal Expansion Materials. JOM 2016;68:2770–5. https://doi.org/10.1007/s11837-016-2071-2.

[27] Bakan E, Mack DE, Mauer G, Vaßen R, Lamon J, Padture NP. High-temperature materials for power generation in gas turbines. Advanced Ceramics for Energy Conversion and Storage, Elsevier; 2020, p. 3–62. https://doi.org/10.1016/B978-0-08-102726-4.00001-6.

[28] Goldmeer DJ. GEA33861 Electrify Europe Whitepaper 2018. /paper/GEA33861-Electrify-Europe-Whitepaper-Goldmeer/ae2b78ad10651c1061918b9030951ac02c1256b5 (accessed July 27, 2020).

[29] Electrical Monitor :: Alstom GT24/GT26 gas turbines create record n.d. http://www.electricalmonitor.com/ArticleDetails.aspx?aid=481&sid=9 (accessed June 27, 2020).

[30] Shaikh AS. Development of a γ' Precipitation Hardening Ni-Base Superalloy for Additive Manufacturing. 2018. https://doi.org/10.13140/RG.2.2.11472.81921.

[31] Pauzi AA, Ghazali MJ, W. Zamri WFH, Rajabi A. Wear Characteristics of Superalloy and Hardface Coatings in Gas Turbine Applications–A Review. Metals 2020;10:1171. https://doi.org/10.3390/met10091171.

[32] Dorcheh AS, Galetz MC. Challenges in Developing Oxidation-Resistant Chromium-Based Alloys for Applications Above 900°C. JOM 2016;68:2793–802. https://doi.org/10.1007/s11837-016-2079-7.

[33] Gu YF, Harada H, Ro Y. Chromium and chromium-based alloys: Problems and possibilities for high-temperature service. JOM 2004;56:28–33. https://doi.org/10.1007/s11837-004-0197-0.

[34] Michalik M, Tobing SL, Hänsel M, Shemet V, Quadakkers WJ, Young DJ. Effects of water vapour on the high temperature nitridation of chromium. Materials and Corrosion 2014;65:260–6. https://doi.org/10.1002/maco.201307160.

[35] Szweda A, Butner S, Ruffoni J, Bacalski C, Lane J, Morrison J, et al. Development and Evaluation of Hybrid Oxide/Oxide Ceramic Matrix Composite Combustor Liners, American Society of Mechanical Engineers Digital Collection; 2008, p. 315–21. https://doi.org/10.1115/GT2005-68496.

[36] Pimentel G, Capdevila C, Bartolome M, Chao J, Serrano M, García-Junceda A, et al. Advanced FeCrAl ODS steels for high-temperature structural applications in energy generation systems. Revista de Metalurgia 2012;48:303. https://doi.org/10.3989/revmetalm.1165.

[37] Furrer D, Fecht H. Ni-based superalloys for turbine discs. JOM 1999;51:14–7. https://doi.org/10.1007/s11837-999-0005-y.

[38] Smith TM, Esser BD, Antolin N, Carlsson A, Williams REA, Wessman A, et al. Phase transformation strengthening of high-temperature superalloys. Nature Communications 2016;7:13434. https://doi.org/10.1038/ncomms13434.

[39] Panwisawas C, Tang YT, Reed RC. Metal 3D printing as a disruptive technology for superalloys. Nature Communications 2020;11:2327. https://doi.org/10.1038/s41467-020-16188-7.

[40] Basoalto HC, Panwisawas C, Sovani Y, Anderson MJ, Turner RP, Saunders B, et al. A computational study on the three-dimensional printability of precipitate-strengthened nickel-based superalloys. Proceedings of the Royal Society A: Mathematical, Physical and Engineering Sciences 2018;474:20180295. https://doi.org/10.1098/rspa.2018.0295.

[41] Chauvet E, Kontis P, Jägle E, Gault B, Raabe D, TASSIN C, et al. Hot cracking mechanism affecting a non-weldable Ni-based superalloy produced by selective electron Beam Melting. Acta Materialia 2018;142:82–94. https://doi.org/10.1016/j.actamat.2017.09.047.

[42] Hojjatzadeh SMH, Parab ND, Yan W, Guo Q, Xiong L, Zhao C, et al. Pore elimination mechanisms during 3D printing of metals. Nature Communications 2019;10:3088. https://doi.org/10.1038/s41467-019-10973-9.

[43] Smialek JL, Miller RA. Revisiting the Birth of 7YSZ Thermal Barrier Coatings: Stephan Stecura †. Coatings 2018;8:255. https://doi.org/10.3390/coatings8070255.

[44] Hasselman DPH, Johnson LF, Bentsen LD, Syed R, Lee HL, Swain MV. Thermal Diffusivity and Conductivity of Dense Polycrystalline Zr02 Ceramics: A Survey 1987;66:9.

[45] Pawlowski L, Lombard D, Fauchais P. Structure-thermal properties—relationship in plasma sprayed zirconia coatings. Journal of Vacuum Science & Technology A: Vacuum, Surfaces, and Films 1985;3:2494–500. https://doi.org/10.1116/1.572865.

[46] Marra J. Advanced Hydrogen Turbine Development. Siemens Energy, Inc., Orlando, FL (United States); 2015. https://doi.org/10.2172/1261639.

[47] Schulz U. Phase Transformation in EB-PVD Yttria Partially Stabilized Zirconia Thermal Barrier Coatings during Annealing. Journal of the American Ceramic Society 2000;83:904–10. https://doi.org/10.1111/j.1151-2916.2000.tb01292.x.

[48] Witz G, Shklover V, Steurer W, Bachegowda S, Bossmann H-P. Phase Evolution in Yttria-Stabilized Zirconia Thermal Barrier Coatings Studied by Rietveld Refinement of X-Ray Powder Diffraction Patterns. Journal of the American Ceramic Society 2007;90:2935–40. https://doi.org/10.1111/j.1551-2916.2007.01785.x.

[49] Liu B, Liu Y, Zhu C, Xiang H, Chen H, Sun L, et al. Advances on strategies for searching for next generation thermal barrier coating materials. Journal of Materials Science & Technology 2019;35:833–51. https://doi.org/10.1016/j.jmst.2018.11.016.

[50] Bakan E, Vaßen R. Ceramic Top Coats of Plasma-Sprayed Thermal Barrier Coatings: Materials, Processes, and Properties. J Therm Spray Tech 2017;26:992–1010. https://doi.org/10.1007/s11666-017-0597-7.

[51] Gok MG, Goller G. State of the Art of Gadolinium Zirconate Based Thermal Barrier Coatings: Design, Processing and Characterization. Methods for Film Synthesis and Coating Procedures 2019. https://doi.org/10.5772/intechopen.85451.

[52] Padture NP, Gell M, Jordan EH. Thermal Barrier Coatings for Gas-Turbine Engine Applications. Science 2002;296:280–4. https://doi.org/10.1126/science.1068609.

[53] Naumenko D, Pillai R, Chyrkin A, Quadakkers WJ. Overview on Recent Developments of Bondcoats for Plasma-Sprayed Thermal Barrier Coatings. J Therm Spray Tech 2017;26:1743–57. https://doi.org/10.1007/s11666-017-0649-z.

[54] Evans AG, Mumm DR, Hutchinson JW, Meier GH, Pettit FS. Mechanisms controlling the durability of thermal barrier coatings. Progress in Materials Science 2001;46:505–53. https://doi.org/10.1016/S0079-6425(00)00020-7.

[55] Quested PN, Brooks RF, Chapman L, Morrell R, Youssef Y, Mills KC. Measurement and estimation of thermophysical properties of nickel based superalloys. Materials Science and Technology 2009;25:154–62. https://doi.org/10.1179/174328408X361454.

[56] Taylor TA, Walsh PN. Thermal expansion of MCrAlY alloys. Surface and Coatings Technology 2004;177–178:24–31. https://doi.org/10.1016/j.surfcoat.2003.05.001.

[57] Taylor TA. Thermal properties and microstructure of two thermal barrier coatings. In: Sartwell BD, McGUIRE GE, Hofmann S, editors. Metallurgical Coatings and Thin Films 1992, Amsterdam: Elsevier; 1992, p. 53–7. https://doi.org/10.1016/B978-0-444-89900-2.50015-4.

[58] Touloukian YS. Thermal Expansion: Nonmetallic Solids. Springer US; 1977.

[59] Martena M, Botto D, Fino P, Sabbadini S, Gola MM, Badini C. Modelling of TBC system failure: Stress distribution as a function of TGO thickness and thermal expansion mismatch. Engineering Failure Analysis 2006;13:409–26. https://doi.org/10.1016/j.engfailanal.2004.12.027.

[60] Eriksson R, Sjöström S, Brodin H, Johansson S, Östergren L, Li X-H. TBC bond coat–top coat interface roughness: Influence on fatigue life and modelling aspects. Surface and Coatings Technology 2013;236:230–8. https://doi.org/10.1016/j.surfcoat.2013.09.051.

[61] Ahrens M, Vaßen R, Stöver D. Stress distributions in plasma-sprayed thermal barrier coatings as a function of interface roughness and oxide scale thickness. Surface and Coatings Technology 2002;161:26–35. https://doi.org/10.1016/S0257-8972(02)00359-6.

[62] Dong H, Yang G-J, Cai H-N, Ding H, Li C-X, Li C-J. The influence of temperature gradient across YSZ on thermal cyclic lifetime of plasma-sprayed thermal barrier coatings. Ceramics International 2015;41:11046–56. https://doi.org/10.1016/j.ceramint.2015.05.049.

[63] Sun J, Wang J, Zhang H, Yuan J, Dong S, Jiang J, et al. Preparation, structure, mechanical properties and thermal cycling behavior of porous LaMgAl11O19 coating. Journal of Alloys and Compounds 2018;750:1007–16. https://doi.org/10.1016/j.jallcom.2018.04.097.

[64] Zhang J, Bai Y, Li E, Dong H, Ma W. Yb2O3-Gd2O3 codoped strontium zirconate composite ceramics for potential thermal barrier coating applications. International Journal of Applied Ceramic Technology 2020;17:1608–18. https://doi.org/10.1111/ijac.13500.

[65] Gell M, Wang J, Kumar R, Roth J, Jiang C, Jordan EH. Higher Temperature Thermal Barrier Coatings with the Combined Use of Yttrium Aluminum Garnet and the Solution Precursor Plasma Spray Process. J Therm Spray Tech 2018;27:543–55. https://doi.org/10.1007/s11666-018-0701-7.

[66] Doleker KM, Karaoglanli AC. Comparison of oxidation behavior of YSZ and Gd2Zr2O7 thermal barrier coatings (TBCs). Surface and Coatings Technology 2017;318:198–207. https://doi.org/10.1016/j.surfcoat.2016.12.078.

[67] Bakan E. Yttria-stabilized zirconia/gadolinium zirconate double-layer plasma-sprayed thermal barrier coating systems (TBCs). Jülich: Forschungszentrum Jülich; 2015.

[68] Pint BA. High-Temperature Corrosion in Fossil Fuel Power Generation: Present and Future. JOM 2013;65:1024–32. https://doi.org/10.1007/s11837-013-0642-z.

[69] Evans HE, Taylor MP. Diffusion Cells and Chemical Failure of MCrAlY Bond Coats in Thermal-Barrier Coating Systems. Oxidation of Metals 2001;55:17–34. https://doi.org/10.1023/A:1010369024142.

[70] Li Z, Bradt RC. Thermal expansion of the cubic (3C) polytype of SiC. J Mater Sci 1986;21:4366–8. https://doi.org/10.1007/BF01106557.

[71] Eaton HE, Linsey GD. Accelerated oxidation of SiC CMC's by water vapor and protection via environmental barrier coating approach. Journal of the European Ceramic Society 2002;22:2741–7. https://doi.org/10.1016/S0955-2219(02)00141-3.

[72] Xu Y, Hu X, Xu F, Li K. Rare earth silicate environmental barrier coatings: Present status and prospective. Ceramics International 2017;43:5847–55. https://doi.org/10.1016/j.ceramint.2017.01.153.

[73] Richards BT, Wadley HNG. Plasma spray deposition of tri-layer environmental barrier coatings. Journal of the European Ceramic Society 2014;34:3069–83. https://doi.org/10.1016/j.jeurceramsoc.2014.04.027.

[74] Lucato SL dos S e, Sudre OH, Marshall DB. A Method for Assessing Reactions of Water Vapor with Materials in High-Speed, High-Temperature Flow. Journal of the American Ceramic Society 2011;94:s186–95. https://doi.org/10.1111/j.1551-2916.2011.04556.x.

[75] Golden RA, Opila EJ. A method for assessing the volatility of oxides in high-temperature high-velocity water vapor. Journal of the European Ceramic Society 2016;36:1135–47. https://doi.org/10.1016/j.jeurceramsoc.2015.11.016.

[76] Mumm D. Mechanisms Underpinning Degradation of Protective Oxides and Thermal Barrier Coatings in High Hydrogen Content (HHC) - Fueled Turbines. 2013. https://doi.org/10.2172/1149472.

[77] Yu CT, Liu H, Zhang J, Ullah A, Bao ZB, Jiang CY, et al. Gradient thermal cycling behavior of a thermal barrier coating system constituted by NiCoCrAlY bond coat and pure metastable tetragonal nano-4YSZ top coat. Ceramics International 2019;45:15281–9. https://doi.org/10.1016/j.ceramint.2019.05.018.

[78] Ziaei-Asl A, Ramezanlou MT. Thermo-mechanical behavior of gas turbine blade equipped with cooling ducts and protective coating with different thicknesses. International Journal of Mechanical Sciences 2019;150:656–64. https://doi.org/10.1016/j.ijmecsci.2018.10.070.

[79] Vaßen R, Kerkhoff G, Stöver D. Development of a micromechanical life prediction model for plasma sprayed thermal barrier coatings. Materials Science and Engineering: A 2001;303:100–9. https://doi.org/10.1016/S0921-5093(00)01853-0.

[80] Saunders SRJ, Monteiro M, Rizzo F. The oxidation behaviour of metals and alloys at high temperatures in atmospheres containing water vapour: A review. Progress in Materials Science 2008;53:775–837. https://doi.org/10.1016/j.pmatsci.2007.11.001.

[81] Meschter PJ, Opila EJ, Jacobson NS. Water Vapor–Mediated Volatilization of High-Temperature Materials. Annual Review of Materials Research 2013;43:559–88. https://doi.org/10.1146/annurev-matsci-071312-121636.

[82] Opila EJ, Myers DL, Jacobson NS, Nielsen IMB, Johnson DF, Olminsky JK, et al. Theoretical and Experimental Investigation of the Thermochemistry of $CrO_2(OH)_2(g)$. J Phys Chem A 2007;111:1971–80. https://doi.org/10.1021/jp0647380.

[83] Asteman H, Svensson J-E, Norell M, Johansson L-G. Influence of Water Vapor and Flow Rate on the High-Temperature Oxidation of 304L; Effect of Chromium Oxide Hydroxide Evaporation. Oxidation of Metals 2000;54:11–26. https://doi.org/10.1023/A:1004642310974.

[84] Tedmon CS. The Effect of Oxide Volatilization on the Oxidation Kinetics of Cr and Fe-Cr Alloys. J Electrochem Soc 1966;113:766–8. https://doi.org/10.1149/1.2424115.

[85] Sachitanand R, Svensson J-E, Froitzheim J. The Influence of Cr Evaporation on Long Term Cr Depletion Rates in Ferritic Stainless Steels. Oxid Met 2015;84:241–57. https://doi.org/10.1007/s11085-015-9552-5.

[86] Hooshyar H, Jonsson T, Hall J, Svensson J-E, Johansson LG, Liske J. The Effect of H2 and H2O on the Oxidation of 304L-Stainless Steel at 600 °C: General Behaviour (Part I). Oxid Met 2016;85:321–42. https://doi.org/10.1007/s11085-015-9597-5.

[87] Henry S, Mougin J, Wouters Y, Petit J-P, Galerie A. Characterization of Chromia Scales Grown on Pure Chromium in Different Oxidizing Atmospheres. Materials at High Temperatures 2000;17:231–4. https://doi.org/10.1179/mht.2000.17.2.008.

[88] Hultquist G, Tveten B, Hörnlund E. Hydrogen in Chromium: Influence on the High-Temperature Oxidation Kinetics in H2O, Oxide-Growth Mechanisms, and Scale Adherence. Oxidation of Metals 2000;54:1–10. https://doi.org/10.1023/A:1004610626903.

[89] Zurek J, Young DJ, Essuman E, Hänsel M, Penkalla HJ, Niewolak L, et al. Growth and adherence of chromia based surface scales on Ni-base alloys in high- and low-pO2 gases. Materials Science and Engineering: A 2008;477:259–70. https://doi.org/10.1016/j.msea.2007.05.035.

[90] Simon D, Gorr B, Christ HJ. Effect of Atmosphere and Sample Thickness on Kinetics, Microstructure, and Compressive Stresses of Chromia Scale Grown on Ni–25Cr. Oxid Met 2017;87:417–29. https://doi.org/10.1007/s11085-016-9702-4.

[91] Sand T, Geers C, Cao Y, Svensson JE, Johansson LG. Effective Reduction of Chromium-oxy-hydroxide Evaporation from Ni-Base Alloy 690. Oxid Met 2019;92:259–79. https://doi.org/10.1007/s11085-019-09935-9.

[92] Pint BA, Dryepondt S, Unocic KA. Oxidation of Superalloys in Extreme Environments. Superalloy 718 and Derivatives, John Wiley & Sons, Ltd; 2012, p. 859–75. https://doi.org/10.1002/9781118495223.ch66.

[93] Maris-Sida MC, Meier GH, Pettit FS. Some Water Vapor Effects during the Oxidation of Alloys that are ⌣-Al2O3 Formers. METALLURGICAL AND MATERIALS TRANSACTIONS A 2003:11.

[94] Zhao W, Gleeson B. Assessment of the Detrimental Effects of Steam on Al2O3-Scale Establishment. Oxid Met 2015;83:607–27. https://doi.org/10.1007/s11085-015-9541-8.

[95] Liu F, Josefsson H, Svensson J-E, Johansson L-G, Halvarsson M. TEM investigation of the oxide scales formed on a FeCrAlRE alloy (Kanthal AF) at 900°C in dry O2 and O2 with 40% H2O. Materials at High Temperatures 2005;22:521–6. https://doi.org/10.1179/mht.2005.062.

[96] Götlind H, Liu F, Svensson J-E, Halvarsson M, Johansson L-G. The Effect of Water Vapor on the Initial Stages of Oxidation of the FeCrAl Alloy Kanthal AF at 900 °C. Oxid Met 2007;67:251–66. https://doi.org/10.1007/s11085-007-9055-0.

[97] Sohlberg K, Pennycook SJ, Pantelides ST. Hydrogen and the Structure of the Transition Aluminas. J Am Chem Soc 1999;121:7493–9. https://doi.org/10.1021/ja991098o.

[98]   Pint BA, Haynes JA, Zhang Y, More KL, Wright IG. The effect of water vapor on the oxidation behavior of Ni–Pt–Al coatings and alloys. Surface and Coatings Technology 2006;201:3852–6. https://doi.org/10.1016/j.surfcoat.2006.07.244.

[99]   Smialek JL. Moisture-Induced TBC Spallation on Turbine Blade Samples. Surface and Coatings Technology 2011;206:1577–85. https://doi.org/10.1016/j.surfcoat.2011.07.015.

[100] Opila EJ, Myers DL. Alumina Volatility in Water Vapor at Elevated Temperatures. Journal of the American Ceramic Society 2004;87:1701–5. https://doi.org/10.1111/j.1551-2916.2004.01701.x.

[101] Sumner J, Simms NJ, Stamm W, Oakey JE. Simulating novel gas turbine conditions for materials assessment: cascade design and operation. Materials Science and Technology 2017;33:1090–9. https://doi.org/10.1080/02670836.2017.1310492.

[102] Zhou C, Yu J, Gong S, Xu H. Influence of water vapor on the high temperature oxidation behavior of thermal barrier coatings. Materials Science and Engineering: A 2003;348:327–32. https://doi.org/10.1016/S0921-5093(02)00742-6.

[103] Cernuschi F, Bison P, Mack DE, Merlini M, Boldrini S, Marchionna S, et al. Thermo-physical properties of as deposited and aged thermal barrier coatings (TBC) for gas turbines: State-of-the art and advanced TBCs. Journal of the European Ceramic Society 2018;38:3945–61. https://doi.org/10.1016/j.jeurceramsoc.2018.04.044.

[104] Sullivan MH, Mumm DR. Transient stage oxidation of MCrAlY bond coat alloys in high temperature, high water vapor content environments. Surface and Coatings Technology 2014;258:963–72. https://doi.org/10.1016/j.surfcoat.2014.07.048.

[105] Unocic KA, Pint BA. Effect of water vapor on thermally grown alumina scales on bond coatings. Surface and Coatings Technology 2013;215:30–8. https://doi.org/10.1016/j.surfcoat.2012.08.100.

[106] Pint BA, Garner GW, Lowe TM, Haynes JA, Zhang Y. Effect of increased water vapor levels on TBC lifetime with Pt-containing bond coatings. Surface and Coatings Technology 2011;206:1566–70. https://doi.org/10.1016/j.surfcoat.2011.06.008.

[107] Nowak W. High Temperature Corrosion of Alloys and Coatings in Gas-Turbines Fired with Hydrogen-Rich Syngas Fuels. 2014.

[108] Opila EJ, Smialek JL, Robinson RC, Fox DS, Jacobson NS. SiC Recession Caused by SiO2 Scale Volatility under Combustion Conditions: II, Thermodynamics and Gaseous-Diffusion Model. Journal of the American Ceramic Society 1999;82:1826–34. https://doi.org/10.1111/j.1151-2916.1999.tb02005.x.

[109] Parker CG, Opila EJ. Stability of the Y2O3–SiO2 system in high-temperature, high-velocity water vapor. Journal of the American Ceramic Society 2020;103:2715–26. https://doi.org/10.1111/jace.16915.

[110] Padture NP. Environmental degradation of high-temperature protective coatings for ceramic-matrix composites in gas-turbine engines. Npj Materials Degradation 2019;3:1–6. https://doi.org/10.1038/s41529-019-0075-4.

[111] Li L, Hitchman N, Knapp J. Failure of Thermal Barrier Coatings Subjected to CMAS Attack. J Therm Spray Tech 2010;19:148–55. https://doi.org/10.1007/s11666-009-9356-8.

[112] Yang Z, Walker MS, Singh P, Stevenson JW. Anomalous Corrosion Behavior of Stainless Steels under SOFC Interconnect Exposure Conditions. Electrochem Solid-State Lett 2003;6:B35–7. https://doi.org/10.1149/1.1603012.

[113] Kurokawa H, Kawamura K, Maruyama T. Oxidation behavior of Fe–16Cr alloy interconnect for SOFC under hydrogen potential gradient. Solid State Ionics 2004;168:13–21. https://doi.org/10.1016/j.ssi.2004.02.008.

[114] Holcomb GR, Ziomek-Moroz M, Cramer SD, Jr BSC, Bullard SJ. Dual-environment effects on the oxidation of metallic interconnects. J of Materi Eng and Perform 2006;15:404–9. https://doi.org/10.1361/105994906X117198.

[115] Alnegren P, Sattari M, Svensson J-E, Froitzheim J. Severe dual atmosphere effect at 600 °C for stainless steel 441. Journal of Power Sources 2016;301:170–8. https://doi.org/10.1016/j.jpowsour.2015.10.001.

[116] Gannon P, Amendola R. High-Temperature, Dual-Atmosphere Corrosion of Solid-Oxide Fuel Cell Interconnects. JOM 2012;64:1470–6. https://doi.org/10.1007/s11837-012-0473-3.

[117] Goebel C, Alnegren P, Faust R, Svensson J-E, Froitzheim J. The effect of pre-oxidation parameters on the corrosion behavior of AISI 441 in dual atmosphere. International Journal of Hydrogen Energy 2018;43:14665–74. https://doi.org/10.1016/j.ijhydene.2018.05.165.

[118] Yang Z, Walker MS, Singh P, Stevenson JW, Norby T. Oxidation Behavior of Ferritic Stainless Steels under SOFC Interconnect Exposure Conditions. J Electrochem Soc 2004;151:B669–78. https://doi.org/10.1149/1.1810393.

[119] Zhao Y, Fergus JW. Oxidation Behavior of Stainless Steel 441 and 430 in Dual Atmosphere: Effects of Alloy Grain Boundaries. J Electrochem Soc 2014;161:C69–76. https://doi.org/10.1149/2.076401jes.

[120] Rufner J, Gannon P, White P, Deibert M, Teintze S, Smith R, et al. Oxidation behavior of stainless steel 430 and 441 at 800 °C in single (air/air) and dual atmosphere (air/hydrogen) exposures. International Journal of Hydrogen Energy 2008;33:1392–8. https://doi.org/10.1016/j.ijhydene.2007.12.067.

[121] Galerie A, Henry S, Wouters Y, Mermoux M, Petit J-P, Antoni L. Mechanisms of chromia scale failure during the course of 15–18Cr ferritic stainless steel oxidation in water vapour. Materials at High Temperatures 2005;22:105–12. https://doi.org/10.1179/mht.2005.012.

[122] Zhao Y, Fergus JW. Oxidation of Alloys 430 and 441 in SOFC Dual Atmospheres: Effects of Flow Rate and Humidity. J Electrochem Soc 2012;159:C109–13. https://doi.org/10.1149/2.013203jes.

[123] Nickel institute: High temperature characteristics of stainless steels n.d.

[124] Nelson GA, Effinger RT. BLISTERING AND EMBRITTLEMENT OF PRESSURE VESSEL STEELS BY HYDROGEN. Welding J (NY) 1955;Vol: 34.

[125] Nibur KA, Somerday BP. 7 - Fracture and fatigue test methods in hydrogen gas. In: Gangloff RP, Somerday BP, editors. Gaseous Hydrogen Embrittlement of Materials in Energy Technologies, vol. 2, Woodhead Publishing; 2012, p. 195–236. https://doi.org/10.1533/9780857093899.2.195.

[126] Gray HR. Embrittlement of nickel-, cobalt-, and iron-base superalloys by exposure to hydrogen. 1975.

[127] Balyts'kyi AI, Kvasnyts'ka YuH, Ivas'kevich LM, Myal'nitsa HP. Corrosion- and Hydrogen-Resistance of Heat-Resistant Blade Nickel-Cobalt Alloys. Mater Sci 2018;54:230–9. https://doi.org/10.1007/s11003-018-0178-z.

[128] Owen D, Tokmo F, Hickey J, Phillips L, Jenkins S, Zhang J. Gas Turbine Engine Components Manufactured via Additive Manufacturing Process. ASTM Project Grant Final Report n.d.:10.

[129] Kellner T. Fired Up: GE Successfully Tested Its Advanced Turboprop Engine With 3D-Printed Parts | GE News n.d. https://www.ge.com/news/reports/ge-fired-its-3d-printed-advanced-turboprop-engine (accessed June 30, 2020).

[130] Additive Manufacturing for Turbomachinery & Turbines | EOS n.d. https://www.eos.info/en/3d-printing-examples-applications/production-and-industry/turbomachinery-turbines (accessed June 24, 2020).

[131] Fu W, Haberland C, Klapdor EV, Rule D, Piegert S. Streamlined frameworks for advancing metal based additive manufacturing technologies. J Glob Power Propuls Soc 2018;2:317–28. https://doi.org/10.22261/JGPPS.QJLS4L.

[132] Gebisa AW, Lemu HG. Additive Manufacturing for the Manufacture of Gas Turbine Engine Components: Literature Review and Future Perspectives, American Society of Mechanical Engineers Digital Collection; 2018. https://doi.org/10.1115/GT2018-76686.

[133] Deng D. Additively Manufactured Inconel 718 : Microstructures and Mechanical Properties 2018.

[134] Zhang F, Levine LE, Allen AJ, Stoudt MR, Lindwall G, Lass EA, et al. Effect of heat treatment on the microstructural evolution of a nickel-based superalloy additive-manufactured by laser powder bed fusion. Acta Materialia 2018;152:200–14. https://doi.org/10.1016/j.actamat.2018.03.017.

[135] Andersson O, Graichen A, Brodin H, Navrotsky V. Developing Additive Manufacturing Technology for Burner Repair. J Eng Gas Turbines Power 2017;139. https://doi.org/10.1115/1.4034235.

[136] Örnek C. Additive manufacturing – a general corrosion perspective. Corrosion Engineering, Science and Technology 2018;53:531–5. https://doi.org/10.1080/1478422X.2018.1511327.

[137] Kong D, Dong C, Ni X, Li X. Corrosion of metallic materials fabricated by selective laser melting. Npj Materials Degradation 2019;3:1–14. https://doi.org/10.1038/s41529-019-0086-1.

[138] Laleh M, Hughes AE, Xu W, Gibson I, Tan MY. A critical review of corrosion characteristics of additively manufactured stainless steels. International Materials Reviews 2020;0:1–37. https://doi.org/10.1080/09506608.2020.1855381.

[139] Baek S-W, Song EJ, Kim JH, Jung M, Baek UB, Nahm SH. Hydrogen embrittlement of 3-D printing manufactured austenitic stainless steel part for hydrogen service. Scripta Materialia 2017;130:87–90. https://doi.org/10.1016/j.scriptamat.2016.11.020.

[140] Smith TR, San Marchi C, Sugar JD, Balch DK. Effects of Extreme Hydrogen Environments on the Fracture and Fatigue Behavior of Additively Manufactured Stainless Steels, American Society of Mechanical Engineers Digital Collection; 2019. https://doi.org/10.1115/PVP2019-93903.

[141] Kong D, Dong C, Ni X, Zhang L, Luo H, Li R, et al. Superior resistance to hydrogen damage for selective laser melted 316L stainless steel in a proton exchange membrane fuel cell environment. Corrosion Science 2020;166:108425. https://doi.org/10.1016/j.corsci.2019.108425.

[142] Kulkarni A. Additive Manufacturing of Nickel Based Superalloy. ArXiv:180511664 [Physics] 2018.

[143] Xu J, Gruber H, Boyd R, Jiang S, Peng RL, Moverare JJ. On the strengthening and embrittlement mechanisms of an additively manufactured Nickel-base superalloy. Materialia 2020;10:100657. https://doi.org/10.1016/j.mtla.2020.100657.

[144] Seifi M, Salem A, Beuth J, Harrysson O, Lewandowski JJ. Overview of Materials Qualification Needs for Metal Additive Manufacturing. JOM 2016;68:747–64. https://doi.org/10.1007/s11837-015-1810-0.

[145] Gorsse S, Hutchinson C, Gouné M, Banerjee R. Additive manufacturing of metals: a brief review of the characteristic microstructures and properties of steels, Ti-6Al-4V and high-entropy alloys. Science and Technology of Advanced Materials 2017;18:584–610. https://doi.org/10.1080/14686996.2017.1361305.

[146] How Mature Are Metal 3D Printing Technologies? AMFG 2019. https://amfg.ai/2019/09/03/how-mature-are-metal-3d-printing-technologies/ (accessed August 7, 2020).

[147] Norsk Titanium Completes TRL 8 Certification: 3D Printed RPD Components Pass Stringent Testing. 3DPrintCom | The Voice of 3D Printing / Additive Manufacturing 2015. https://3dprint.com/112084/norsk-titanium-trl8/ (accessed August 7, 2020).

[148] Metal Materials for 3D printing | EOS GmbH n.d. https://www.eos.info/en/additive-manufacturing/3d-printing-metal/dmls-metal-materials (accessed August 7, 2020).

[149] TRLs Promise Quality in 3D Printing | EOS GmbH n.d. https://www.eos.info/en/additive-manufacturing/3d-printing-metal/trl (accessed August 7, 2020).

[150] Silverstein R, Eliezer D. Hydrogen trapping in 3D-printed (additive manufactured) Ti-6Al-4V. Materials Characterization 2018;144:297–304. https://doi.org/10.1016/j.matchar.2018.07.029.

[151] Hong Y, Zhou C, Zheng Y, Zhang L, Zheng J, Chen X, et al. Formation of strain-induced martensite in selective laser melting austenitic stainless steel. Materials Science and Engineering: A 2019;740–741:420–6. https://doi.org/10.1016/j.msea.2018.10.121.

[152] Zheng L, Schmitz G, Meng Y, Chellali M, Schlesiger R. Mechanism of Intermediate Temperature Embrittlement of Ni and Ni-based Superalloys. Critical Reviews in Solid State and Material Sciences 2012;37:181–214. https://doi.org/10.1080/10408436.2011.613492.

[153] Varela A de V, de Deus HD, de Siqueira MC, Rezende MC, de Almeida LH. Oxidation assisted intergranular cracking in 718 Nickel Superalloy: on the mechanism of dynamic embrittlement. Journal of Materials Research and Technology 2018;7:319–25. https://doi.org/10.1016/j.jmrt.2018.02.008.

[154] Saarimäki J. Cracks in superalloys. 2018. https://doi.org/10.3384/diss.diva-144397.

[155] Chan K. A Grain Boundary Fracture Model for Predicting Dynamic Embrittlement and Oxidation-Induced Cracking in Superalloys. Metallurgical and Materials Transactions A 2015;46. https://doi.org/10.1007/s11661-015-2860-1.

[156] Németh AAN, Crudden DJ, Armstrong DEJ, Collins DM, Li K, Wilkinson AJ, et al. Environmentally-assisted grain boundary attack as a mechanism of embrittlement in a nickel-based superalloy. Acta Materialia 2017;126:361–71. https://doi.org/10.1016/j.actamat.2016.12.039.

[157] Deng D, Peng RL, Moverare J. On the dwell-fatigue crack propagation behavior of a high strength superalloy manufactured by electron beam melting. Materials Science and Engineering: A 2019;760:448–57. https://doi.org/10.1016/j.msea.2019.06.013.